Stochastic Fluctuations in Signaling, Gene Control and Pattern Formation

A DISSERTATION
SUBMITTED TO THE FACULTY OF THE GRADUATE SCHOOL
OF THE UNIVERSITY OF MINNESOTA
BY

Likun Zheng

IN PARTIAL FULFILLMENT OF THE REQUIREMENTS
FOR THE DEGREE OF
Doctor of Philosophy

Hans G. Othmer

September, 2011

Acknowledgements

I would like to express my sincere thanks and gratitude to my thesis advisor Hans G. Othmer for his constant encouragement, infinite patience and valuable guidance through these years of my graduate study. I would like to thank Hye-Won Kang for her helpful discussion on stochastic background and analysis. I would like to thank Christina Brakken-Thal and Mike O'Connor for the discussion on the single cell model. I would like to thank Jifeng Hu for the discussion on Fourier transformation. I would like to thank all other members of Hans Othmer's group for their comments and support, especially my officemates Chuan Xue, Qixuan Wang and Hua Nie.

I would like to thank my parents for their unconditional trust, love and freedom. I also want to thank my husband Yu Gu for his faithful love and encouragement. I want to thank my sister Yakun Zheng for her support and understanding in the past 20 years.

Dedication

Dedicated to my parents.

Abstract

Stochasticity is inherent in biochemical systems. Noise can come from internal sources such as the random motion and reactions of molecules, and external sources such as environmental fluctuations. The main purpose of this thesis is to study how fluctuations propagate in biological systems.

First, we focus on how a signaling molecule called a ligand searches for and binds to its target (receptor). There exist membrane proteins that can bind to the ligand molecule and localize it near receptors, affecting the association between it and the receptor. Our analysis shows that although the membrane protein can concentrate the ligand molecule near the receptor surface, the membrane protein has to pass the localized ligand molecule to the receptor fast enough, in order to enhance signaling. Otherwise, the membrane protein inhibits signaling. Moreover, we also study the effect of localization on signal specificity. In particular, we discuss how the membrane proteins bind to ligand molecules and distribute them to different downstream signaling pathways.

Upon ligand binding to receptors, bound receptors can initiate the downstream network, which may finally lead to gene expression. We then study how the noise from the initiation step of transcription propagates in the elongation step. Elongation can be interrupted by the pauses of the transcription complex on the DNA sequence. We give a condition under which the pause of the transcription complex can cause bursts of mRNA production.

Finally, we use stochastic simulations to study dorsal-ventral patterning in *Drosophila* numerically. Our results indicate that a feedback loop can stabilize the determination of the amnioserosa boundary. We then propose a detailed single cell system for the downstream network in nuclei. Our analysis of time scales of reactions and molecular transport shows the phosphorylation of Mad and transport of mRNA across the nuclear membrane are the major limiting steps in the signal transduction pathway. Simulations results show noises are amplified at these limiting steps.

Contents

List of Tables

List of Figures

Chapter 1

Introduction

Randomness is inherent in biological reaction systems: "At each instant, the exact sequence of reactions that fires is a matter of chance [7]." Certain biochemical systems can start with the same input but produce different outputs with a probability density. In gene regulatory networks, stochasticity can come from the transcription and translation levels. The fluctuations can lead to phenotypically distinct groups within genetically identical cells [8]. For example, in the λ phage evolution process, the fluctuations in the degradation of the λ repressor can cause the switch between the two stable points in the bistable steady-state concentration of the λ repressor [9]. This switch may lead to the *lysis/lysogeny* switch of the λ phage.

Noise arises from two kinds of sources in a biochemical system: external noise and internal noise. External noise comes from environmental fluctuations, which results in the random variation of the control parameters, such as the rate of a reaction. On the other hand, internal noise originates from the small number of reactant molecules. A small number of molecules imply a small number of reaction occurrences, since the probability of a particular reaction occurrence in a time interval is proportional to the product of the number of reactant molecules [10]. As a result, the microscopic event that governs which reaction happens and in what order is stochastic.

In this thesis, different kinds of stochastic models and simulations are used to explore how noise propagates along diffusion-reaction networks and affects gene expression in cells. Chapter 1 provides the essential background. In Chapter 2, deterministic and

stochastic models are formulated and analyzed to study how a signaling molecule diffuses and searches for its signal targets. The role of different localization mechanisms of signaling molecules has been discussed. The signaling molecule binding to its signal targets can promote or inhibit transcription. Chapter 3 focuses on fluctuations in transcription processes. In particular, how noise propagates along the initiation and elongation steps of transcription has been analyzed by stochastic differential equations and master equations. In Chapter 4, the reliability of Dorsal surface patterning in early *Drosophila* is examined by stochastic simulations, with the objective to understand how the system responds to noise.

1.1 Biochemical systems

1.1.1 Diffusion

In a spatially inhomogeneous system, molecules can spread from a region of a higher concentration to one of a lower concentration by random motion. The process, in which the molecules intermingle as a result of random motion, is called diffusion. Mathematical theories of diffusion are based on the hypothesis that the spread rate of the diffusant through unit area of a section is proportional to the concentration gradient measured normal to the section [11]. Let $u(x,t)$ be the concentration of the diffusant at location x at time t and F be the transfer rate. Then

$$F = -D\nabla u(x,t) \tag{1.1}$$

where D is the proportionality constant and ∇ is the differential operator acting on the space coordinates. D is called the diffusion coefficient and depends on the temperature, the solution viscosity, and the molecular weight. Following Eq. (1.1), the governing equation for the temporal evolution of u is:

$$\frac{\partial u(x,t)}{\partial t} = \nabla[D\nabla u(x,t)].$$

Brownian motion is often used to describe the motion of a molecule. In particular, assume there is only one kind of molecule in an infinitely large biochemical system and the diffusion coefficient is constant. Then the probability density function of the

location of a tagged molecule at time t is the following normal distribution

$$x(t) \sim \frac{1}{\sqrt{4D\pi(t-t_0)}} e^{-\frac{(x-x_0)^2}{4D(t-t_0)}},$$

where x_0 is the location of the molecule at time t_0.

1.1.2 Chemoreception

Chemoreception is a process by which a living organism senses an external stimulus and it is one specific kind of bimolecular reaction. In chemoreception, a ligand molecule has to bind to another molecule whose motion is restricted in some region of the system. Chemoreception has three sequential stages: detection, amplification and signaling [12].

In the detection stage, a ligand molecule binds to a receptor protein on the surface of the organism, causing a change in the receptor protein. The reaction is as follows:

$$R + P \underset{k_-}{\overset{k_+}{\rightleftharpoons}} RP, \tag{1.2}$$

where P is the binding ligand and R is the receptor protein. In the amplification stage, the organism transforms the change in the receptor into biochemical signals through the reaction networks inside the organism. Then in the signaling stage, a biological response is triggered by the amplified signal [12].

Chemoreception is commonly observed in the biological world. One example can be seen in the dorsal surface pattern formation process discussed later. Dpp/Scw binds to the receptor on the embryo surface, which phosphorylates Mad and initiates the downstream network to determine cell fates. Another common example is chemotaxis, where a cell determines the concentration gradient of the binding ligand by sensing the difference in receptor occupation across its body. Then it may move towards the direction of higher concentrations.

1.1.3 Morphogens

A morphogen is a substance that governs the pattern of tissue development in a concentration-dependent manner. The morphogen secreted from a local source spreads across the developing tissue and forms a concentration gradient that determines cell fates differentially. To regulate cellular responses, morphogens can be transcription factors to control gene expression, or can be ligand molecules that bind to receptors on cell surfaces.

1.2 Mathematical models

1.2.1 Stochastic background

Let $X(t) = (X_1(t), X_2(t), \ldots, X_M(t))$ be a time-dependent random variable vector for a stochastic process. $X(t)$ is a Markov process, if for all $t_1 \geqslant \tau_1 \geqslant \tau_2 \cdots \geqslant \tau_k$,

$$p(x(t_1), t_1 | x(\tau_1), \tau_1, x(\tau_2), \tau_2 \ldots, x(\tau_{k_2}), \tau_k) \quad = \quad p(x(t_1), t_1 | x(\tau_1), \tau_1)$$

where $x(t)$ is an M-component vector and $p(x(t_1), t_1 | x(\tau_1), \tau_1, x(\tau_2), \tau_2, \ldots, x(\tau_k), \tau_k)$ is the conditional probability density function that $X(t_1) = x(t_1)$ given $X(\tau_1) = x(\tau_1), X(\tau_2) = x(\tau_2), \ldots, X(\tau_k) = x(\tau_k)$ [13].

The Chapman-Kolmogorov equation

If $X(t)$ is a Markov process and has a probability density function $p(x(t), t)$, then $p(x(t), t)$ obeys the Chapman-Kolmogorov equation:

$$p(x(t_1), t_1 | x(t_3), t_3) = \int dx(t_2) p(x(t_1), t_1 | x(t_2), t_2) p(x(t_2), t_2 | x(t_3), t_3),$$

where $x(t_1)$, $x(t_2)$ and $x(t_3)$ are $X(t)$ at time t_1, t_2 and t_3, respectively. If $p(x(t), t)$ satisfies the following conditions:
for all $\varepsilon > 0$

1. $\lim\limits_{\Delta t \to 0} p(x, t + \Delta t | y, t)/\Delta t = W(x \mid y, t)$ uniformly in x,y and t for $\mid x - y \mid \geqslant \varepsilon$;
2. $\lim\limits_{\Delta t \to 0} \dfrac{1}{\Delta t} \displaystyle\int_{|x-y|<\varepsilon} (x_i - y_i) p(x, t + \Delta t | y, t) dx = A_i(y, t) + O(\varepsilon)$ uniformly in y, ε and t;
3. $\lim\limits_{\Delta t \to 0} \dfrac{1}{\Delta t} \displaystyle\int_{|x-y|<\varepsilon} (x_i - y_i)(x_j - y_j) p(x, t + \Delta t | y, t) dx = B_{ij}(y, t) + O(\varepsilon)$ uniformly in y, ε and t,

where $x = (x_1, x_2, \ldots, x_M)$ and $y = (y_1, y_2, \ldots, y_M)$, then the differential-integral Chapman-Kolmogorov equation can be derived as

$$\partial_t p(x, t | y, t') \quad = \quad -\sum_i \frac{\partial}{\partial x_i} [A_i(x, t) p(x, t | y, t')]$$

$$+\sum_{i,j}\frac{1}{2}\frac{\partial^2}{\partial x_i \partial x_j}[B_{ij}(x,t)p(x,t|y,t^{'})]$$
$$+\int dz[W(x|z,t)p(z,t|y,t^{'})-W(z|x,t)p(x,t|y,t^{'})]$$

for x and y in the region of X. The details of the derivation can be found in [14].

The Fokker-Planck equation

If $W(x|z,t)=0$, the differential-integral Chapman-Kolmogorov equation becomes the Fokker-Planck equation:

$$\partial_t p(x,t|y,t^{'})=-\sum_i \frac{\partial}{\partial x_i}[A_i(x,t)p(x,t|y,t^{'})]+\sum_{i,j}\frac{1}{2}\frac{\partial^2}{\partial x_i \partial x_j}[B_{ij}(x,t)p(x,t|y,t^{'})]. \quad (1.3)$$

Since $W(x|z,t)=\lim_{\Delta t\to 0} p(x,t+\Delta t|z,t)/\Delta t=0$, the probability that the final position x is finitely different from z goes to zero faster than Δt. Hence the path of $X(t)$ is necessarily continuous under this condition [14].

The Langevin equation

Given that $\widetilde{X}(0)$ has a probability density $p(x,0)$, the solution $\widetilde{X}(t)$ of the following stochastic differential equation has a probability density function satisfying the Fokker-Planck equation (1.3) [13]:

$$d\widetilde{X}(t)=\mu(\widetilde{X}(t),t)dt+\sigma(\widetilde{X}(t),t)d\widetilde{W}(t),$$

where $\widetilde{W}(t)$ is a standard M-dimensional Brownian motion, and $\mu(x,t)$ and $\sigma(x,t)$ satisfy these two conditions: $\mu_i(x,t)=A_i(x,t)$, $B_{ij}(x,t)=\sum_k \sigma_{ik}(x,t)\sigma^T_{kj}(x,t)$.

The Langevin equation and the Fokker-Planck equation can be used to describe the motions of individual molecules in a biological system [13]. Moreover, although the number of molecules is not continuous, it is shown in [15] and [16] that the Langevin equation can still be applicable to approximate the evolution of the number of molecules in a biological network when the number of molecules is large enough.

The Master equation

If $A_i(z,t) = B_{ij}(z,t) = 0$, then the differential-integral Chapman-Kolmogorov equation will become the Master equation

$$\partial_t p(x,t \mid y,t^{'}) = \int dz[W(x \mid z,t)p(z,t \mid y,t^{'}) - W(z \mid x,t)p(x,t \mid y,t^{'})].$$

For example, if $X(t)$ is integer valued, then $A_i(z,t) = B_{ij}(z,t) = 0$, and we have the master equation

$$\partial_t p(n,t \mid n^{'},t^{'}) = \Sigma_m[W(n \mid m,t)p(m,t \mid n^{'},t^{'}) - W(m \mid n,t)p(n,t \mid n^{'},t^{'})]. \quad (1.4)$$

In a biological system, we can let $X(t)$ be a state vector representing the number of molecules of species. Then $X(t)$ is integer valued and the above master equation can be used to study the temporal evolution of the system.

1.2.2 Stochastic models of a reaction network

Suppose there are M species in a biological system that undergo r reactions and denote the jth reaction as follows

$$\upsilon_{1j}^{reac}M_1 + \upsilon_{2j}^{reac}M_2 + \ldots, + \upsilon_{Mj}^{reac}M_M \longrightarrow \upsilon_{1j}^{prod}M_1 + \upsilon_{2j}^{prod}M_2 + \ldots, + \upsilon_{Mj}^{prod}M_M, \quad (1.5)$$

where M_i is the ith species and υ_{ij}^{reac} (υ_{ij}^{prod}) represents the number of molecules of the ith species consumed (produced) in the j reaction. In the stochastic model, $\alpha_j^V(x,t)$ is defined in [17] and [18] so that the chance of the jth reaction occurrence in $(t, t+\Delta t)$ is taken to be

$$V\alpha_j^V(x,t)\Delta t = \mu_j V[\prod_{i=1}^{M}(V^{\upsilon_{ij}^{reac}})^{-1}\frac{X_i(t)!}{\upsilon_{ij}^{reac}!(X_i(t)-\upsilon_{ij}^{reac})!}]\Delta t,$$

where $X(t) = (X_1(t), X_2(t), \ldots, X_M(t))$ is the vector representing the numbers of the molecules of each species, V is the volume of the system, and $\mu_j\Delta t$ is the probability that a particular combination of reactant molecules with integral coefficients υ_{ij}^{reac} will take the jth reaction in time interval Δt in a system of volume 1.

Let $p(x,t)$ be the probability function that $X(t) = x$ at time t. Then the governing equation for $p(x,t)$ can be written as follows:

$$\frac{dp(x,t)}{dt} = \sum_{y \in S_p(x)} V\alpha_{j_{y,x}}^V(y,t) - \sum_{y \in S_s(x)} V\alpha_{j_{x,y}}^V(x,t), \quad (1.6)$$

where $S_p(x)$ is the set of the system states from which the system can reach state x after one reaction step, $S_s(x)$ is the set of the system states which the system can reach from state x after one reaction step, and $j_{y,x}$ specifies the reaction that happens to change the system state from y to x.

1.2.3 Deterministic models of a reaction network

The deterministic model, described in [19], expresses the instantaneous change of the concentration of each species in terms of the concentrations of all species. Let c_i be the concentration of the ith species. Then the deterministic equation for the reaction network (1.5) can be written as

$$\frac{dc_i}{dt} = -\sum_{j=1}^{j=r} \upsilon_{ij}^{reac} R_j(c) + \sum_{j=1}^{j=r} \upsilon_{ij}^{prod} R_j(c), \quad c(0) = c_0 \tag{1.7}$$

where $c = (c_1, c_2, \ldots, c_M)$ and R_j is a function of c that describes the rate of reaction j. According to the mass action rate law, the rate function for reaction j is

$$R_j(c) = k_j \prod_{i=1}^{i=M} (c_i)^{\upsilon_{ij}^{reac}},$$

where k_j is the reaction constant determined by the temperature, the pressure and the volume of the system.

1.2.4 The relation between deterministic and stochastic models

In the deterministic model, each reaction happens with certainty at the concentration-dependent rate and the concentration of each species can be uniquely determined by Eq. (1.7). As a result, the system is deterministic and there are no fluctuations. On the other hand, the stochastic model takes the randomness of reactions into account and includes the resulting fluctuation in the number of the molecules of each species.

To make the deterministic model and the stochastic model consistent, there is a relationship between μ_j and k_j [18]:

$$k_j = \frac{\mu_j}{\prod_{i=1}^{M} \upsilon_{ij}^{reac}!}. \tag{1.8}$$

Based on Eq. (1.8), in [17] Kurtz proves that,
if $\lim_{V\to\infty} V^{-1}X(0) = c_0$, then for any finite t and $\epsilon > 0$,

$$\lim_{V\to\infty} P\{sup_{s\leq t} \mid V^{-1}X(s) - c(s, c_0) \mid > \epsilon\} = 0,$$

where $c(s, c_0)$ is the solution to Eq. (1.7) and $X(t)$ represents the number of the molecules with the probability function satisfying Eq. (1.6).

The condition $\lim_{V\to\infty} V^{-1}X(0) = c_0$ implies that if the number of the molecules is big enough to make X/V meaningful as V becomes large, then the solution to the deterministic model will be close to the solution to the stochastic model.

If the system only consists of first-order reactions, then Eq. (1.7) and Eq. (1.6) will be linear; otherwise, they will contain nonlinear terms and be difficult to handle. Moreover, in an open system, the number of molecules of species can range from zero to infinity. Then there will be infinite states of the system, which leads to an infinite number of equations for $p(x, t)$. Then the stochastic model can be very complicated to analyze.

1.3 The Gillespie algorithm for diffusion-reaction systems

1.3.1 Reaction systems

If the evolution of a reaction system is a Markov process, the Gillespie simulation method derived in [20] is commonly used. In [10], Erban et al. explain the Gillespie method clearly using the following system:

1. $A + A \xrightarrow{k_1} \Phi$,
2. $A + B \xrightarrow{k_2} \Phi$,
3. $\Phi \xrightarrow{k_3} A$,
4. $\Phi \xrightarrow{k_4} B$

where Φ denotes the species they are not interested in, and k_1, k_2, k_3 and k_4 are the reaction rate constants. Let $a(t)$ and $b(t)$ be the numbers of molecules of species A and

B at time t. As shown in [21], the probability for each reaction occurrence between $[t, t+dt)$ are

$$a(t)(a(t)-1)k_1dt/(2V), \quad a(t)b(t)k_2dt/V, \quad k_3dt, \quad k_4dt,$$

where V is the volume of the system and $a(t)(a(t)-1)k_1/(2V)$, $a(t)b(t)k_2/V$, k_3 and k_4 are called the propensity functions of reactions. In the Gillespie simulation method, the waiting time for each reaction to happen is assumed to be exponentially distributed. The propensity function is the control parameter of the exponential distribution. In particular, given a molecules of species A and b molecules of species B at time t, let $\alpha^i(a,b)$ be the propensity function of reaction i. Then in [20] it is shown that the probability that the first occurrence of the ith reaction after time t is in $[t+\tau, t+\tau+d\tau)$ is

$$p(\tau, i \mid a, b, t)d\tau = \alpha^i(a,b)e^{-\alpha^i(a,b)\tau}d\tau. \tag{1.9}$$

Assume that only one reaction can happen every time. Then the next reaction time τ after time t has the following probability density function:

$$p(\tau \mid a, b, t) = \sum_{i=1}^{4} \alpha^i e^{-(\sum_{i=1}^{i=4}\alpha^i)\tau}. \tag{1.10}$$

The probability that the jth reaction is the first reaction happening in $[t+\tau, t+\tau+d\tau)$ is

$$\frac{\alpha^j}{\sum_{i=1}^{4}\alpha^i}$$

Using $p(\tau, i \mid a, b, t)$ and $p(\tau \mid a, b, t)$ in Eq. (1.9) and (1.10), the reaction processes can be simulated by the Gillespie method :

1. At time $t = 0$, set initial numbers of molecules of species A and B as $a(0)$ and $b(0)$ respectively.
2. Calculate α^i and $\alpha = \sum_{i=1}^{i=4}\alpha^i$.
3. Generate two random numbers r_1 and r_2 uniformly distributed in $[0,1]$.
4. Compute the next reaction time τ with the following formula

$$\tau = \frac{1}{\alpha} ln[\frac{1}{r_1}].$$

5. Find j such that
$$\frac{1}{\alpha}\sum_{i=1}^{j-1}\alpha^i \leqslant r_2 < \frac{1}{\alpha}\sum_{i=1}^{i=j}\alpha^i.$$
Let the jth reaction happen and update the numbers of molecules A and B after the reaction.

6. Add τ to t and repeat the above calculations from step 2.

The reaction probability during a time interval only depends on the product of the numbers of the molecules of each reactant species. So each molecule of a reactant species has the same chance to react. However, the reactant molecules that are close have a large chance to react, while the reactant molecules that are far away from each other would have a small chance to react. Therefore, if the species in the system are not uniformly distributed, the Gillespie method is not directly applicable and must be modified.

1.3.2 Diffusion-reaction systems

If the biochemical system in Section 1.3.1 is not well-mixed, to incorporate the spatial factor in simulation, the whole domain of the system can be discretized into small compartments and each compartment can be treated as being well-mixed approximately. The same species in different compartments can be treated as different species to differentiate the molecules in different locations. Only molecules in the same compartment can react with each other. For example, assume the whole domain of the system is $[0, L]$ with reflecting boundaries. Then the domain can be discretized into M intervals with equal length :
$$\{[0, h), [h, 2h), \cdots, [(M-1)h, L]\},$$
where $h = L/M$. The molecules of species A in the ith interval is denoted as A_i and B_i is similarly defined. The whole diffusion and reaction processes can be converted into pure reaction processes consisting of the following reactions:
$$A_1 \underset{d_a}{\overset{d_a}{\rightleftharpoons}} A_2 \underset{d_a}{\overset{d_a}{\rightleftharpoons}} A_3 \cdots \underset{d_a}{\overset{d_a}{\rightleftharpoons}} A_M,$$
$$B_1 \underset{d_b}{\overset{d_b}{\rightleftharpoons}} B_2 \underset{d_b}{\overset{d_b}{\rightleftharpoons}} B_3 \cdots \underset{d_b}{\overset{d_b}{\rightleftharpoons}} B_M,$$

$$A_i + A_i \xrightarrow{k_1} \Phi, A_i + B_i \xrightarrow{k_2} \Phi, \Phi \xrightarrow{k_3} A_i,$$
$$\Phi \xrightarrow{k_4} B_i, i = 1, 2, \cdots, M,$$

where $d_a = \frac{D_a}{h^2}$, $d_b = \frac{D_b}{h^2}$, and D_a and D_b are diffusion constants of species A and B. The propensity functions for reactions in the ith $(1 < i < M)$ compartment are

$$a_i * d_a, \quad a_i * d_a, \quad b_i * d_a, \quad b_i * d_a, \quad a_i * (a_i - 1) * k1/(2V_i), \quad a_i * b_i * k1/V_i, k_3,$$

where V_i is the volume of the ith compartment. For the first and Mth compartments, one $a_i * d_a$ and one $b_i * d_a$ is removed due to the reflective boundaries. Then the Gillespie method can be applied.

Appropriate discretization is very essential for the application of the Gillespie method to spatially inhomogeneous systems. Discretization has to be fine enough to ensure each compartment can be treated as being well-mixed approximately. However, it has been shown the master equations for a system with two reactant molecules will approach a model of two independently diffusing molecules as the compartment size approaches zero [22]. Moreover, if the compartment size is too small, the simulation will spend most of time on tracking the diffusion of molecules among compartments. As a result, computation will be time-consuming. Therefore, choosing the right criterion for discretization is important. In [23], we have suggested the minimal compartment size so that the solution to the deterministic model of the species concentrations in the compartment approaches a spatially uniform solution exponentially at the steady state.

1.4 The early development of *Drosophila* embryo

All our analysis and computations have been to applied to dorsal surface patterning in the early development of *Drosophila* embryo. Here we introduce the basic background and previous results in these areas. *Drosophila melanogaster* is one of the most interesting subjects in biological studies, as its small size, short life time and large number of offspring make it ideal for research. In addition, the completed *Drosophila* genome project has provided a huge amount of genetic information. *Drosophila melanogaster* has been a powerful model for genetic, developmental biology and biochemistry studies. Studies have shown that the gradients of species concentrations are established during

the early development of *Drosophila* [2, 4, 24, 25]. Here we introduce the spatial pattern establishment briefly.

1.4.1 Oogenesis

During early oogenesis, a developing oocyte is placed in an egg chamber covered by a thin fluid-filled shell called the perivitelline (PV) space. The PV space is surrounded by the follicular support cells. The structure of the egg chamber is shown in Fig. 1.1, where the egg chamber is approximately a prolate ellipsoid. A coordinate system is defined as the Anterior-Posterior (AP) axis in the lateral direction and the Dorsal-Ventral (DV) axis in the vertical direction. The gradients of species concentrations are established along these axis's in the early development of *Drosophila* [2, 4, 24, 25].

In the oocyte, Gurken, a signaling molecule, is produced in the dorsal-anterior cortex of the oocyte. Gurken can be transported to the oocyte surface, where it binds to Torpedo, the *Drosophila* homologue of the Epidermal Growth Factor (EGF) receptor on the surrounding follicle cells. The localized production of *Gurken* and extracellular transportation establish a graded distribution of Gurken, which leads to a graded activation of Torpedo along the DV axis. As a result, a DV polarity is formed [24].

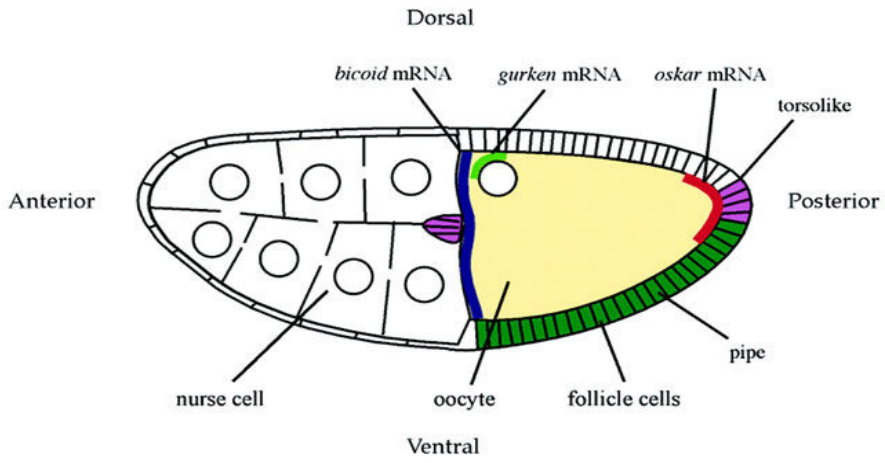

Figure 1.1: The structure of an egg chamber [1].

1.4.2 DV pattern formation

After fertilization, the egg is laid and embryogenesis begins. The whole process is divided into 17 stages. Nuclear division happens in the first five stages, which are divided into 14 division cycles based on the number of nuclei. From the fifth division cycle on, the nuclei begin to spread. By the end of the eighth division cycle, the nuclei are distributed evenly in the embryo [26]. In the tenth division cycle, the nuclei migrate to the embryo surface. In the 13th division cycle, the nuclei perform the last cleavage division, and in the 14th division cycle, the cell membrane begins to invaginate, partitioning the nuclei into individual cells. After cellularization, gastrulation begins.

In addition to nuclear division, the concentration gradients of species form in the first five stages. The AP and DV polarities will be inherited from follicle cells. The key maternal gene for the DV axis maintenance is the Toll receptor. It is uniformly distributed around the embryo surface. Toll is the receptor for Spätzle, which is activated and proteolytically processed at the ventral side of the PV space. Spätzle-bound Toll receptors initiate a cascade that causes Cactus to degrade. Dorsal, a transcription factor, is bound to Cactus and Cactus/Dorsal is distributed throughout the embryo. The removal of Cactus frees Dorsal and allows Dorsal to enter the nuclei around the embryo surface [27, 28]. Consequently, the Dorsal nuclear gradient shown in Fig. 1.2 is formed. The concentration gradient of Dorsal is shallow in the ventral region and quite steep in the lateral region. It becomes shallow again in the descending dorsal region (DR). The graded downstream gene expressions established by the gradient of Dorsal concentration divides the whole PV space into three domains along the DV axis. They are the Mesoderm (M), Neurogenic Ectoderm (NE) and Dorsal Region (DR). The DR is also denoted as Dorsal Ectoderm(DE).

Once in the nuclei, Dorsal initiates the transcription of target genes in a concentration-dependent manner. Two of the earliest genes activated by the high and intermediate Dorsal levels in the M and the NE are Twist and Snail. Dorsal binds to DNA as a homodimer and enhances Twist transcription. Fig. 1.3 shows that Twist expression is sharper than the Dorsal gradient. This may be explained by the cooperative interaction between Dorsal dimers. Dorsal dimer, strongly enhanced by Twist, can initiate Snail transcription. The cooperation between Dorsal and Twist gives a significantly sharper expression of Snail in the lateral region. The high concentration of Snail specifies the

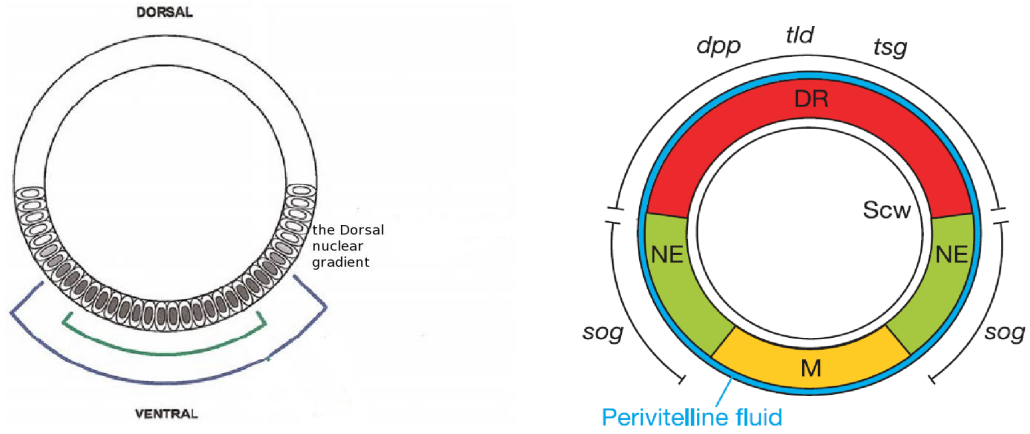

Figure 1.2: The gradient of Dorsal concentration [2] and the division of the whole PV space [3] .

M region in the ventral most side and the steep gradient of Snail concentration defines the boundary between the M and the NE [2].

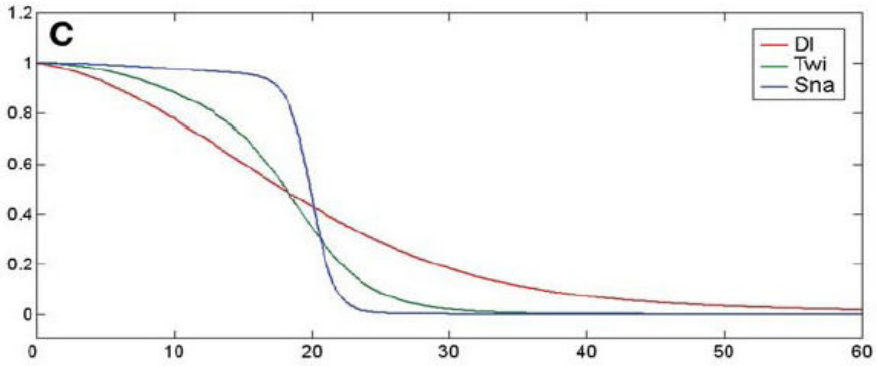

Figure 1.3: The normalized result of gene expressions from experiments [4].

The next target genes are sim, rho and sog. Dorsal, Twist, Snail and another transcription factor "Suppressor of Hairless (SuH)" cooperate to produce a one cell wide expression of sim at the boundary of the M [4]. Twist and Dorsal work together to initiate sim transcription, while Snail acts as a repressor. The one cell wide expression of sim at the boundary of M can be explained by the sharp decrease of Snail concentration there. However, the absence of sim expression outside of the M can only be

explained by the role of SuH. Hence, SuH is essential for the one cell wide expression of sim. Rho is expressed in the ventral most 8-10 nuclei of the NE. Dorsal, Twist and Daughterless/Scute heterodimers promote rho transcription, while Snail is a repressor of rho expression [2]. Another important gene sog is regulated by Dorsal. It has four binding sites for Dorsal in its enhancer region. It is expressed almost over the entire NE region [2].

In the DR, where the concentration of Dorsal is low, the gene repressed by Dorsal such as decapentaplegic (dpp) and tolloid (tld) are expressed [29]. Dpp has many low affinity binding sites for Dorsal, while tld has only two binding sites for Dorsal [29].

1.4.3 Subdivision of the DR

After the early patterning along the DV axis, Bone Morphogenetic Proteins (BMP) Decapentaplegic (Dpp) and Screw (Scw) begin to interact with other proteins in the PV space, which leads to a high concentration of the heterodimer Dpp/Scw around the dorsal midline (DM). The heterodimers bind to receptors and the bound receptors phosphorylate the intracellular transcription factors Mad to pMad. As a result, the level of pMad is higher around the DM than the level in other areas. The area with the highest pMad signaling specifies the amnioserosa, while the remaining area in the DR becomes dorsal epidermis [5].

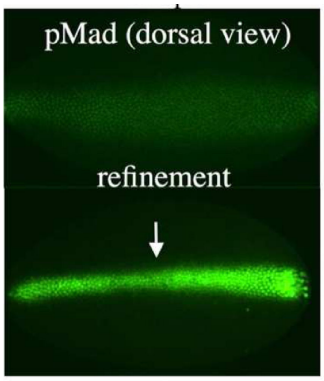

Figure 1.4: Signal contraction.

The determination of the aminoserosa boundary involves signal contraction. Initially

Dpp levels are moderate throughout the dorsal ectoderm, and pMad is broadly distributed. Later pMad begins to concentrate at the dorsal midline. Wang and Ferguson have proposed a feedback loop that could account for the contraction and intensification of signaling [30]. Umulis et al. use deterministic models to study the pattern formation process in detail and demonstrate the feedback loop for the signal contraction around the DM [5]. Umulis et al. identify the following reactant species that are involved in the signal contraction process:

1. Dpp: it is expressed in the DR. Two Dpp molecules can form a homodimer, but most of Dpp binds to Scw to form heterodimers Dpp/Scw.

2. Scw: it is distributed all throughout the PV space. Two Scw molecules can form a homodimer, but most of Scw binds to Dpp to form heterodimers Dpp/Scw.

3. Twisted gastrulation (Tsg): it is expressed in the DR. It can bind to Sog to form Sog/Tsg, which can transport Dpp/Scw to the DM.

4. Sog: it is expressed in the neighboring NE.

5. Tld: it is also expressed in the DR. It can cut Sog from Sog/Tsg/Dpp/Scw and then free Dpp/Scw can bind to receptors.

6. Thickveins (Tkv): it is a TGF-β type I receptor and Dpp can bind to it.

7. Saxaphone (Sax): it is a TGF-β type I receptor and Scw can bind to it.

8. Punt: it is a TGF-β type II receptor. BMP-bound Punt can phosphorylate the type I receptor. Genetic analysis shows that the signal must be integrated downstream of multiple receptors. In addition, it has been found that Dpp/Scw binds to Tkv and then Dpp/Scw/Tkv recruits Sax [31]. For simplicity, it is assumed that Tkv, Sax and Punt always bind together as a single unit (R). Moreover, it is uniformly distributed all throughout the PV space. If a receptor R is bound by a Dpp/Scw, we denote it by BR.

9. Surface-bound BMP binding protein (SBP): it is a potent protein which leads to the future contraction of pMad signaling around the DM. SBP has a high binding affinity for both BMP and R. BMP can bind to SBP easily and BMP/SBP bind

to R easily. Then the release of SBP leaves BMP bound to R. The enhanced signaling cascade can lead to more generation of SBP in the downstream network, which becomes a feedback loop.

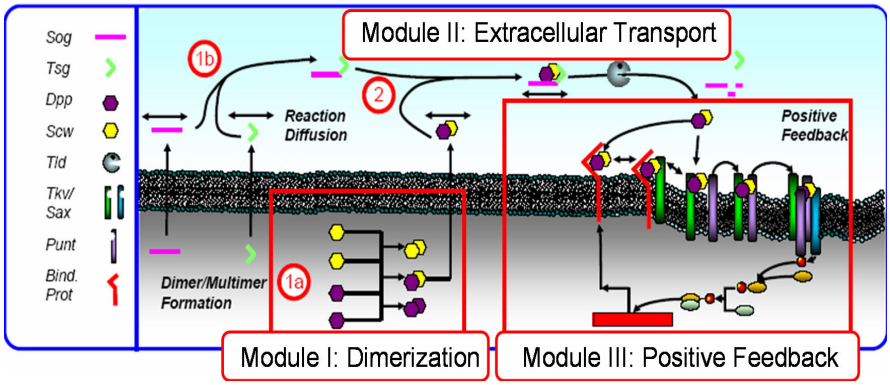

Figure 1.5: The reaction network for the DR pattern formation [5].

Fig. 1.5 shows the whole reaction network. Dpp and Scw form heterodimers and homodimers within the DR, while Tsg and Sog form heterodimers around the boundary between the NE and the DR. Then Dpp/Scw binds to Sog/Tsg between the NE and the DR, which prevents Dpp/Scw from binding to receptors and forms a flux of Dpp/Scw/Sog/Tsg towards the DM. Sog in Dpp/Scw/Sog/Tsg is cleaved off by Tld in the DR, which frees Dpp/Scw to bind to receptors. Dpp/Scw can either bind to receptors R or SBP. If Dpp/Scw binds to R to become BR, BR can either phosphorylate mad or release Dpp/Scw in the PV space. If Dpp/Scw binds to SBP, Dpp/Scw/SBP can bind to R and Dpp/Scw/SBP/R can release SBP. The pMad expression can lead to the generation of SBP in the downstream network.

1.4.4 Deterministic model

In [5], Umulis et al. construct a deterministic model based on the reaction network shown in Fig. 1.5. They study the concentration of each species along the Dorsal-Ventral line. Here we introduce their deterministic model briefly as a background for our study in the following sections. For their model, they make several assumptions :

1. The total number of receptors R on the surface remains constant.

2. All non-surface-associated species diffuse.

3. The initial amount of all species is zero except receptor R and Tld.

4. Intracellular reactions are at quasi-equilibrium.

In addition to their assumptions, we make some simplification of their models without losing the main features of the signal here. Although two Dpp molecules can form a homodimer in the PV space, experiments show that signals through the homodimers are much less intense than the heterodimer. Therefore, we only focus on signaling through heterodimers. Since the production of Dpp and Scw is steady at the beginning of the DR pattern formation process, for simplicity we assume that the production of heterodimer Dpp/Scw is steady all through the surface pattern formation process. Moreover, the analysis from Umulis et al. shows that SBP may undergo degradation and endocytosis and the signal contracts fastest when SBP only undergoes endocytosis [5]. Therefore, we assume that SBP only undergoes endocytosis. Then as suggested in [5], Dpp/Scw is not involved in extracellular degradation as well.

Then, denoting each species by the simple symbols,

Species	Sog	Tsg	Tld	Sog/Tsg	Dpp/Scw	Dpp/Scw/Sog/Tsg	R	SBP
Symbol	S	T	Tol	I	B	IB	R	C

the reactions involved in the pattern formation process are as follows:

1. $\emptyset \xrightarrow{s(x)} B$

2. $\emptyset \xrightarrow{\phi_S} S$

3. $S \xrightarrow{\delta_S} \emptyset$

4. $\emptyset \xrightarrow{\phi_T} T$

5. $T \xrightarrow{\delta_T} \emptyset$

6. $S + T \underset{k_{-2}}{\overset{k_2}{\rightleftharpoons}} I$

7. $I + B \underset{k_{-3}}{\overset{k_3}{\rightleftharpoons}} IB$

8. $IB \xrightarrow{Told} B + T$
9. $B + C \underset{k_{-4}}{\overset{k_4}{\rightleftharpoons}} BC$
10. $B + R \underset{k_{-5}}{\overset{k_5}{\rightleftharpoons}} BR$
11. $BC + R \underset{k_{-6}}{\overset{k_6}{\rightleftharpoons}} BCR$
12. $BR + C \underset{k_{-7}}{\overset{k_7}{\rightleftharpoons}} BCR$
13. $BR \xrightarrow{f_{BR}} C$
14. $BR \xrightarrow{\delta_e} \emptyset$
15. $BCR \xrightarrow{\delta_e} \emptyset$
16. $BC \xrightarrow{\delta_e} \emptyset$.

All reaction rates can be found in [5], except that $s(x)$ is the production rate of heterodimer Dpp/Scw. As suggested from [5] $s(x)$ is $1nMmin^{-1}$ in the DR and zero anywhere else. $f_{BR} = \frac{\Lambda \bullet [BR]^\nu}{K_{h1}^\nu + [BR]^\nu}$ is the production rate of C by the feedback loop.

Therefore, the governing equations for the concentration of each species become

1. $\frac{\partial [B]}{\partial t} = D_B \frac{\partial^2 [B]}{\partial x^2} + s(x) - k_3[I][B] + k_{-3}[IB] + \lambda[Tol][IB] - k_4[B][C] + k_{-4}[BC] - k_5[B][R] + k_{-5}[BR]$
2. $\frac{\partial [S]}{\partial t} = D_S \frac{\partial^2 S}{\partial x^2} + \phi_S - k_2[S][T] + k_{-2}[I] - \delta_S[S]$
3. $\frac{\partial [T]}{\partial t} = D_T \frac{\partial^2 [T]}{\partial x^2} + \phi_T - k_2[S][T] + k_{-2}[I] + \lambda[Tol][IB] - \delta_T[T]$
4. $\frac{\partial [I]}{\partial t} = D_I \frac{\partial^2 [I]}{\partial x^2} + k_2[S][T] - k_{-2}[I] - k_3[I][B] + k_{-3}[IB]$
5. $\frac{\partial [IB]}{\partial t} = D_{IB} \frac{\partial^2 [IB]}{\partial x^2} + k_3[I][B] - k_{-3}[IB] - \lambda[Tol][IB]$
6. $\frac{\partial [C]}{\partial t} = \frac{\Lambda \bullet [BR]^\nu}{K_{h1}^\nu + [BR]^\nu} - k_4[B][C] + k_{-4}[BC] - k_7[BR][C] + k_{-7}[BCR] - \delta_E[C]$
7. $\frac{\partial [BC]}{\partial t} = k_4[B][C] - k_{-4}[BC] - k_6[BC][R] + k_{-6}[BCR] - \delta_E[BC]$
8. $\frac{\partial [BCR]}{\partial t} = k_7[BR][C] - k_{-7}[BCR] - k_6[BC][R] + k_{-6}[BCR] - \delta_E[BCR]$

9. $\frac{\partial[BR]}{\partial t} = k_5[B][R] - k_{-5}[BR] + k_{-7}[BCR] - k_7[BR][C] - \delta_E[BR]$

and $[R_{tot}] = [R] + [BR] + [BCR]$. Here [*] means the concentration of that species.

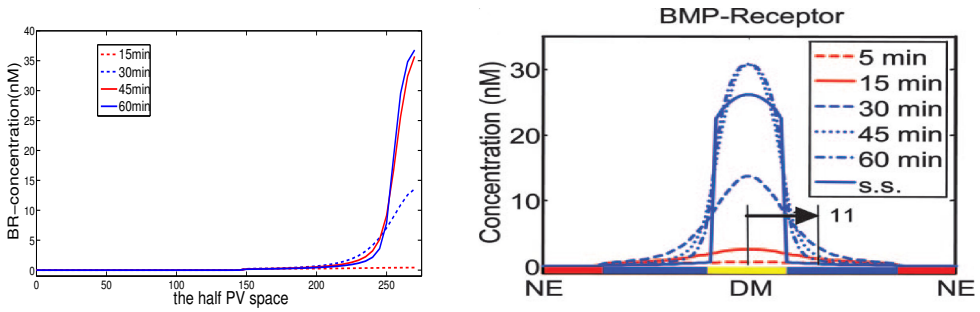

Figure 1.6: The temporal evolution of the BR concentration.

By symmetry, we only consider a half of the PV space, which is from the DM to the ventral midline. The temporal evolution of the concentration of BR along the DV axis is shown in Fig. 1.6. The left figure in Fig. 1.6 shows the concentration of BR calculated from the above equations. In the left figure, the DM is at x=275, and the ventral midline is at x=0. The right figure is from [5] and it shows the concentration of BR between the two NE's.

The nonlinear property of the governing equations yields bistability, which explains the sharp increase of the signal around the DM in Fig. 1.6. As shown in Fig. 1.7, if the concentration of B is low, the BR concentration remains below the red dashed line; once the concentration exceeds Point 1, the BR concentration reaches the upper branch. Once on the upper branch, the BR concentration stays on the upper branch, until the B concentration drops below Point 2. Therefore, the concentration of B at Point 1 identifies the threshold of the high signal in the pattern formation process. Moreover, the threshold of the high signal gives the aminoserosa boundary. Fig. 1.6 demonstrates that the position of the threshold is around $x = 250\mu m$.

1.4.5 Motivation

Here we examine the number of signaling molecules involved in the process of boundary determination. We consider the numbers of BR and B molecules in a slice of the half PV space. We choose the width of the slice to be $5\mu m$. Since the PV space is a shell of height

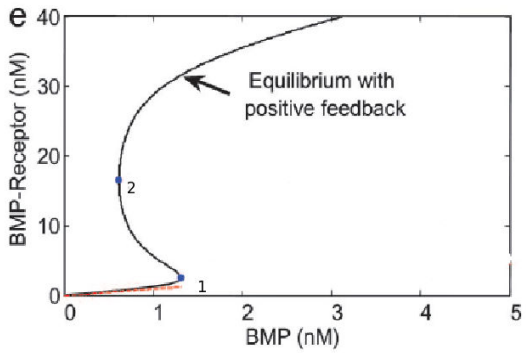

Figure 1.7: The steady response of BR to the level of B [5].

$0.5\mu m$, the slice can be approximated as a cuboid of dimension $5\mu m \times 0.5\mu m \times 275\mu m$ as shown in Fig. 1.8 from Radek Erban. The whole slice is divided into 55 sub-cuboids of length $5\mu m$ and each species in each sub-cuboid is assumed to be well-mixed. The compartment adjacent to the ventral midline is labeled with 1 and the number increases towards the dorsal midline. The diameters of the nuclei in nuclear cycles 10-14 are $10\mu m, 9.2\mu m, 8.2\mu m$ and $6.5\mu m$ respectively [32]. The dimensions of the slice are chosen to describe the change of the signal level within an individual nucleus. Using the concentrations of species from the deterministic model, we calculate the number of molecules in different compartments. Fig. 1.9 shows the numbers of the BR molecules and the B molecules at 60 minutes, which is the end of the pattern formation process.

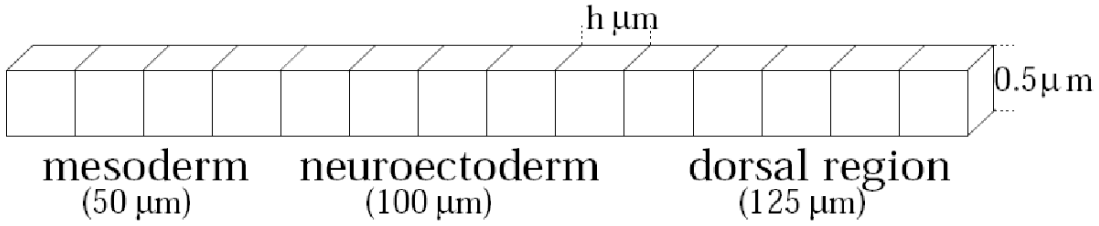

Figure 1.8: The discretized structure of a slice of the half PV space.

However, as shown in Fig. 1.9, the number of the B molecules is less than 10 in every compartment and the number of the BR molecules is less than 25 in most compartments except several compartments around the DM. As a result, the small

numbers of these species requires a model at the molecular level. Individual reaction is inherently stochastic, which may cause fluctuations in the dynamics of the pattern formation process [7, 19]. Noise can play a pivotal role in a biological process. It can make biological systems choose different outcomes even with the same input [7, 8, 9].

However, embryonic development has a remarkable property of being extremely reliable and reproducible despite fluctuations in the environment surrounding the embryo, noise in genome expression, and variations in the compositions of the proteome. Despite these complications, for *Drosophila*, the survival rate of embryos hatching to larvae is nearly 80-90% in a laboratory setting [33, 34]. How nuclei handle the stochastic and spatially inhomogeneous signal and choose their fates reliably has not been fully understood.

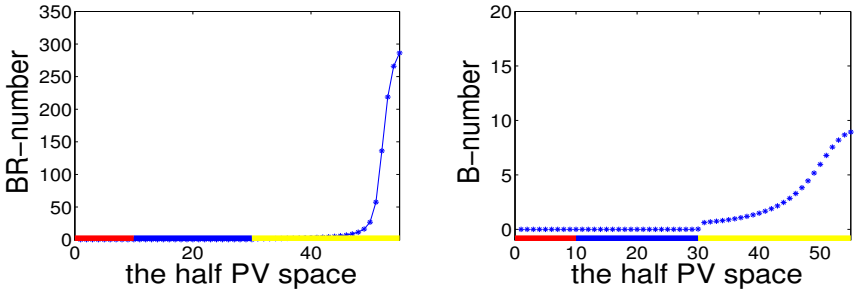

Figure 1.9: The numbers of BR and B molecules in each compartment at 60 minutes.

Chapter 2

Ligand signaling in a complex medium

2.1 Introduction

2.1.1 Biological background

Most signal transduction processes involve the proper binding of signaling molecules to cell-surface receptors to form a signaling complex, which triggers downstream intracellular reactions to achieve appropriate cellular responses such as cell differentiation, proliferation, death and so on. Upon stimulation, protein kinases, phosphatases and other players located near the bound receptors get activated and transfer the signal to downstream species. For example, morphogens, which are secreted from a local source and distributed in a spatially non-uniform pattern, can bind to the receptors on the extracellular membrane and determine the cell fate in a concentration-dependent manner. Since morphogen patterning is a dynamic process, the position and the timing of the bound receptors on the cell membrane determine whether the response of cells to the stimulus is appropriate.

The number of signaling molecules is usually small. For example, in cell culture the dynamic range for Bone Morphogenetic Protein (BMP) signaling is $10^{-10} - 10^{-9}$ M, which equals 10-100 BMP molecules for each nucleus at the cell differentiation stage of early *Drosophila*. This small number of BMP molecules may lead to large fluctuations

in the downstream network. Then how does the biological system interpret such a weak input accurately and place the boundary between cells of different types reliably? There are many kinds of signal transducing auxiliary proteins that can bind to multiple members of a signaling pathway, localize them to specific areas of the cell, and concentrate the signal in a small region. For example, heparan sulfate in the brain extracellular matrix can bind to humane lactoferrin (Lf) and slow Lf diffusion, which may attenuate the spread of diffusible signals in brain extracellular space [35].

Moreover, the localization of signaling molecules can increase the encounter chance between reactants and potentially facilitate the formation of the signaling complex. For example, on the extracellular membrane, coreceptors serve to bind to signaling molecules first and orient them in the right way to improve their affinities to receptors. One example is the vertebrate TGFβ coreceptor TGFβR3, which binds to BMP and acts as a coreceptor [36]. In the intracellular downstream reaction networks, scaffold proteins can bring all signaling molecules together and form multimolecular complexes that can respond rapidly to the incoming signal. For example, in the mitogen-activated protein kinase (MAPK) cascade, where MAPK is activated by the phosphorylation at amino acids by MAPKK and MAPKK is activated by the phosphorylation at amino acids by MAPKKK, the assumption that the scaffold protein binds to all these three species increases the sensitivity of the MAPK activation to the incoming signal [37].

Furthermore, the localization of signaling molecules can protect the signaling molecules from degradation or deactivation, thereby maintaining the signal and attenuating the fluctuations. For example, mathematical simulation shows that in the MAPK pathway with a high level of phosphatases, scaffold protein can reduce the probability for kinases to get deactivated by phosphatases and increase the time for kinases to activate downstream target genes [38].

However, the localization can also inhibit signaling under certain conditions. On the extracellular membrane, there exists some proteins that can localize signaling molecules on the membrane and block the signaling molecules from receptors. As a result, once the signaling molecule binds to the protein, the signaling molecule can only bind to the receptors after it is detached from the protein. Therefore, the protein slows the movement of the signaling molecule approaching to the receptors and may inhibit signaling. The trade-off between promoting signaling by concentrating signaling molecules

around the receptors and inhibiting signaling by slowing down the movement of the signaling molecules towards the receptors has to be considered carefully. Moreover, coreceptors can also inhibit signaling in a similar way. At an appropriate level, they can help receptors recruit signaling molecules by localizing molecules around receptors and promoting the association between receptors and signaling molecules. However, when the level of the coreceptor is high, they will compete with receptors for signaling molecules and form non-functional complexes, thereby blocking signaling molecules from receptors. Therefore, the effect of coreceptor is biphasic. One example is Cv-2 in the pupal wing of *Drosophila*, which binds to BMP and acts as a coreceptor. As the concentration of Cv-2 increases, BMP signaling first increases and then decreases [36]. Furthermore, Levchenko et al. have shown the biphasic effect of scaffold proteins on signaling and discovered that there exists the optimal concentration of scaffold protein for the maximal amplitude of the signal [37].

By promoting certain reactions and inhibiting others, the localization of signaling molecules can govern the selection of signaling pathways and regulate signal output. For example, scaffold proteins determine the specificity of Rho GTPase-signaling [39]. Upon Rho activation, Rho can induce the polymerization of actin into stress fibers and cause the enhanced expression from the c-fos serum-response element (SRE). At the same time, Rho can control the activity of the c-Jun N-terminal kinase (JNK) and regulate the expression of $c-jun$ in an independent pathway. It has been found that the scaffold protein hCNK1 links Rho and Rho guanine-nucleotide-exchange factors to JNK and limits stress-fiber formation, leading to the preferential activation of JNK and the regulation of $c-jun$ expression.

From the macroscopic perspective, the localization of signaling molecules regulates the temporal and spatial evolution of signaling. By limiting the movement of signaling molecules and promoting the association between receptors and signaling molecules, localization can concentrate the signal within certain regions and accelerate the temporal evolution of signaling. For example, a coreceptor called surface-bound protein (SBP) helps concentrate the signal and accelerate the signaling process in Dorsal surface patterning in *Drosophila*. Wang and Ferguson have suggested a feedback step, in which SBP is produced in proportion to the level of BMP-bound receptors and helps receptors recruit BMPs as a coreceptor in the high signaling region, in order to explain signal

contraction in dorsal-ventral patterning in *Drosophila* [30]. Moreover, the stochastic simulations in Chapter 4 show that the signal transduction process evolves faster with SBP than without SBP. In addition, since the localization can protect signaling molecules from degradation, and the localizing species carry the signaling molecules during their transport process, the localization can also spread the signal and slow the signal transduction process. In the wing disc epithelium of *Drosophila*, the localization of the morphogen Wingless (Wg) may contribute to the long-range signal. Wg can be localized within cells by associating with heparin sulfate proteoglypcans on small labeled vesicles (called argosome in [40]). Argosomes are secreted by cells and can be trafficked among cells by transcytosis consisting of iterative internalizations and externalizations. Once internalized, Wg can undergo degradation via the lysosome or get recycled to a different place in the extracellular environment via the externalization of argosomes. As a result, the temporal and spatial evolution of the Wg signal is mediated by recycling and intracellular degradation. The long-range signal may result from fast recycling or slow intracellular degradation. Similarly, the localization of Dpp by the receptor Thickvein in an endocytic compartment can spread the Dpp signal [41, 42].

The effect of the localization of signaling molecules on signaling depends on many factors. These factors can be divided into two groups according to the following two aspects: 1) the rate for the signaling molecule to become localized; and 2) the rate for the localized molecule to form a signaling complex.

The localization rate depends on the capture region of the localizing species and the affinity of the signaling molecules for the localizing molecules. Since the localizing species can only affect the signal around them, the distributions of the localizing molecules and the signaling molecules are very important. The distribution of the signaling molecules results from an interplay of various reaction-diffusion processes, such as the production process of the signaling species, the transport process of the signaling species and the endocytosis process of the signaling species and so on.

The rate for the localized molecule to form a signaling complex can range from zero to infinity. Consider the association between signaling molecules and receptors as an example. If the localized signaling molecules can only bind to the receptors after they are released by localizing molecules, the effect of localization on signaling depends on how long the signaling molecules can be held by localizing molecules and how fast the

signaling molecules can reach the receptors . If the localized signaling molecule can be passed to the receptors directly, the transfer rate is important to determine the effect of localization. If the transfer rate is higher than the association rate between free signaling molecules and the receptors, localization may promote signaling. Otherwise, the localized signaling molecules are partially blocked from the receptors and the signaling may be inhibited by localization.

2.1.2 Previous work

One widely-studied example of the localization of signaling molecules is a two-step process involving dimensionality reduction in ligand diffusion. In the first step, the ligand molecules perform three-dimensional diffusion until they reach the cell membrane. Upon hitting the cell membrane, the ligand molecules get attached to the cell membrane. Then in the second step, the ligand molecules perform two-dimensional diffusion over the cell membrane until they bind to receptors or detach from the cell membrane. Such non-specific binding to the cell membrane localizes the ligand molecules around the receptors, which can promote or inhibit the association between receptors and ligand molecules. To understand the effect of dimensionality reduction on signaling, the two-step process has been compared with the one-step process, in which the ligand molecules reach the receptors by three-dimensional diffusion.

Adam and Delbrück suggested that for signaling efficiency and timing, the ligand molecules may use the two-step diffusion process to reach receptors instead of using the one-step process [43]. They compared the first passage times for the ligand molecule to reach a receptor through the one-step process and through the two-step diffusion process. They assumed that a spherical receptor of radius a is located in the center of a large sphere of radius b and a ligand molecule is initially uniformly distributed between the large sphere and the receptor. Define $\tau^{(3)}$ as the mean time for the ligand molecule to reach the receptor by three-dimensional diffusion in the large sphere. Define $\tau^{(3,2)}$ as the mean time for the ligand molecule to reach the receptor through the two-step process, in which the ligand first reaches the equatorial plane of the large sphere by three-dimensional diffusion and then performs two-dimensional diffusion on the equatorial plane to reach the receptor. Define $D^{(3)}$ and $D^{(2)}$ as the three- and two-dimensional

diffusion coefficients, respectively. They found the ratio of τ^3 and $\tau^{(3,2)}$ as follows:

$$\frac{\tau^{(3,2)}}{\tau^{(3)}} = \left\{ \frac{1}{3}\frac{D^{(2)}}{D^{(3)}} \left[y_1 \left(\frac{b}{a} \right) \right]^2 \frac{b}{a} \left(1 - \frac{a}{b} \right)^2 \right\}^{-1} \tag{2.1}$$

where $y_1\left(\frac{b}{a}\right)$ represents the dependence of y_1 on $\frac{b}{a}$. $y = y_1$ is the root of

$$J_0\left(\frac{a}{b}y\right) Y_1(y) - Y_0\left(\frac{a}{b}y\right) J_1(y) \quad = \quad 0$$

where $J_n(y)$ and $Y_n(y)$ are Bessel functions of order n. When $\frac{D^{(2)}}{D^{(3)}} > 10^{-2}$, $\frac{\tau^{(3,2)}}{\tau^{(3)}} < 1$ requires $\frac{b}{a} > 10^3$. Then Adam and Delbrück claimed that $\frac{b}{a} > 10^3$ is in the range of bacterial systems and hence dimensionality reduction in the two-step process can promote the association between ligand molecules and receptors. In biological systems, the average cell radius is $10\,\mu m$ and average receptor radius is $5\,nm$, which gives $\frac{b}{a} \approx 2 \times 10^3$ [44]. Therefore, their result implies that location of ligand molecules by dimensionality reduction can promote signaling.

Berg and Purcell studied the effect of dimensionality reduction on signaling in a cell with multiple receptors on the cell membrane by comparing the ligand currents to all the receptors from ligand molecules using the one-step process and using the two-step process [45]. They assumed that the cell is a sphere of radius a and N circular receptors of radius s are uniformly distributed on the cell membrane. They also assumed that the receptors are perfectly absorbing, i.e., any ligand molecule that touches a receptor is captured immediately by the receptor and is transported into the cell. Define J and J' as the average current of ligand molecules to all the receptors through the one-step process and the two-step process, respectively. Define D and D' as the diffusion coefficients of the ligand molecules for the three-dimensional diffusion in the solution and for the two-dimensional diffusion on the cell membrane, respectively. To derive J', they considered the mean time, $\bar{t_c}$, for the membrane-attached ligand molecules to get absorbed by receptors. They approximated $\bar{t_c}$ as

$$\bar{t_c} \quad \cong \quad \frac{a^2}{ND'} \ln(\frac{a^2}{Ns^2}).$$

Moreover, they looked at the mean number of the ligand molecules attached to the cell membrane, $\bar{m}$. Assuming that the ligand concentration is in equilibrium and the ligand

concentration in the solution is c_∞, they approximated $\bar{m}$ as

$$\bar{m} \cong 4\pi a^2 d c_\infty \exp\left(\frac{E_A}{kT}\right)$$

where d is the height of the layer of the membrane-attached ligand molecules, E_A is the energy of adsorption, and kT is the energy of thermal fluctuation. They then computed J' as follows:

$$J' = \frac{\bar{m}}{\bar{t}_c}. \tag{2.2}$$

For J, they assumed that each receptor is independent of each other and can absorb ligand molecules as a single disk. Then they got J as

$$J = 4NDsc_\infty. \tag{2.3}$$

They derived the following condition in order that $J' > J$:

$$\left(\frac{\pi d}{s}\right)\left(\frac{D'}{D}\right)\exp\left(\frac{E_A}{kT}\right) > \ln\left(\frac{a^2}{Ns^2}\right)$$

The receptors are assumed to be independent in the calculation of J, which implies that the number of receptors has to be small. When the number of receptors is not small, Berg and Purcell claimed that the two-step process may be not necessary for efficient collections of ligand molecules by a cell. Moreover, they proposed that $\bar{t}_c$, which measures the difficulty for the membrane-attached ligand molecule to reach receptors on the cell membrane, is essential for the effect of dimensionality reduction on signaling. Their discussion about $\bar{t}_c$ is consistent with our discussion about the rate at which the localized signaling molecules are passed to receptors. They assumed that c_∞ is constant in their calculation. However, the actual concentration of the ligand in the medium is not uniform but graded, since the receptors on the cell surface are assumed to perfectly absorb the ligand molecules.

In [46], Wiegel and Delisi also compared the currents to receptors on the cell membrane from ligand molecules using the one-step process and the two-step process. All of their settings are exactly the same as the settings of Berg and Purcell except the following assumption: the ligand molecules bind to the receptors using both processes. Define $c_\infty(r)$ as the steady-state concentration of the ligand at a distance r from the

center of the cell. They took J and J' very similar to the ones in Eq. (2.2) and (2.3) except that they replace c_∞ by $c_\infty(a)$ and ND' in Eq. (2.3)) is replaced by $a^2\alpha$ where α is the mean collision rate between a membrane-attached ligand molecule and receptors. After that, they claimed that the following condition has to be satisfied to make $J' > J$:

$$3 \times 10^{-7} N < \frac{D' K^*}{D} < 10^{-3}, \tag{2.4}$$

where K^* is the overall nonspecific affinity. They calculated the number of ligand molecules per unit concentration in the layer of membrane-attached ligand molecules, and then estimated K^* is in the range of $[10, 10^2]$. They then obtained $N < 3000$ per cell and $\frac{D'}{D} < 10^{-4}$ using inequality Eq. (2.4) . Moreover, they found that the reduction of dimensionality has little effect on enhancement of signal unless the number of free receptors per cell is reduced to 100. However, following from [44], cells can exhibit a few receptor types (about $10-40$) with high numbers (about 10^5 per cell), or a lot of receptor types (about $2000-30000$) with small numbers (about 10^2 per cell). Therefore, in case there are about 10^5 receptors in the cell, the small number of free receptors indicates over 99% receptor occupancy for most eukaryotes, which is usually not true. Hence, they concluded that the reduction of dimensionality is of little effect on signaling.

In addition to the association between ligand molecules and receptors on the cell membrane, it is suggested that dimensionality reduction is involved in target site localization of gene regulatory proteins on DNA [47, 48]. Proteins exhibit appreciable affinities for functional specific sites and nonfunctional nonspecific sites on DNA sequences, making dimension reduction possible in the search process of target sites. Furthermore, the reactions between proteins and DNA occur several-magnitude-faster than the diffusion-limited rates. Therefore, to explain the rapid reactions, it is commonly assumed that target site location occurs via two steps: one-dimensional motion along a DNA segment and three-dimensional excursion in the solution. The optimum search strategy has been suggested by using the minimal mean search time as the criterion [48].

All the above previous work assumes receptors are perfectly absorbing or studies how proteins search for the target site on DNA. They all focus on the time for signaling molecules to first encounter their targets. None of them consider the case that the signaling molecule in the proximity region of receptors diffuses away before binding to

any receptors. When the signaling molecule is close enough to bind to the receptors, the reaction rate between the signaling molecule and receptors is called the intrinsic reaction rate. If the intrinsic reaction rate is small, then the signaling molecule starting close enough to receptors can diffuse away before binding to any receptors.

Kholodenko et al. considered the role of localization of signaling molecules in reaction-limited signal transduction pathways [49]. In the reaction-limited reactions, the intrinsic reaction rate is much slower than the first-encounter rate, which is the inverse of the time for the signaling molecule to reach its target. As a result, only a small fraction of collisions leads to association reactions that can last long enough to transfer signal into downstream networks. Therefore, Kholodenko et al. asserted that the effect of localization on the first-encounter rate can be neglected, and they considered the effect of localization on the number of signaling complexes formed by signaling molecules and their target proteins at the steady state. They first considered the system in which only the target proteins are anchored in a layer around the cell membrane. Define A as the total number of the signaling molecules in the cytoplasm, T as the number of membrane-associated target proteins, and AT as the total number of the signaling complex. Define V_m and V_c as the volume of the layer and the cytosol volume of the cell, respectively. Using the law of mass action, Kholodenko et al. wrote the dissociation constant, K_d for the binding reaction to form a signaling complex as follows:

$$K_d \equiv \frac{\left(\frac{A}{V_c}\right) \cdot \left(\frac{T}{V_m}\right)}{\left(\frac{AT}{V_m}\right)} = \left(\frac{1}{V_c}\right) \cdot \left(\frac{A \cdot T}{AT}\right). \tag{2.5}$$

Then they claimed that K_d does not depend on V_m and localization of only the target proteins does not affect the number of signaling complexes. After calculation of Eq. (2.5)), they then considered another system in which the signaling molecules and their target proteins are both anchored in the layer and only anchored signaling molecules can bind to the target proteins. Define RAT as the total number of the signaling complexes formed by the anchored signaling molecules and their target proteins. Assuming the number of molecules that can anchor signaling molecules in the layer is in excess, Kholodenko et al. obtained the dissociation constants for the formation of the signaling

complex as follows

$$K_d^{app} \equiv \frac{\left(\frac{A}{V_c}\right) \cdot \left(\frac{T}{V_m}\right)}{\left(\frac{RAT}{V_m}\right)} = K_d \cdot \left(\frac{V_m}{Vc}\right) \cdot (1+\alpha)\,, \tag{2.6}$$

where α is a dimensionless factor. α was claimed to be less than one. Therefore, they insisted that $K_d^{app} < K_d$ and localization can increase the number of signaling complexes. In the calculation of Eq. (2.5))and (2.6)), the concentration of the signaling species was assumed to be spatially uniform. However, the concentration of the signaling species within the layer is different from the one outside the layer. Similarly, the dissociation constant K_d is different for binding reactions within/outside the layer. As a result, the dependence of K_d on the layer may lead to the dependence of AT on the layer. Moreover, it was assumed the dissociation constant for the binding between anchored signaling molecules and targets proteins is the same as K_d in the calculation of Eq. (2.6). Since the localization of signaling molecules can change the orientation of the signaling molecules and thereby change the association rate, the assumption is not appropriate.

Wofsy and Goldstein considered a system with a binding layer around the cell membrane [50], in which receptors are located and ligand diffusion is slowed. Wofsy and Goldstein quantified the effect of the binding layer by estimating the effective association and dissociation rate coefficients for binding between the ligands and the receptors. Their effective rate coefficients were used to approximate the system with the binding layer by a model with surface binding but without a binding layer. Define R_{tot} as the total number of receptors in the binding layer. Define k_+ as the transport-limited forward rate for the ligand to bind to the surface as the concentration of the receptors goes to infinity to make the surface perfectly absorbing. Define k_a as the intrinsic association rate between ligands and receptors. Define γ as the ratio of the height of the binding layer to the mean path for the ligand molecule to travel within the layer before binding to any receptor. Then they derived a formula for the effective association rate between ligands and receptors, k_a^e, as follows:

$$k_a^e = \frac{T(\gamma)}{1 + T(\gamma) k_a R_{tot}/k_+} k_a \tag{2.7}$$

where $T(\gamma) \equiv \frac{\tanh(\gamma)}{\gamma}$ is a decreasing function of γ and approaches to one as γ goes to zero. Therefore, Wofsy and Goldstein claimed that when $\gamma \equiv \sqrt{\frac{k_a R_{tot} d}{A \Phi D_i}} \ll 1$, the

binding layer can be neglected and the binding reaction can be modeled as the one on the surface. Since $T(\gamma) < 1$ for $\gamma > 0$, $T(\gamma)$ plays a role as a reduction factor on k_a and the binding layer slows the effective association rate. In the system of Wofsy and Goldstein, the concentration of the ligand approaches to its maximal level far away from the binding layer and decreases towards the binding layer. If the ligand is produced around the binding layer, the effect of the binding layer on k_a^e is different from the one in the system of Wofsy and Goldstein, as we will discuss in this chapter.

In addition to the above work on the formation of the signaling complexes, there exists work on the effect of localization on the spatial and temporal evolution of signaling from the macroscopic perspective. Bollenbach et al. studied how the localization of morphogens by transcytosis mediates morphogen transport and the formation of the concentration gradient of the morphogen [42]. They have formulated effective nonlinear transport equations for the total concentration of morphogens present in all forms, including the free morphogens, the receptor-bound morphogens in the extracellular space and in the intracellular space. They have derived how the effective transport and degradation rates depend on the total concentration of the morphogen. They also showed that morphogen gradients can be extremely robust to changes in the morphogen production rate if morphogen transport is dominated by transcytosis. However, they did not discuss how transcytosis affects the effective transport and degradation rates. As a result, the effect of transcytosis on the concentration gradient formation is not clear. Umulis (2009) discussed the temporal evolution of the concentration gradient of the ligand in a one-dimensional line with an input flux of ligands at one end of the line and a uniform level of receptors everywhere [51]. He gave conditions under which the system can achieve dynamical scale invariance, i.e., the concentration gradient of the ligand can keep the same proportion regardless of the size of the system during its transient approach to equilibrium. However, he did not consider the effect of localization. If receptors are only localized in some part of the system with adapter receptors nearby, can the conditions for the scale invariance of the system with uniformly distributed receptors still work? Apparently, there are some extra requirements for scale invariance. For example, the distributions of receptors and adapter receptors have to be spatially scale invariant.

Using different approaches and different settings of the systems, all the above previous work indicates that localization plays a diverse role in the signal transduction process. Their results can only apply to specific situations and some may even lead to contradictory conclusions about the effect of localization. Furthermore, the effect of localization on the temporal and spatial evolution of the signal is not clear.

2.1.3 Overview

In this chapter, our objective is to systematically explore localization mechanisms and gain a better understanding of how localization regulates signaling, from the temporal and spatial evolution of the signal at the macroscopic level to the motion of signaling molecules and the formation of signaling complexes at the microscopic level. To this end, we consider the system with ligands, receptors and membrane proteins, with the potential to be extended to other localization systems. Here membrane proteins are defined as any proteins that stay near the membrane and can bind to ligand molecules. We incorporate the important factors for localization in our deterministic and stochastic models of the system, including the distribution region of the membrane protein, the diffusion coefficient of the ligand, the on/off rate of binding reactions between the ligand and the membrane proteins, and the on/off rate of binding reaction between free/localized ligand molecules and receptors. We aim to examine how these factors interact with each other to determine the effect of localization on signaling.

To understand how localization adjusts the temporal and spatial scale of the evolution of the signal, we look the concentration of the ligand with spatially varying diffusion coefficients and degradation rates in the deterministic model in Section 2.2. To understand how localization affects the noise propagation along the signal pathway, we look at the stochastic motion of a single ligand molecule in Section 2.3. In Section 2.3.1 and Section 2.3.2, we add membrane proteins in the system and analyze the effect of localization on the distribution of the ligand molecule in a stochastic model. In Section 2.3.3, we first assume only the free ligand molecule can bind to receptors and receptors can catch the free ligand molecule once it touches receptors. With this assumption, we estimate the extent to which the localization by the membrane proteins can slow the association between the receptor and the ligand. Then we consider the case that when

the ligand molecule and receptors are close enough, they can react with a finite probability per unit time. We discuss under what conditions the localization can enhance or inhibit the association between ligands and receptors. At the end of Section 2.3.3, we analyze the effect of the membrane proteins on signal specificity.

2.2 Deterministic Model

In the section, we study how the localization of the ligand affects the temporal and spatial evolution of the extracellular signal by constructing deterministic diffusion-reaction models. Ligand diffusion is restricted by the membrane proteins around the cell membrane in the extracellular space. Once internalized, ligand can be transported via transcytosis, get recycled to the cell membrane or decay intracellularly. Therefore, the rate at which the ligand spreads around the cell membrane is different from the rate far away from the membrane. Moreover, due to recycling and different degradation mechanisms within/outside the cell, the decay rate of the ligand around the cell membrane is different from the decay rate far away from the cell membrane. Therefore, we can consider a two-layered system to differentiate the domain near the cell membrane and the domain far away.

Fig. 2.1 shows our general two-layered rectangular system, where the lower layer corresponds to the domain near the cell membrane and the upper layer corresponds to the domain far away. For the signaling in the lower layer, Bollenbach et al. have shown that the evolution of the total morphogen concentration can be described approximately by a diffusion-reaction equation with an effective diffusion coefficient and an effective degradation rate [42]. The effective diffusion coefficient and degradation rate are complicated functions of the system kinetics, the total morphogen concentration and the total receptor concentration. However, the effective diffusion coefficient and the effective degradation rate approach finite values in the limit of low morphogen level. As the signaling molecules are usually present in small numbers in signaling systems, we assume that the diffusion coefficient and the degradation rate for the ligand concentration are constants. In the upper layer, the ligand diffuses with a different diffusion coefficient and decays with a different degradation rate.

In Fig. 2.1, the input flux of the ligand on the $y = 0$ boundary corresponds to

cell secretion, while the input flux on the $x = 0$ face corresponds to the flux from the concentration gradient of the ligand. First assuming the ligand is uniformly distributed in the x- and z-directions in Section 2.2.1, we consider a one-dimensional system with the input flux in the y-direction and study the effect of localization on the time for the system to evolve to the steady state. Then assuming the ligand is uniformly distributed in the z-direction, we consider the two-dimensional system in the $x - y$ plane with the input flux in the x-direction to understand the effect of localization on the spatial pattern of the signal at the steady state.

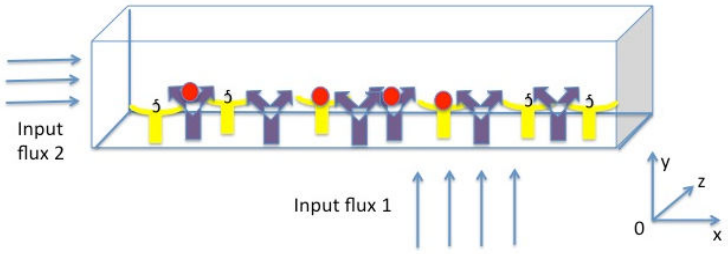

Figure 2.1: The schematic of a biological system with ligands binding to surface receptors

2.2.1 One-dimensional model

In this section we study the concentration of the ligand in the y-direction. We consider the one-dimensional system consisting of two layers with heights H_1 and H_2. In the lower layer, the ligand diffuses with diffusion constant D_1 and decays with rate k_1, while in the upper layer, the ligand diffuses with diffusion constant D_2 and decays with rate k_2. At $y = 0$, there is an input flux of the ligand j. At $y = H_1 + H_2$, the boundary is reflective. Here D_1 and k_1 are the effective diffusion coefficient and the effective degradation rate for the signal level around the cell membrane. In this section, we study the time for the ligand concentration to relax to the steady state given different D_1's and k_1's. Let $C(y,t)$ denote the concentration of the ligand at y at time t. We have the governing equations of $C(y,t)$ as follows:

$$\frac{\partial C(y,t)}{\partial t} = D_1 \frac{\partial^2 C(y,t)}{\partial y^2} - k_1 C(y,t) \quad \text{for } y \in [0, H_1) \tag{2.8a}$$

$$\frac{\partial C(y,t)}{\partial t} = D_2 \frac{\partial^2 C(y,t)}{\partial y^2} - k_2 C(y,t) \quad \text{for } y \in (H_1, H_1 + H_2] \tag{2.8b}$$

$$-D_1 \frac{\partial C(y,t)}{\partial y} = j \quad \text{at } y = 0 \tag{2.8c}$$

$$-D_2 \frac{\partial C(y,t)}{\partial y} = 0 \quad \text{at } y = H_1 + H_2 \tag{2.8d}$$

$$\lim_{y \to H_1^-} D_1 \frac{\partial C(y,t)}{\partial y} = \lim_{y \to H_1^+} D_2 \frac{\partial C(y,t)}{\partial y} \tag{2.8e}$$

$$\lim_{y \to H_1^-} C(y,t) = \lim_{y \to H_1^+} \Gamma C(y,t) \tag{2.8f}$$

$$C(y,0) = 0 \tag{2.8g}$$

where Γ is the partition coefficient that reflects the equilibrium partitioning between two different domains. We assume that there is no capacity or transport resistance at the interface, and set the equal flux at the boundary between two layers in Eq. (2.8e).

To simplify the system, we define the following dimensionless variables and coordinates as in [52]:

$$u \equiv \frac{C}{C_0}, \quad \eta \equiv \frac{y}{H_1 + H_2}, \quad \tau \equiv t \times k_1,$$

C_0 is a reference concentration of the ligand. To explore how the different reaction and diffusion time scales in the two layers affect each other and influence the temporal evolution of the whole system in Eq. (2.8), we define the scaled parameters as follows:

$$\theta \equiv \frac{k_1}{k_2}, \quad \delta \equiv \frac{D_1}{D_2}, \quad \epsilon \equiv \frac{H_1}{H_1 + H_2},$$
$$J \equiv \frac{j(H_1 + H_2)}{D_1}, \quad \Lambda \equiv \frac{D_1}{k_1 (H_1 + H_2)^2}.$$

We express the equations in Eq. (2.8) in terms of the scaled variables and parameters as follows:

$$\begin{aligned}
\frac{\partial u(\eta,\tau)}{\partial \tau} &= \Lambda \frac{\partial^2 u(\eta,\tau)}{\partial \eta^2} - u(\eta,\tau) \quad \text{when } \eta \in [0, \epsilon) \\
\frac{\partial u(\eta,\tau)}{\partial \tau} &= \frac{\Lambda}{\delta} \frac{\partial^2 u(\eta,\tau)}{\partial \eta^2} - \frac{1}{\theta} u(\eta,\tau) \quad \text{when } \eta \in (\epsilon, 1] \\
-\frac{\partial u(\eta,\tau)}{\partial \eta} &= J \quad \text{at } \eta = 0 \\
\frac{\partial u(\eta,\tau)}{\partial \eta} &= 0 \quad \text{at } \eta = 1
\end{aligned}$$

$$\begin{aligned} \lim_{\eta\to\epsilon^-} \frac{\partial u(\eta,\tau)}{\partial \eta} &= \lim_{\eta\to\epsilon^+} \frac{1}{\delta}\frac{\partial u(\eta,\tau)}{\partial \eta} \\ \lim_{\eta\to\epsilon-} u(\eta,\tau) &= \lim_{\eta\to\epsilon^+} \Gamma u(\eta,\tau) \\ u(\eta,0) &= 0. \end{aligned} \tag{2.9}$$

For the transient evolution of $u(\eta,\tau)$, we compute the Laplace transform of $u(\eta,\tau)$ with respect to τ and obtain the following results:

1. for $\eta \in [0,\epsilon)$

$$\begin{aligned} & \mathcal{L}[u](\eta,s) \\ = \; & \frac{J\sqrt{\Lambda}\cosh\left((1-\frac{\eta}{\epsilon})\beta\sqrt{s+1}\right)}{\sqrt{s+1}} \\ \times \; & \frac{\left\{\Gamma\sqrt{\delta(s+1)}\cosh\left(\alpha\sqrt{s+\frac{1}{\theta}}\right)-\sqrt{(s+\frac{1}{\theta})}\sinh\left(\alpha\sqrt{s+\frac{1}{\theta}}\right)\tanh\left((1-\frac{\eta}{\epsilon})\beta\sqrt{s+1}\right)\right\}}{s\left\{\Gamma\sqrt{\delta(s+1)}\cosh(\alpha\sqrt{s+\frac{1}{\theta}})\sinh(\beta\sqrt{s+1})+\sqrt{(s+\frac{1}{\theta})}\sinh(\alpha\sqrt{s+\frac{1}{\theta}})\cosh(\beta\sqrt{s+1})\right\}} \end{aligned} \tag{2.10}$$

2. for $\eta \in (\epsilon,1]$

$$\begin{aligned} & \mathcal{L}[u](\eta,s) \\ = \; & \frac{J\sqrt{\delta}\sqrt{\Lambda}\cosh\left(\frac{(1-\eta)\alpha\sqrt{s+\frac{1}{\theta}}}{1-\epsilon}\right)}{s\left\{\Gamma\sqrt{\delta}\sqrt{s+1}\cosh(\alpha\sqrt{s+\frac{1}{\theta}})\sinh(\beta\sqrt{s+1})+\sqrt{(s+\frac{1}{\theta})}\sinh(\alpha\sqrt{s+\frac{1}{\theta}})\cosh(\beta\sqrt{s+1})\right\}} \end{aligned} \tag{2.11}$$

Here $\alpha \equiv \sqrt{\frac{\delta(1-\epsilon)^2}{\Lambda}}$ and $\beta \equiv \sqrt{\frac{\epsilon^2}{\Lambda}}$. $u(\eta,\tau)$ can be obtained using the inverse Laplace transform. Due to different degradation mechanisms in the two layers, we can assume that $\theta \neq 1$. Then $\mathcal{L}[u](\eta,s)$ is a single-valued function of s with poles at $s=0$ and at s's satisfying the following equation:

$$\begin{aligned} & \Gamma\sqrt{\delta}\sqrt{s+1}\cosh\left(\alpha\sqrt{s+\frac{1}{\theta}}\right)\sinh\left(\beta\sqrt{s+1}\right) \\ + \; & \sqrt{\left(s+\frac{1}{\theta}\right)}\sinh\left(\alpha\sqrt{s+\frac{1}{\theta}}\right)\cosh\left(\beta\sqrt{s+1}\right)=0 \end{aligned} \tag{2.12}$$

To estimate the rate at which $u(\eta,\tau)$ relaxes to the steady state, we look at the smallest pole (in magnitude) of $\mathcal{L}[u](\eta,s)$. In our system, $\eta \ll 1$ and we assume that $\alpha \ll 1$ and $\beta \ll 1$. In fact, $\alpha \ll 1$ and $\beta \ll 1$ are true in many biological systems. One example is Dorsal-Ventral patterning in *Drosophila* embryo where BMP is the signaling

species and collagen is the extracellular matrix protein [53]. In *Drosophila* embryo, the height of the collagen layer is only $0.1\,\mu m$ [54], i.e., $\epsilon(H_1 + H_2) = 0.1\,\mu m$. To decide k_1 and k_2, we consider the following reactions which can lead to the degradation of BMP eventually: the degradation of BMPs, the association reaction between BMPs and receptors, and the association association between BMPs and collagens, which may result in the intracellular degradation. In [53], the reaction rate between BMP and collagen is only $3.9 \times 10^{-6}\, nM^{-1}\, sec^{-1}$. The concentration of collagen is much less than the maximal level of the collagen $3.5 \times 10^6\, nM$, which we estimate. The reaction rate between BMP and receptors is only $4 \times 10^{-4}\, nM^{-1}\, sec^{-1}$ and the maximal level of free receptor is $320\, nM$ [5]. The maximal degradation rate of free BMP is $3 \times 10^{-2}\, sec^{-1}$ [5]. Therefore, we get

$$\begin{aligned} k_1 &\ll \left((3.5 \times 10^6) \times (3.9 \times 10^{-6}) + (4 \times 10^{-4}) \times 320 + 3 \times 10^{-2}\right) sec^{-1} = 13.8\, sec^{-1} \\ k_2 &< 3 \times 10^{-2}\, sec^{-1}. \end{aligned}$$

From [5], $D_2 = 73\,\mu m^2\, sec^{-1}$. Thorne et al. show that the extracellular matrix protein heparan sulfate can slow Lf diffusion by 30% [35]. Therefore, we let $D_1 = 0.7 D_2$. Then we get

$$\beta = \sqrt{\frac{\epsilon^2 (H_1 + H_2)^2 k_1}{D_1}} \ll \sqrt{\frac{0.1^2 \times 13.8}{73 \times 0.7}} = 0.05 < 1. \tag{2.13}$$

Using the fact that the total height of the PV space is less than $1\,\mu m$, we get

$$\alpha = \sqrt{\frac{(1-\epsilon)^2 (H_1 + H_2)^2 k_1}{D_2}} \ll \sqrt{\frac{1^2 \times 13.8}{73}} = 0.43 < 1. \tag{2.14}$$

In Appendix 6.1.1, assuming $\alpha \ll 1$ and $\beta \ll 1$, we estimate the smallest nonzero real pole, $s_{\min}$, (in magnitude) of $\mathcal{L}[u](\eta, s)$ as follows:
For $\eta \in [\epsilon, 1)$,

$$s_{\min} \approx -1 + \frac{1 - \frac{1}{\theta}}{1 + \Gamma\rho} + \frac{\Gamma\rho^3 (1 - \frac{1}{\theta})^2}{3\Lambda(1+\rho)^2 (1 + \frac{\Gamma\rho^3}{\delta})(1 + \Gamma\rho)} \tag{2.15}$$

where $\rho \equiv \frac{\epsilon}{1-\epsilon}$.

When Γ goes to infinity in Eq. (2.15), $s_{\min}$ approaches to -1 in Eq. (2.15) and $u(\eta, \tau)$ approaches to zero for $\eta \geqslant \epsilon$ from Eq. (2.9). As a result, $u(\eta, \tau)$ can be considered as

a solution of a single-layered system with $\eta \in [0, \epsilon]$. Moreover, -1 becomes an essential singularity of $\mathcal{L}[u](\eta, s)$ in Eq. (2.10) as Γ goes to infinity. As a result, $s_{\min} = -1$ cannot be used to estimate the relaxation time of the system to the steady state. In fact, as Γ goes to infinity, the exact temporal solution for $\eta \in [0, \epsilon)$ is given as

$$u(\eta, \tau) = \frac{J\sqrt{\Lambda}\sinh\left(\beta(1-\frac{\eta}{\epsilon})\right)}{\cosh(\beta)} + \sum_{n=0}^{\infty} A_n e^{-\left[1+\Lambda\left(\frac{2n\pi+\pi}{2\epsilon}\right)^2\right]t}\cos\left(\frac{(2n\pi+\pi)\eta}{\epsilon}\right)$$

where $A_n = -\frac{J\sqrt{\Lambda}\left[4\beta e^{\beta}+(-1)^n(2n\pi+\pi)^2\right]}{2\cosh(\beta)[(2n\pi+\pi)^2+4\beta^2]}$. Therefore, the relaxation time depends on $1 + \Lambda\left(\frac{2n\pi+\pi}{2\epsilon}\right)^2$.

Similarly to Γ, when ρ (or ϵ) goes to zero, $s_{\min} = -\frac{1}{\theta}$ is an essential singularity of Eq. (2.11) and $u(\eta, \tau)$ can be considered as a solution of the one-layered system in $y \in [\epsilon, 1]$. The temporal solution of $u(\eta, \tau)$ for $\eta \in [\epsilon, 1]$ can be obtained in the same way as when Γ approaches to infinity. When $\theta = 1$, i.e., $k_1 = k_2$, $s_{\min} = -1$ is an essential singularity and cannot be used to estimate the relaxation time.

When $\mathcal{L}[u](\eta, s)$ does not have any essential singularity, i.e. $\theta \neq 1$, $\Gamma < \infty$, and $\eta \neq 0$, $s_{\min}$ can be used to estimate the relaxation time. In our system, $\epsilon \ll 1$ and this gives $\rho \ll 1$. Since $\rho \ll 1$, the relation between $s_{\min}$ and θ depends on the second term in the right side of Eq. (2.15), which is an increasing function of θ. Note that $\theta = \frac{k_1}{k_2}$ and $s_{\min}$ is the pole of the Laplace transform of u with respect to $\tau = k_1 t$. Therefore, fixing k_1 and increasing k_2 decreases $s_{\min}$ and the relaxation time, i.e, faster degradation in the upper layer leads to faster relaxation to the steady state. On the other hand, decreasing k_1 and fixing k_2 decreases s. As a result, $|s|$ increases due to the fact that $s < 0$, while $|sk_1|$ may not. Therefore, it is hard to tell how k_1 influences the relaxation time from Eq. (2.15). To understand the effect of k_1 on the steady state, we can normalize the time t by $\frac{1}{k_2}$, follow the above procedure to obtain $s_{\min}$, and analyze the effect of k_1 on $s_{\min}$ as we do for k_2 here.

Similar to θ, the relation between s and ρ (or ϵ) depends on the second term in the right side of Eq. (2.15). The effect of ρ (ϵ) on $s_{\min}$ depends on θ. When $\theta > 1$, s_{min} is approximately an decreasing function of ρ (or ϵ), i.e., the relaxation time is a decreasing function of ϵ when $k_2 < k_1$. Increasing ϵ enlarges the lower layer, where the ligand molecule decays faster than the upper layer. Therefore, the relaxation time may decrease due to the amplification of the fast degradation by increasing ϵ. Similarly, when

$\theta < 1$,i.e., $k_1 < k_2$, $s_{\min}$ is approximately an increasing function of ρ (or ϵ). Increasing ϵ enlarges the domain of the slow degradation, which may increase the relaxation time. In addition to degradation, changing ϵ also changes the domain for diffusion. However, the effect of diffusion on the relationship between ϵ and $s_{\min}$ is very small. This is due to the small effect of δ on $s_{\min}$, as we discuss below.

In Eq. (2.15), we substitute Λ by $\frac{\delta D_2}{k_1(H_1+H_2)^2}$, fix D_2 and change δ by changing D_1, in order to study the effect of δ on $s_{\min}$. We first assume that δ is independent of Γ, θ and ρ. Then $s_{\min}$ is a decreasing function of δ and the effect of δ on s_{min} is very small, since δ only appears in the third term on the right side of Eq. (2.15) and $\rho \ll 1$. However, δ and Γ may be related. For example, if we decrease D_1, the ligand molecule diffuses more slowly in the lower layer and It will take longer time for the ligand molecules to enter the upper layer on average. So decreasing D_1 can increase the concentration of the ligand in the lower layer and hence increase Γ. Therefore, δ and the partition coefficient Γ are related. The effect of the relation between δ and Γ on s_{min} will be discussed in the stochastic model in Section 2.3.

Since $\rho \ll 1$ in Eq. (2.15), the relationship between s_{min} and Γ also depends on the second term in the right side of Eq. (2.15). Therefore, the effect of Γ on s_{min} depends on θ in the same way as the effect of ρ on s_{min} does.

In Fig. 2.2, we plot how the solution of Eq. (2.12) depends on the scaled variables ϵ, δ, Γ, and θ, which gives the smallest pole in magnitude of $\mathcal{L}[u](\eta, s)$. The numerical solution is the value where the left side of Eq. (2.15) changes its sign, and the approximate solution is from Eq. (2.15). As we expect, the approximate solution in Eq. (2.15) gives a good estimation for the numerical solution, and the dependence of s_{min} on the scaled parameters in Fig. 2.2 is consistent with our previous analysis. Here all parameters used in Fig. 2.2 are given in Table 2.1, whose values are estimated based on Dorsal-Ventral patterning in *Drosophila* [5]. In each figure of Fig. 2.2, we change one of the parameters and fix the remaining parameters as given in Table 2.1. Fixing D_2 and k_2, we change D_1 and k_1 by changing δ and θ respectively. When $\theta = 1$, $\mathcal{L}[u](\eta, s)$ has an essential singularity. Therefore, we avoid $\theta = 1$ when calculating $s_{\min}$ in Fig. 2.2 -(a).

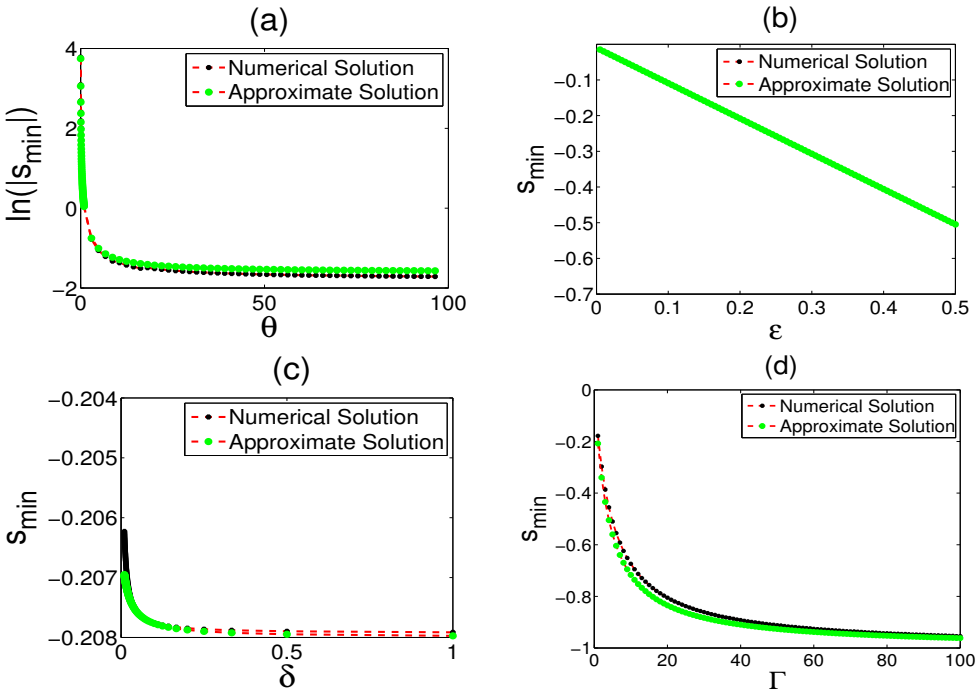

Figure 2.2: The pole closest to zero.

Parameters	$H_1 + H_2$	D_2	j	k_2	Γ	$\epsilon \equiv \frac{H_1}{H_1+H_2}$	$\delta \equiv \left(\frac{D_1}{D_2}\right)$	$\theta \equiv \frac{k_1}{k_2}$
Values	$0.5\,\mu m$	$73\frac{\mu m^2}{sec}$	$1\frac{mol}{sec}$	$0.03\frac{1}{sec}$	1	0.2	0.7	100

Table 2.1: The parameters for the one-dimensional system.

2.2.2 Two-dimensional model

In this section we study the steady-state concentration of a locally produced ligand in the $x-y$ plane to study the spatial distribution of the signal. We consider the two-dimensional system of dimension $L \times (H_1 + H_2)$ consisting of two layers of dimension $L \times H_1$ and $L \times H_2$. In the lower layer, the ligand diffuses with diffusion constant D_1 and decays with rate k_1, while in the upper layer, the ligand diffuses with diffusion constant D_2 and decays with rate k_2. There is an input flux of the ligand at $x = 0$. All other boundaries are reflective. Here we study how the concentration gradient of the ligand

depends on all parameters.

Let $C(x,y)$ be the steady-state concentrations of the ligand at (x,y). Then $C(x,y)$ obeys the following equations:

$$\begin{aligned}
D_1\Delta C(x,y) - k_1 C(x,y) &= 0 \quad \text{for } (x,y) \in [0,L]\times[0,H_1)\\
D_2\Delta C(x,y) - k_2 C(x,y) &= 0 \quad \text{for } (x,y) \in [0,L]\times(H_1,H_1+H_2]\\
-D_1\frac{\partial C(x,y)}{\partial x} &= j \quad \text{at } x=0,\ y\in[0,H_1)\\
-D_2\frac{\partial C(x,y)}{\partial x} &= j \quad \text{at } x=0,\ y\in(H_1,H_1+H_2]\\
\frac{\partial C(x,y)}{\partial x} &= 0 \quad \text{at } x=L
\end{aligned}$$

$$\begin{aligned}
\frac{\partial C(x,y)}{\partial y} &= 0 \quad \text{at } y=0 \text{ and } y=H_1+H_2\\
\lim_{y\to H_1^-} D_1\frac{\partial C(x,y)}{\partial y} &= \lim_{y\to H_1^+} D_2\frac{\partial C(x,y)}{\partial y}\\
\lim_{y\to H_1^-} C(x,y) &= \lim_{y\to H_1^+} \Gamma C(x,y),
\end{aligned}$$

Let C_0 be a reference concentration of the ligand. Similar to the one-dimensional model in Section 2.2.1, we define the dimensionless variables, coordinates and parameters as follows:

$$\begin{aligned}
&u \equiv \frac{C}{C_0}, \quad \xi \equiv \frac{x}{L}, \quad \eta \equiv \frac{y}{H_1+H_2},\\
&J \equiv \frac{jL}{D_1}, \quad \delta \equiv \frac{D_1}{D_2}, \quad \theta \equiv \frac{k_1}{k_2}, \quad \epsilon \equiv \frac{H_1}{H_1+H_2},\\
&\Lambda \equiv \frac{D_1}{k_1L^2}, \quad \Upsilon \equiv \frac{D_2}{k_2L^2}, \quad \mu \equiv \frac{H_1+H_2}{L}.
\end{aligned}$$

Therefore, $\Upsilon = \Lambda * \frac{\theta}{\delta}$. The governing equations of $u(\xi,\eta)$ become

$$\begin{aligned}
\Lambda\left(\frac{\partial^2 u}{\partial\xi^2} + \frac{1}{\mu^2}\frac{\partial^2 u}{\partial\eta^2}\right) - u &= 0 \quad \text{for } (\xi,\eta)\in[0,1]\times[0,\epsilon)\\
\Upsilon\left(\frac{\partial^2 u}{\partial\xi^2} + \frac{1}{\mu^2}\frac{\partial^2 u}{\partial\eta^2}\right) - u &= 0 \quad \text{for } (\xi,\eta)\in[0,1]\times(\epsilon,1]\\
-\frac{\partial u}{\partial\xi} &= J \quad \text{at } \xi=0,\ \eta\in[0,\epsilon)
\end{aligned}$$

$$
\begin{aligned}
-\frac{\partial u}{\partial \xi} &= J\delta \quad \text{at } \xi = 0,\ \eta \in (\epsilon, 1] \\
\frac{\partial u}{\partial \xi} &= 0 \quad \text{at } \xi = 1 \\
\frac{\partial u}{\partial \eta} &= 0 \quad \text{at } \eta = 0 \text{ and } \eta = 1 \\
\lim_{\eta \to \epsilon^-} \delta \frac{\partial u}{\partial \eta} &= \lim_{\eta \to \epsilon^+} \frac{\partial u}{\partial \eta} \\
\lim_{\eta \to \epsilon^-} u &= \lim_{\eta \to \epsilon^+} \Gamma u,
\end{aligned}
$$

Letting $\alpha_n = \sqrt{\frac{\mu^2\epsilon^2(1+n^2\pi^2\Lambda)}{\Lambda}}$ and $\beta_n = \sqrt{\frac{\mu^2(1-\epsilon)^2(1+n^2\pi^2\Upsilon)}{\Upsilon}}$ for $n = 0, 1, 2, \ldots$, we solve the above equations of u and represent u as follows:
For $\eta \in [0, \epsilon)$

$$
u = \frac{J}{2}(\xi - 1)^2 + \sum_{n=0}^{\infty} A_n(\eta) \cos(n\pi\xi) \tag{2.16}
$$

where

$$
\begin{aligned}
A_n(\eta) &= J\Lambda - \frac{J}{6} - \frac{J\sqrt{\Lambda}(\Lambda - \delta\Gamma\Upsilon)\sinh(\beta_0)\cosh\left(\alpha_0\frac{\eta}{\epsilon}\right)}{\delta\Gamma\sqrt{\Upsilon}\sinh(\alpha_0)\cosh(\beta_0) + \sqrt{\Lambda}\cosh(\alpha_0)\sinh(\beta_0)}, \quad \text{for } n = 0, \\
A_n(\eta) &= -\frac{2J}{n^2\pi^2(1+n^2\pi^2\Lambda)} \\
&\quad -\frac{2J\epsilon\beta_n\sinh(\beta_n)\cosh\left(\alpha_n\frac{\eta}{\epsilon}\right)\left(\frac{\Lambda}{1+n^2\pi^2\Lambda} - \frac{\delta\Gamma\Upsilon}{1+n^2\pi^2\Upsilon}\right)}{\Gamma\delta(1-\epsilon)\alpha_n\sinh(\alpha_n)\cosh(\beta_n) + \epsilon\beta_n\cosh(\alpha_n)\sinh(\beta_n)}, \quad \text{for } n > 0.
\end{aligned}
$$

For $\eta \in (\epsilon, 1]$, we have

$$
u = \frac{J\delta}{2}(\xi - 1)^2 + \sum_{n=0}^{\infty} B_n(\eta) \cos(n\pi\xi) \tag{2.17}
$$

where

$$
\begin{aligned}
B_n(\eta) &= J\delta\Upsilon - \frac{J\delta}{6} + \frac{J\delta\sqrt{\Upsilon}(\Lambda - \delta\Gamma\Upsilon)\sinh(\alpha_0)\cosh\left(\beta_0\frac{1-\eta}{1-\epsilon}\right)}{\Gamma\delta\sqrt{\Upsilon}\sinh(\alpha_0)\cosh(\beta_0) + \sqrt{\Lambda}\cosh(\alpha_0)\sinh(\beta_0)}, \quad \text{for } n = 0, \\
B_n(\eta) &= -\frac{2J\delta}{n^2\pi^2(1+n^2\pi^2\Upsilon)} \\
&\quad +\frac{2J(1-\epsilon)\alpha_n\sinh(\alpha_n)\cosh\left(\beta_n\frac{(1-\eta)}{1-\epsilon}\right)\left(\frac{\Lambda}{1+n^2\pi^2\Lambda} - \frac{\delta\Gamma\Upsilon}{1+n^2\pi^2\Upsilon}\right)}{\Gamma\delta(1-\epsilon)\alpha_n\sinh(\alpha_n)\cosh(\beta_n) + \epsilon\beta_n\cosh(\alpha_n)\sinh(\beta_n)}, \quad \text{for } n > 0.
\end{aligned}
$$

Using Eq. (2.16) and Eq. (2.17) we first discuss how the system can achieve scale-invariance, i.e., the concentration gradient of the ligand can keep the same proportion regardless of the system size. From Eq. (2.16) and (2.17), the following expressions have to be independent of L, H_1 and H_2 for the system to be scale-invariant:

$$J = \frac{jL}{D_1}, \quad \eta = \frac{H_1}{H_1 + H_2}, \quad \mu = \frac{L}{H_1 + H_2},$$
$$\Lambda = \frac{D_1}{k_1 L^2}, \quad \Upsilon = \frac{D_2}{k_2 L^2}, \quad \frac{\Lambda}{\mu^2 \epsilon^2} = \frac{D_1}{k_1 H_1^2}, \quad \frac{\Upsilon^2}{\mu^2 (1-\epsilon)^2} = \frac{D_2}{k_2 H_2^2}.$$

Scale-invariance related to $J = \frac{jL}{D_1}$ has been discussed by Umulis in [51]. The fact that $\eta = \frac{H_1}{H_1+H_2}$ is independent of H_1 and H_2 indicates that the caption region of the receptors occupy a certain proportion of the system. The fact that $\mu = \frac{L}{H_1+H_2}$ is independent of L and $H_1 + H_2$ is natural, since μ represents the ratio of two sides of the system.

$\Lambda = \frac{D_1}{k_1 L^2}$ is the ratio of two characteristics times: $\frac{1}{k_1}$ is the characteristic life time of the ligand molecule in the lower layer; and $\frac{L^2}{D_1}$ is the characteristic diffusion time for the ligand molecule in the lower layer. If $\frac{D_1}{k_1 L^2}$ is small, then the ligand molecules spread to a small region of the system, since the ligand molecules decay so quickly that they can not diffuse far away. For the two-dimensional system to be scale-invariant, $\frac{D_1}{k_1 L^2}$ has to be independent of L. Similarly, the independence of $\frac{D_2}{k_2 L^2}$ and $\frac{D_1}{k_1 H_1^2}$ and $\frac{D_2}{k_2 H_2^2}$ can be explained.

In Fig. 2.3, using Eq. (2.16), we observe how u changes at $\eta = 0$ as we change the values of the parameters. Since the downstream signal transduction pathway is initiated by a signaling complex forming near the receptors, we only consider the concentration of ligand at $\eta = 0$. All parameters used in Fig. 2.3 are given in Table 2.2, whose values are estimated based on Dorsal-Ventral patterning in *Drosophila* [5]. In each figure of Fig. 2.3, we change one parameter and keep the remaining parameters as in Table 2.2.

In Fig. 2.3-(a), we fix k_2 and increase θ by increasing k_1. Fig. 2.3-(a) shows that as θ (k_1) increases, the maximal level of u decreases and the concentration gradient becomes sharper (data not shown here). Please note that the degradation in the lower layer is the ligand degradation mechanism around the cell membrane, which consists of the extracellular degradation around cell membrane and the intracellular degradation of the internalized ligand molecules. Therefore, increasing the extracellular degradation rate,

the internalization rate or the intracellular degradation rate of the ligand can increase k_1 and decrease the life time of the ligand, which sharpens the concentration gradient and decreases the level of u.

In Fig. 2.3-(b), we fix D_2 and increase δ by increasing D_1. Fig. 2.3-(b) shows that changing δ does not change the level of u much, which is consistent with our result about the relationship between δ and $s_{\min}$ in Section 2.2.1. In fact, as δ (D_1) decrease, the characteristic times $\frac{L^2}{D_1}$ and $\frac{H_1^2}{D_1}$ increase so it takes longer time for the ligand molecule to leave the lower layer. As a result, the ligand molecules have more chance to decay before diffusing away. Therefore, the concentration gradient of the ligand becomes sharper, which is shown in Fig. 2.3-(b).

In Fig. 2.3-(c), as ϵ increases, u decreases and the concentration gradient of u becomes sharper. As the lower layer becomes large, the region for the ligand to decay fast becomes large. Moreover, the region for the slow diffusion of the ligand becomes larger.

In Fig. 2.3-(d), we fix L and increase μ by increasing $H_1 + H_2$. We find the overall level of the concentration decreases as μ increases. As μ increases, H_1 and H_2 increases and the characteristic times of diffusion, $\frac{H_1^2}{D_1}$ and $\frac{H_2^2}{D_2}$, increase. Therefore, the ligand molecules in the lower layer leaves the lower layer more slowly and it takes longer time the ligand molecules in the upper layer to diffuse into the lower layer. Then the molecules in the lower layer have more chance to decay before diffusing away. Therefore, the overall level of the ligand in the lower layer decreases. One more important thing is that changing μ rarely changes u if μ is small enough. This implies that as the height of the rectangular system becomes small enough relative to the length and the width, the concentration becomes robust to the change of μ. This is because that the rectangular system becomes thin enough so that it can be considered as a one-dimensional line.

In Fig. 2.3-(e), when we increases Γ, which concentrates the ligand molecules in the lower layer, the gradient of u becomes sharper.

In this section, we show that if the ligand degrades faster in the lower layer than it does in the upper layer, localization can decrease the relaxation time of the ligand concentration to reach the steady state in the one-dimensional model and can sharpen the concentration gradient in the two-dimensional model. However, since the number of ligand molecules involved in the signaling process is small in general, the fluctuations of

the number of ligand molecules may play a significant role in signaling process. Therefore in the next section, we consider stochastic models of the signaling systems with ligands, membrane proteins, and receptors.

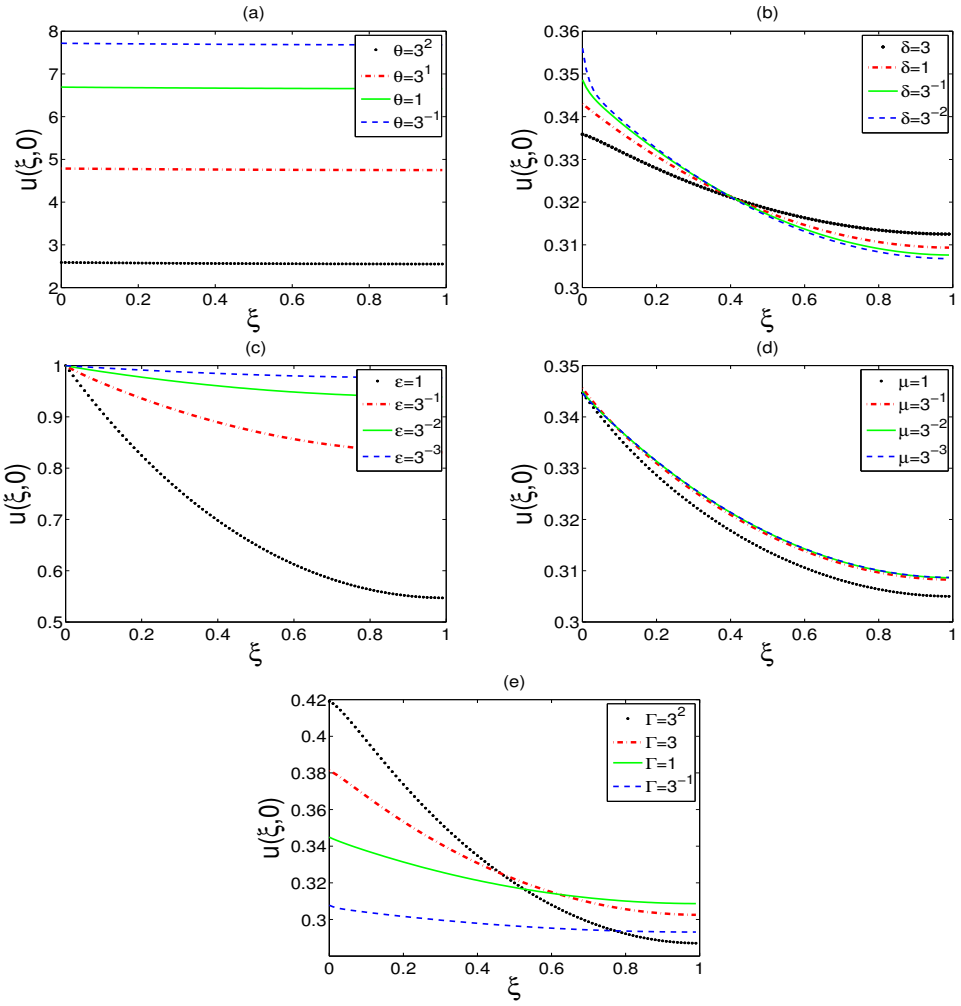

Figure 2.3: The steady-state concentration, $u(\xi, \eta)$, at $\eta = 0$.

Parameters	L	D_2	j	k_2	Γ	$\mu \equiv \frac{H_1+H_2}{L}$	$\epsilon \equiv \frac{H_1}{H_1+H_2}$	$\delta \equiv \frac{D_1}{D_2}$	$\theta \equiv \frac{k_1}{k_2}$
Values	$5\,\mu m$	$73\frac{\mu m^2}{sec}$	$1\frac{mol}{sec}$	$0.03\frac{1}{sec}$	1	0.2	0.7	0.1	100

Table 2.2: The parameters for the two-dimensional system.

2.3 Stochastic Model of ligand movement and reception

We look at the effect of localization on signaling by analyzing the transport of an individual ligand molecule in two-dimensional two-layered systems. The two-dimensional two-layered systems are chosen as the signaling systems in the x-y plane in Fig. 2.1, in the lower layer of which lie the membrane proteins and the receptors. First, we consider the system with a ligand molecule and the membrane proteins to understand the extent of localization by the association between the ligand and the membrane protein. Then in the next system, we add receptors to study the interaction among ligands, receptors and membrane proteins. At the end, we analyze the effect of the localization on signaling specificity.

2.3.1 The residence time of a ligand molecule

We consider a two-dimensional two-layered system with the ligand (B) and the membrane protein. We denote as BC the immobile complex of the ligand molecule and the membrane protein located in the lower layer. We compute the mean time for a ligand molecule starting in each layer to enter into the other layer, in order to evaluate how the motion of the ligand molecule is restricted by the membrane protein.

Fig. 2.4 shows the two-layered system with the ligand (B) and the membrane protein. In the lower layer $[0, L] \times [0, H_1]$, denoted as Region I, a ligand molecule of species B diffuses with diffusion coefficient D_1. Moreover, the ligand molecule becomes an immobile molecule of species BC with rate k_+ and a molecule of species BC becomes a molecule of species B with rate k_-. In using k_+, we are assuming that the membrane protein is uniformly distributed in the lower layer and is in excess. In the upper layer $[0, L] \times [H_1, H_1 + H_2]$, denoted as Region II, the ligand molecule of species B diffuses with diffusion coefficient D_2.

For simplicity, we assume the boundary between the two layers is 'perfectly absorbing': in the sense that, once the ligand molecule of species B reaches the line $y = H_1$ from Region I, it automatically moves into Region II. Similarly, once the ligand molecule reaches the line $y = H_1$ from Region II, it moves into Region I automatically. All the other boundaries of the system are reflective.

We analyze two separate cases when the molecule of species B is located in Region I

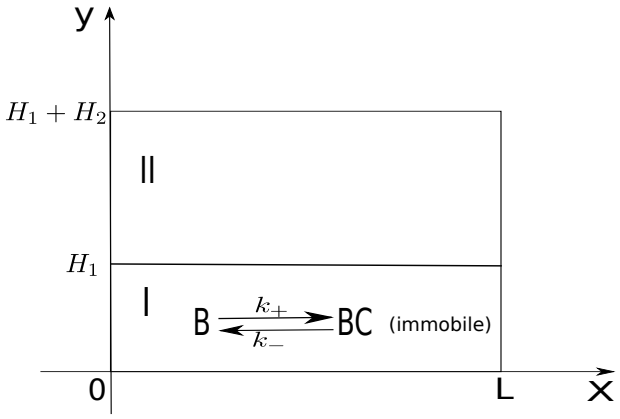

Figure 2.4: The schematic of the two-layered system with binding to immobile proteins

or Region II initially. First, assume the molecule of species B starts at position (x_0, y_0) in Region I. Define $p_{1b}(x, y, t|x_0, y_0, 0)$ and $p_{1bc}(x, y, t|x_0, y_0, 0)$ as the probability density functions such that $p_{1b}(x, y, t|x_0, y_0, 0)\, dx\, dy$ and $p_{1bc}(x, y, t|x_0, y_0, 0)\, dx\, dy$ are the probabilities that without leaving region I, the molecule stays in $(x, x+dx] \times (y, y+dy]$ as a molecule of species B and species BC at time t respectively.

Then for $y \in [0, H_1]$, we have the governing equations as follows:

$$\begin{aligned}
\frac{\partial p_{1b}(x, y, t|x_0, y_0, 0)}{\partial t} &= D_1 \Delta_{xx+yy} p_{1b}(x, y, t|x_0, y_0, 0) \\
&\quad - k_+ p_{1b}(x, y, t|x_0, y_0, 0) + k_- p_{1bc}(x, y, t|x_0, y_0, 0), && \text{(2.18a)} \\
\frac{\partial p_{1bc}(x, y, t|x_0, y_0, 0)}{\partial t} &= k_+ p_{1b}(x, y, t|x_0, y_0, 0) - k_- p_{1bc}(x, y, t|x_0, y_0, 0), && \text{(2.18b)} \\
p_{1b}(x, y, t|x_0, y_0, 0) &= \delta(x - x_0)\delta(y - y_0), && \text{(2.18c)} \\
p_{1bc}(x, y, t|x_0, y_0, 0) &= 0, && \text{(2.18d)} \\
\frac{\partial p_{1b}(x, y, t|x_0, y_0, 0)}{\partial y} &= 0, \quad \text{at } y = 0, && \text{(2.18e)} \\
p_{1b}(x, y, t|x_0, y_0, 0) &= 0, \quad \text{at } y = H_1 && \text{(2.18f)} \\
\frac{\partial p_{1b}(x, y, t|x_0, y_0, 0)}{\partial x} &= 0, \quad \text{at } x = 0 \text{ and } x = L, && \text{(2.18g)}
\end{aligned}$$

where Δ_{xx+yy} is the Laplace operator acting on x and y. Let $S_1(t|x_0, y_0, 0)$ be the probability that the ligand molecule never leaves Region I before t given it starts at (x_0, y_0) in Region I. Define T_1 as the random variable of the time when the molecule

leaves Region I for the first time. Then

$$\begin{aligned} S_1(t|x_0,y_0,0) &= \int_0^{H_1}\int_0^{L}\{p_{1b}(x,y,t|x_0,y_0,0)+p_{1bc}(x,y,t|x_0,y_0,0)\}\,dx\,dy \\ P\left(T_1>t|x_0,y_0,0\right) &= S_1(t|x_0,y_0,0) \end{aligned}$$

Letting

$$p_{\bar{1}b}(y,t|x_0,y_0,0)=\int_0^{L}p_{1b}(x,y,t|x_0,y_0,0)dx$$

and

$$p_{\bar{1}bc}(y,t|x_0,y_0,0)=\int_0^{L}p_{1bc}(x,y,t|x_0,y_0,0)dx,$$

Eq. (2.18) leads to

$$\begin{aligned} \frac{\partial p_{\bar{1}b}(y,t|x_0,y_0,0)}{\partial t} &= D_1\Delta p_{\bar{1}b}(y,t|x_0,y_0,0) \\ &\quad - k_+p_{\bar{1}b}(y,t|x_0,y_0,0)+k_-p_{\bar{1}bc}(y,t|x_0,y_0,0), && \text{(2.19a)} \\ \frac{\partial p_{\bar{1}bc}(y,t|x_0,y_0,0)}{\partial t} &= k_+p_{\bar{1}b}(y,t|x_0,y_0,0)-k_-p_{\bar{1}bc}(y,t|x_0,y_0,0), && \text{(2.19b)} \\ p_{\bar{1}b}(y,t|x_0,y_0,0) &= \delta(y-y_0), && \text{(2.19c)} \\ p_{\bar{1}bc}(y,t|x_0,y_0,0) &= 0, && \text{(2.19d)} \\ \frac{\partial p_{\bar{1}b}(y,t|x_0,y_0,0)}{\partial y} &= 0, \quad \text{at } y=0, && \text{(2.19e)} \\ p_{\bar{1}b}(y,t|x_0,y_0,0) &= 0, \quad \text{at } y=H_1 && \text{(2.19f)} \end{aligned}$$

where Δ_{yy} is the Laplace operator acting on y. So $p_{1b}(y,t|x_0,y_0,0)$ and $p_{\bar{1}bc}(y,t|x_0,y_0,0)$ do not dependent on x_0. As a result, S_1 and $P\left(T_1>t|x_0,y_0,0\right)$ do not depend on x_0. We only have to consider the evolution of the y-coordinate of the position of the ligand molecule. For simplicity, we denote $p_{\bar{1}b}(y,t|x_0,y_0,0)$ as $p_{1b}(y,t|y_0,0)$ and $p_{\bar{1}bc}(y,t|x_0,y_0,0)$ as $p_{\bar{1}bc}(y,t|y_0,0)$. In addition, Δ_{yy} is denoted as Δ.

In Appendix 6.1.2, we compute $p_{1b}(y,t|y_0,0)$ and $p_{1bc}(y,t|y_0,0)$, from which we obtain S_1 as follows:

$$\begin{aligned} & S_1(t|y_0,0) \\ = & \sum_{n=0}^{\infty}\frac{2(-1)^n}{(2n+1)\pi\upsilon_n}\cos\frac{(2n+1)\pi y_0}{2H_1} \\ \times & \left[e^{\lambda_{n+}t}(\upsilon_n-\omega_n^2D_1+k_++k_-)+e^{\lambda_{n-}t}(\upsilon_n+\omega_n^2D_1-k_+-k_-)\right], \qquad \text{(2.20)} \end{aligned}$$

where $\omega_n = \frac{(2n+1)\pi}{2H_1}$, $\upsilon_n = \sqrt{(k_+ + k_- + \omega_n^2 D_1)^2 - 4k_-\omega_n^2 D_1}$ and $\lambda_{n\pm} = \frac{-(k_+ + k_- + \omega_n^2 D_1) \pm \upsilon_n}{2}$. Moreover,

$$\begin{aligned} E[T_1|y_0, 0] &= \int_0^\infty S_1(t|y_0, 0)\, dt \\ &= \frac{16H_1^2(k_+ + k_-)}{D_1 k_-} \sum_{n=0}^{\infty} \frac{(-1)^n}{(2n\pi + \pi)^3} \cos\frac{(2n+1)\pi y_0}{2H_1}. \end{aligned}$$

Assuming that the position of the ligand molecule is uniformly distributed in Region I initially, the expected value of T_1 is [1]

$$\begin{aligned} E[T_1] &= \frac{1}{H_1}\int_0^{H_1} E[T_1|y_0, 0]\ dy_0 \\ &= \frac{\tau_1(1 + K_D)}{3}, \end{aligned}$$

where $\tau_1 = \frac{H_1^2}{D_1}$ and $K_D = \frac{k_+}{k_-}$.

Next we consider the stochastic motion of the ligand molecule in region II. Similarly, we only have to consider the evolution of the y-coordinate of the position of the ligand molecule. Assume the molecule starts in y_0 in Region II as a molecule of species B. Define $p_2(y, t|y_0, 0)$ as the probability density function such that $p_2(y, t|y_0, 0)\, dy$ is the probability that without leaving Region II, the molecule stays in $(y, y+dy]$ as a molecule of species B at time t. Then the governing equation of $p_2(y, t|y_0, 0)$ is

$$\frac{\partial p_2(y, t|y_0, 0)}{\partial t} = D_2 \Delta p_2(y, t|y_0, 0), \tag{2.21a}$$

$$p_2(y, 0|y_0, 0) = \delta(y - y_0), \tag{2.21b}$$

$$p_2(y, t|y_0, 0) = 0, \quad \text{at } y = H_1, \tag{2.21c}$$

$$\frac{\partial p_2(y, t|y_0, 0)}{\partial y} = 0, \quad \text{at } y = H_1 + H_2, \tag{2.21d}$$

We solve Eq. (2.21) in Appendix 6.1.2. Define $S_2(t|y_0, 0)$ as the probability that the molecule never leaves Region II before time t given it starts at y_0 in Region II. Then we have $S_2(t|y_0, 0)$ as follows:

$$S_2(t|y_0, 0) \equiv \int_{H_1}^{H_1+H_2} p_2(x, y, t|y_0, 0)\, dy$$

[1] In the calculation of $E[T_1]$, we use $\sum_{n=0}^{\infty} \frac{1}{(2n\pi + \pi)^4} = \frac{1}{96}$.

$$= \sum_{n=0}^{\infty} \frac{4e^{-D_2\left(\frac{2n\pi+\pi}{2H_2}\right)^2 t}}{(2n+1)\pi} \sin\frac{(2n+1)\pi(y_0-H_1)}{2H_2}. \tag{2.22}$$

Define T_2 be the random variable of the time when the molecule leaves Region II for the first time. Then the expectation of T_2 is [2]

$$\begin{aligned} E\left[T_2|y_0,0\right] &= \int_0^{\infty} S_2(t|y_0,0)\,dt \\ &= \tau_2\left\{\frac{y_0-H_1}{H_2} - \frac{1}{2}\left(\frac{y_0-H_1}{H_2}\right)^2\right\} \end{aligned} \tag{2.23}$$

where $\tau_2 = \frac{H_2^2}{D_2}$. Assuming that the position of the ligand molecule is uniformly distributed in Region II initially, we have

$$\begin{aligned} E\left[T_2\right] &= \frac{1}{H_2}\int_{H_1}^{H_1+H_2} E\left[T_2|y_0,0\right]\,dy_0 \\ &= \frac{\tau_2}{3} \end{aligned} \tag{2.24}$$

Therefore, we have

$$\frac{E\left[T_1\right]}{E\left[T_2\right]} = \frac{\tau_1(1+K_D)}{\tau_2} \tag{2.25}$$

where τ_1 (τ_2) is the characteristic time for a ligand molecule to diffuse freely throughout a one-dimensional system of length H_1 (H_2) with diffusion coefficient D_1 (D_2). The association between the ligand and the membrane protein increases the time for the ligand molecule to stay in the lower layer by $1+K_D$ times. Therefore, the membrane protein holds the ligand molecule in the lower layer.

Here, we assume the interface between the two layers is perfectly 'absorbing' for simplicity. However, when the molecule reaches the interface, it may not cross the interface and stay in its starting layer. As a result, due to the assumption that the interface is perfectly absorbing, $S_2(t|y_0,0)$ is underestimated in the case that the molecule starts at y_0 in Region II. Similarly, $S_1(t|y_0,0)$ is also underestimated in the case that the molecule starts at y_0 in Region I. We have to compare the underestimation amounts of $S_1(t|y_0,0)$ and $S_2(t|y_0,0)$ and the frequencies of the ligand molecule hitting the interface from two layers, in order to find whether the perfectly absorbing boundary at the

[2] In the calculation of $E\left[T_2|y_0,0\right]$, we use that for $x\in[0,2]$, $\sum_{n=0}^{\infty}\frac{16}{(2n\pi+\pi)^3}\sin\frac{(2n\pi+\pi)x}{2} = x-\frac{x^2}{2}$.

interface causes underestimation or overestimation of the probability that the molecule stays in each layer.

For example, we approximate the exit rates of the ligand molecule from the lower and upper layers as $\frac{1}{E[T_1]}$ and $\frac{1}{E[T_2]}$. Denote B_1 and B_2 as ligands in the lower layer and in the upper layer, respectively. Then we can approximate the movement of the ligand between two layers as the following first-order reactions:

$$B_1 \underset{k_2}{\overset{k_1}{\rightleftharpoons}} B_2,$$

where $k_1 = \frac{1}{E[T_1]}$ and $k_2 = \frac{1}{E[T_2]}$. In the case that $\frac{E[T_1]}{E[T_2]} > 1$, i.e., $k_1 < k_2$, the ligand molecule from the upper layer hits the absorbing interface more frequently than that from the lower layer. Assume the underestimation amounts of $S_1(t|y_0, 0)$ and $S_2(t|y_0, 0)$ are the same. Then we can conclude that the perfectly absorbing condition leads to underestimation of the chance for the ligand molecule to become a species B_2 in the upper layer. Similarly, in the case that $\frac{E[T_1]}{E[T_2]} < 1$, the chance for the ligand molecule to become a species B_1 in the lower layer is underestimated.

2.3.2 The ligand density at the steady state

In Section 2.3.1, we consider the two-layered system with the perfectly absorbing boundary condition at the interface between two layers. Due to the perfectly absorbing boundary condition, once the ligand molecule hits the interface, the ligand molecule leaves its starting region and enters the other region. However, when the ligand molecule reaches the interface, it can cross the interface to enter the other region or return to its starting region. So here we introduce an artificial layer around the interface to model the possibility that the ligand molecule does not cross the interface at the interface. With the help of the artificial layer, we can evaluate the effect of membrane proteins on the distribution of the ligand molecule more accurately.

To model how the ligand molecule crosses the interface by diffusing from one of the layers, we introduce an artificial layer of height $2h$ as shown in Fig. 2.5. We denote $[0, L] \times [0, H_1 + h]$ as Region I' and $[0, L] \times [H_1 - h, H_1 + H_2]$ as Region II'. If the molecule starts in $[0, L] \times [0, H_1]$, then the molecule is a molecule in Region I' where the molecule can be diffusing species B with diffusion coefficient D_1 or immobile species BC until it hits $y = H_1 + h$. Once the molecule in Region I' hits $H_1 + h$, it becomes

diffusing species B in Region II' with diffusion coefficient D_2 until it hits $y = H_1 - h$. Once the molecule in Region II' hits $y = H_1 - h$, it becomes a molecule in Region I'. Then the molecule repeatedly switches between Region I' and II'. If the molecule starts in $[0, L] \times (H_1, H_1 + H_2]$, it is species B with diffusion coefficient D_2 in Region II' until it hits $y = H_1 - h$. Once it hits $y = H_1 - h$, it becomes a molecule in Region I'. Then it repeats the process as it starts in Region I'. Since the molecule has to diffuse to $H_1 + h$ to enter Region II', our model requires the ligand cross the interface to leave the lower layer. Therefore, our model includes the possibility that the molecule arriving at $y = H_1$ from the lower layer returns to the lower layer. Similarly, it also includes the case that the molecule arriving at $y = H_1$ from the upper layer returns to the upper layer.

Similarly to Section 2.3.1, we only have to consider the evolution of the y-coordinate of the molecule position if we are only interested in which layer the molecule lies. Define $p_{1b}(y, t|y_0, 0)$ ($p_{1bc}(y, t|y_0, 0)$) to be the probability density function such that $p_{1b}(y, t|y_0, 0)\, dy$ ($p_{1bc}(y, t|y_0, 0)\, dy$) is the probability that the molecule of species B starting at y_0 in Region I' lies in $[y, y + dy)$ as a molecule of species B (BC) at time t without leaving Region I' before. Similarly, define $p_2(y, t|y_0, 0)$ as a probability density function such that $p_2(y, t|y_0, 0)\, dy$ is the probability that the molecule of species B starting at y_0 in Region II' lies in $[y, y + dy)$ at time t without leaving Region II' before. Then the governing equations for $p_{1b}(y, t|y_0, 0)$, $p_{1bc}(y, t|y_0, 0)$ and $p_2(y, t|y_0, 0)$ are the same as Eq. (2.19) and (2.21) except that the absorbing boundaries in (2.19f) and (2.21c) are replaced by the ones at $y = H_1 + h$ and $y = H_1 - h$, respectively. Therefore, $p_{1b}(y, t|y_0, 0)$, $p_{1bc}(y, t|y_0, 0)$ and $p_2(y, t|y_0, 0)$ are obtained the same way as in Appendix 6.1.2.

Define $S_1(t|y_0, 0)$ as the probability that the molecule starting in y_0 in Region I' stays in Region I' at time t and never leaves Region I' before time t. Similarly to Section 2.3.1, we obtain $S_1(t|y_0, 0)$ as follows:

$$
\begin{aligned}
& S_1(t|y_0, 0) \\
\equiv\ & \int_0^{H_1+h} \{p_{1b}(y, t|y_0, 0) + p_{1bc}(y, t|y_0, 0)\}\, dy \\
=\ & \sum_{n=0}^{\infty} \frac{2(-1)^n}{(2n+1)\pi\upsilon_n} \cos\frac{(2n+1)\pi y_0}{2H_1} \left[e^{\lambda_{n+}t}(\upsilon_n - \omega_n^2 D_1 + k_+ + k_-) \right.
\end{aligned}
$$

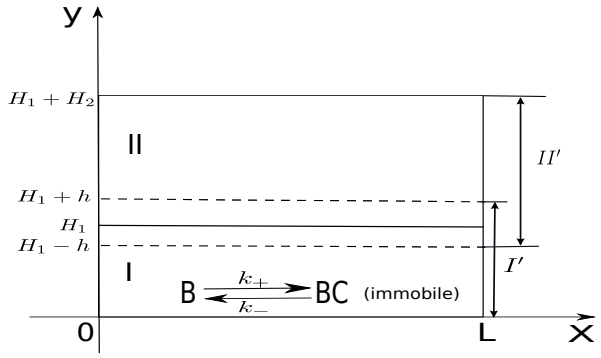

Figure 2.5: The two-layered system with an artificial layer.

$$+ \quad e^{\lambda_{n-}t}(\upsilon_n + \omega_n^2 D_1 - k_+ - k_-)\Big], \tag{2.26}$$

where $\omega_n = \frac{(2n+1)\pi}{2(H_1+h)}$, $\upsilon_n = \sqrt{(k_+ + k_- + \omega_n^2 D_1)^2 - 4k_-\omega_n^2 D_1}$ and $\lambda_{n\pm} = \frac{-(k_+ + k_- + \omega_n^2 D_1) \pm \upsilon_n}{2}$.

Define $S_2(t|y_0, 0)$ as the probability such that the molecule starting in y_0 in Region II' stays in Region II' at time t and never leaves Region II' before time t. Similarly to Section 2.3.1, we obtain $S_2(t|y_0, 0)$ as follows:

$$\begin{aligned} & S_2(t|y_0, 0) \\ \equiv & \int_{H_1-h}^{H_1+H_2} p_2(y, t|y_0, 0)\, dy \\ = & \sum_{n=0}^{\infty} \frac{4e^{-\left(\frac{2n\pi+\pi}{2H_2+2h}\right)^2 D_2 t}}{(2n+1)\pi} \sin \frac{(2n+1)\pi\,(y_0 - (H_1 - h))}{2(H_2 + h)}. \end{aligned} \tag{2.27}$$

We consider the probability that the ligand molecule starting in Region I (II) ends in Region I' (II') at time t after switching between Region I' and Region II' several times. For $y \in [0, H_1 + h)$ and $y_0 \in [0, H_1]$, define $G_1(y, t|y_0, 0)$ as the probability density function such that $G_1(y, t|y_0, 0)\, dy$ is the probability that the molecule starting at y_0 as a molecule of species B lies in $[y, y + dy)$ of Region I' as a molecule of species B or BC at time t. Similarly, define $G_{1B}(y, t|y_0, 0)$ as the probability density function such that $G_{1B}(y, t|y_0, 0)\, dy$ is the probability that the molecule starting at y_0 as a molecule of species B lies in $[y, y + dy)$ of Region I' as a molecule of species B at time t. For $y \in (H_1 - h, H_1 + H_2]$, define $G_2(y, t|y_0, 0)$ as a probability density function such that

$G_2(y,t|y_0,0)\,dy$ is the probability that the molecule starting in $[y_0, y_0+dy)$ as a molecule of species B lies in $[y, y+dy)$ of Region II' as a molecule of species B at time t.

Now we focus on the case when the ligand molecule starts in region I. But the following results and procedure can be extended to the case when the molecule starts in region II. If the ligand molecule starts in Region I, it will switch between Region I' and II' after it reaches $y = H_1 + h$ for the first time. Therefore, for $y_0 \in [0, H_1]$ and $t > 0$, we have

$$
\begin{aligned}
& G_{1B}(y,t|y_0) && (2.28)\\
= \; & p_{1b}(y,t|y_0) && (2.29)\\
& + \int_0^t \int_0^{t-\tau} \left\{ -\frac{\partial S_1(\tau|y_0)}{\partial \tau} \right\} \left\{ -\frac{\partial S_2(\tau'|H_1+h)}{\partial \tau'} \right\} G_{1B}(y, t-\tau-\tau'|H_1-h)\, d\tau'\, d\tau.
\end{aligned}
$$

$\left\{ -\frac{\partial S_1(\tau|y_0)}{\partial \tau} \right\} d\tau$ gives the probability that the molecule starting at y_0 leaves Region I' for the first time in $[\tau, \tau + d\tau)$. Upon entering Region II' at $y = H_1 + h$, the molecule diffuses with diffusion coefficient D_2 and leaves Region II' for the first time in $[\tau+\tau', \tau+\tau'+d\tau')$ with probability $\left\{ -\frac{\partial S_2(\tau'|H_1+h)}{\partial \tau'} \right\} d\tau'$. Then the molecule starts at $y = H_1 - h$ in Region I' and stays in $[y, y+dy)$ as a molecule of species B after time $t-\tau-\tau'$ with probability $G_{1B}(y, t-\tau-\tau'|H_1-h)$.

Similarly, for $y_0 \in [0, H_1]$ and $t > 0$, we get

$$
\begin{aligned}
& G_1(y,t|y_0)\\
& = p_{1b}(y,t|y_0) + p_{1bc}(y,t|y_0)\\
& + \textstyle\int_0^t \int_0^{t-\tau} \left\{ -\frac{\partial S_1(\tau|y_0)}{\partial \tau} \right\} \left\{ -\frac{\partial S_2(\tau'|H_1+h)}{\partial \tau'} \right\} G_1(y, t-\tau-\tau'|H_1-h)\, d\tau'\, d\tau.\\
& G_2(y,t|y_0)\\
& = \textstyle\int_0^t \left\{ -\frac{\partial S_1(\eta|y_0)}{\partial \eta} \right\} [p_2(y, t-\eta|y_0)\\
& + \textstyle\int_0^{t-\eta} \int_0^{t-\eta-\tau} \left\{ -\frac{\partial S_2(\tau|y_0)}{\partial \tau} \right\} \left\{ -\frac{\partial S_1(\tau'|H_1-h)}{\partial \tau'} \right\} G_2(y, t-\eta-\tau-\tau'|H_1+h)\, d\tau'\, d\tau \Big]\, d\eta
\end{aligned}
$$

Using the calculation in Section 6.1.3, we get

$$
\begin{aligned}
\lim_{h\to 0} \lim_{t\to\infty} G_{1B}(y,t|y_0) &= \frac{\frac{1}{D_1}}{\frac{H_1(1+K_D)}{D_1} + \frac{H_2}{D_2}}, \quad \text{for } y < H_1,\\
\lim_{h\to 0} \lim_{t\to\infty} G_1(y,t|y_0) &= \frac{\frac{(1+K_D)}{D_1}}{\frac{H_1(1+K_D)}{D_1} + \frac{H_2}{D_2}}, \quad \text{for } y < H_1,
\end{aligned}
$$

$$\lim_{h\to 0}\lim_{t\to\infty} G_2(y,t|y_0) = \frac{\frac{1}{D_2}}{\frac{H_1(1+K_D)}{D_1}+\frac{H_2}{D_2}}, \quad \text{for } H_1 < y < H_1+H_2.$$

Therefore, the ratio of the steady-state concentrations of molecules in Region I and Region II is as follows:

$$\begin{aligned} R_{d12} &\equiv \frac{\lim_{h\to 0}\lim_{t\to\infty} G_1(y,t|y_0)}{\lim_{h\to 0}\lim_{t\to\infty} G_2(y,t|y_0)} \\ &= \frac{\frac{(1+K_D)}{D_1}}{\frac{1}{D_2}}. \end{aligned} \tag{2.31}$$

In (2.31), $1+K_D$ shows that the association between the ligand and the membrane protein can hold the ligand in the lower layer and increases the concentration of the ligand in the lower layer by $1+K_D$, which is consistent with our conclusion about the time for the ligand molecule to leave the lower layers in Section 2.3.1.

2.3.3 The context-dependent effect of localization on signaling

From the analysis of the transport of a ligand molecule in Section 2.3.2, we conclude that the membrane protein can concentrate the ligand molecules around the receptor surface. However, once the ligand molecules bind to the membrane protein, they are not free any more. The ligand molecules may not be as accessible to receptors as there is no membrane protein. As a result, the signal transmitted to the downstream reaction network may be changed. In this section, we consider how the time for a ligand molecule to bind to the receptors is influenced by interactions among the ligand, the membrane protein and the receptor. We first study a system with perfectly absorbing receptor surface, which absorbs the ligand molecule immediately once the ligand molecule hits the surface. After that, we look at the system in which the receptor can react with the ligand with only a finite rate in the lower layer.

Signaling through perfectly-absorbing receptors

In Section 2.3.2, we consider the two-layered system with membrane proteins in the lower layer. In this section, we add receptors at $y=0$ in the two-dimensional rectangle $[0,L]\times[0,H_1+H_2]$ and assume the receptor surface are perfectly absorbing, i.e., the

ligand molecule gets absorbed once it hits the receptor surface. Then we compare the first passage times for a ligand molecule to get absorbed in the systems with and without the localization layer. In system (a) of Fig. 2.6, the ligand molecule of species B can diffuse freely in $[0, L] \times [0, H_1 + H_2]$ with diffusion constant D_2 and can get absorbed immediately when it hits $y = 0$. In system (b) of Fig. 2.6, the molecule can diffuse with diffusion coefficient D_1 and attach to/detach from the membrane protein with rate k_+/k_- in the lower layer. Once the molecule of species B hits $y = 0$, it gets absorbed immediately. In the upper layer of system (b), the ligand molecule diffuses with diffusion coefficient D_2. As in Section 2.3.2, we set an artificial layer around the interface in system (b) in order to reflect the fact the ligand molecule may stay in the starting layer even though it hits the interface. As defined in Section 2.3.2, let $[0, L] \times [0, H_1 + h]$ be Region I' and $[0, L] \times [H_1 - h, H_1 + H_2]$ be Region II'. The ligand molecule switches between two regions as in Section 2.3.2 except that the ligand molecule may get absorbed by the perfectly absorbing receptor surface at $y = 0$ in Region I'.

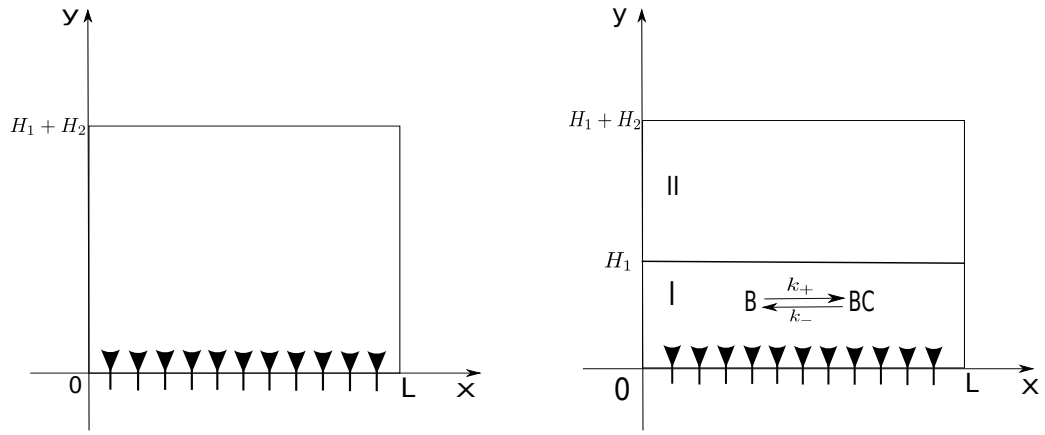

Figure 2.6: Systems with perfectly absorbing receptors.

We first estimate the first passage time for the ligand molecule to bind to receptors in system (b). Similarly to Section 2.3.1, we only have to consider the evolution of the y-coordinate of the molecule position. Let $p_{1b}^{(b)}(y, t|y_0, 0)$ ($p_{1bc}^{(b)}(y, t|y_0, 0)$) be the probability density function such that $p_{1b}^{(b)}(y, t|y_0, 0)\, dy$ ($p_{1bc}^{(b)}(y, t|y_0, 0)\, dy$) is the probability that the molecule starting at y_0 in Region I' as a molecule of species B lies in $[y, y + dy)$ as a

molecule of species B (BC) at time t without leaving Region I' before. Therefore, if $y_0 \in [0, H_1 + h]$, the governing equations for $p_{1b}^{(b)}(y,t|y_0,0)$ and $p_{1bc}^{(b)}(y,t|y_0,0)$ are the same as Eq. (2.18) except that $p_{1b}^{(b)}(y,t|y_0,0) = 0$ at the boundaries $y = 0$ and $y = H_1+h$ [3] .

Using the similar procedure in Section 6.1.2, we can obtain $p_{1b}^{(b)}(y,t|y_0,0)$ and $p_{1bc}^{(b)}(y,t|y_0,0)$. Define $S_1^{(b)}(t|y_0,0)$ as the survival probability such that the molecule starting at y_0 in Region I' is still in Region I' at time t without leaving Region I' before. We get

$$\begin{aligned} & S_1^{(b)}(t|y_0,0) \\ \equiv & \int_0^{H_1+h} \left\{ p_{1b}^{(b)}(y,t|y_0,0) + p_{1bc}^{(b)}(y,t|y_0,0) \right\} dy \\ = & \sum_{n=0}^{\infty} \frac{4 \sin \frac{(2n+1)\pi y_0}{H_1+h}}{(2n+1)\pi \upsilon_n} \\ \times & \left[e^{\lambda_{n+} t} (\upsilon_n - \omega_n^2 D_1 + k_+ + k_-) + e^{\lambda_{n-} t} (\upsilon_n + \omega_n^2 D_1 - k_+ - k_-) \right] \end{aligned}$$

where $\omega_n = \frac{(2n+1)\pi}{H_1+h}$, $\upsilon_n = \sqrt{(k_+ + k_- + \omega_n^2 D_1)^2 - 4k_- D_1 \omega_n^2}$, and $\lambda_{n\pm} = \frac{-(k_+ + k_- + \omega_n^2 D_1)^2 \pm \upsilon_n}{2}$.

Define $T_{1h}^{(b)}$ as the random variable of the time when the molecule starting at y_0 in Region I' leaves Region I' for the first time either by being absorbed at $y = 0$ or at $y = H_1 + h$. Then we have[4]

$$\begin{aligned} P\left(T_{1h}^{(b)} > t|x_0,y_0,0\right) &= S_1^{(b)}(t|y_0,0), \\ E\left[T_{1h}^{(b)}|x_0,y_0,0\right] &= \int_0^{\infty} S_1^{(b)}(t|y_0,0)\, dt \\ &= \frac{(1+K_D)(H_1+h)^2}{4D_1} \left[\frac{2y_0}{H_1+h} - \frac{1}{2} \left(\frac{2y_0}{H_1+h} \right)^2 \right] \end{aligned}$$

Define $T_{2h}^{(b)}$ as the random variable for the time when the molecule starting at y_0 in Region II' leaves Region II' for the first time. To calculate $E\left[T_{2h}^{(b)}|x_0,y_0,0\right]$, we can use the result in Section 2.3.1. The difference between Region II in Section 2.3.1 and Region II' in system (b) is that the absorbing boundary is at $y = H_1$ in Region II

[3] The boundary conditions at $y = 0$ and $y = H_1 + h$ are the homogeneous Dirichlet boundary condition.

[4] In the calculation of $E\left[T_{1h}^{(b)}|y_0,0\right]$, we use that for $x \in [0,2]$, $\sum_{j=0}^{\infty} \frac{16 \sin \frac{(2j+1)\pi x}{2}}{(2j\pi+\pi)^3} = x - \frac{x^2}{2}$.

while the absorbing boundary is at $y = H_1 - h$ in Region II'. Therefore, based on Eq. (2.23), we have

$$E\left[T_{2h}^{(b)}|y_0, 0\right] = \frac{(H_2+h)^2}{D_2}\left\{\frac{y_0-(H_1-h)}{H_2+h} - \frac{1}{2}\left(\frac{y_0-(H_1-h)}{H_2+h}\right)^2\right\}.$$

To connect the motion of the molecule between Region I' and II', we define $P_{H_1+h,0}(y_0)$ as the probability that the molecule starting at $y = y_0$ in Region I' hits $y = H_1 + h$ before getting absorbed at $y = 0$. Using the calculation in Appendix 6.1.4, we have

$$P_{H_1+h,0}(y_0) = \frac{y_0}{H_1+h}. \tag{2.32}$$

Let $T_{1,i}^{(b)}$ ($T_{2,i}^{(b)}$) be the random variable of the time that the molecule spends in Region I' (II') during its ith visit. Let $y_{1,i}$ ($y_{2,i}$) be the starting position when the molecule enters Region I' (II') for the ith time. Assume that the molecule starts at y_0. Then if $y_0 > H_1$, $y_{2,1} = y_0$ and $y_{1,1} = H_1 - h$. Similarly, if $y < H_1$, $y_{1,1} = y_0$ and $y_{2,1} = H_1 + h$. Define $T^{(b)}$ as the random variable of the time when the molecule gets absorbed by the receptors at $y = 0$. When $y_0 > H_1$, we have

$$\begin{aligned}
& E\left[T^{(b)}|y_0, 0\right] \\
= & \lim_{h\to 0}\Big\{E\left[T_{2,1}^{(b)}|y_0, 0\right] + E\left[T_{1,1}^{(b)}|H_1-h, 0\right] \\
& + \sum_{i=2}^{\infty} E\left[T_{2,i}^{(b)}|H_1+h, 0\right] + E\left[T_{1,i}^{(b)}|H_1-h, 0\right]\Big\} \\
= & \lim_{h\to 0}\Big\{E\left[T_{2h}^{(b)}|y_0, 0\right] + E\left[T_{1h}^{(b)}|H_1-h, 0\right] \\
& + \sum_{i=1}^{\infty} P_{H_1+h,0}(H_1-h)^i\left(E\left[T_{2h}^{(b)}|H_1+h, 0\right] + E\left[T_{1h}^{(b)}|H_1-h, 0\right]\right)\Big\} \\
= & \frac{(1+K_D)\tau_1}{2} + \frac{H_1H_2}{D_2} + \tau_2\left[\frac{y_0-H_1}{H_2} - \frac{1}{2}\left(\frac{y_0-H_1}{H_2}\right)^2\right].
\end{aligned} \tag{2.33}$$

When $y_0 < H_1$, we have

$$\begin{aligned}
E\left[T^{(b)}|y_0, 0\right] &= \lim_{h\to 0}\left\{E\left[T_{1h}^{(b)}|y_0, 0\right] + P_{H_1+h,0}(y_0)E\left[T^{(b)}|H_1+h, 0\right]\right\} \\
&= (1+K_D)\left(\frac{H_1y_0}{D_1} - \frac{y_0^2}{2D_1}\right) + \frac{H_2y_0}{D_2}.
\end{aligned} \tag{2.34}$$

Assuming that y_0 is uniformly distributed in $[0, H_1 + H_2]$, we have

$$\begin{aligned} E\left[T^{(b)}\right] &= \frac{1}{H_1+H_2}\int_0^{H_1+H_2} E\left[T^{(b)}|x_0, y_0, 0\right]\, dy_0 \\ &= \frac{1}{H_1+H_2}\left\{\frac{(1+K_D)(3H_2+2H_1)\tau_1}{6} + \frac{H_1H_2(H_1+2H_2)}{2D_2} + \frac{H_2\tau_2}{3}\right\}. \end{aligned}$$

In system (a) of Fig. 2.6, there is no membrane-protein layer. Let $p^{(a)}(y, t|y_0, 0)$ be the probability density function such that $p^{(a)}(y, t|y_0, 0)\, dy$ is the probability that the molecule starting at y_0 lies in $[y, y + dy)$ at time t. Then given the molecule starts from y_0 initially, the governing equation for $p^{(a)}(y, t|y_0, 0)$ is the same as Eq. (2.21) in Section 2.3.1 except that Eq. (2.21c) is replaced by $p^{(a)}(y, t|y_0, 0) = 0$ at $y = 0$. Using the same procedure to obtain $E[T_2|y_0, 0]$ and $E[T_2]$ in Section 2.3.1, we get the mean time for the ligand molecule to get absorbed in system (a) as follows:

$$E\left[T^{(a)}|y_0, 0\right] = \frac{(H_1+H_2)^2}{D_2}\left\{\frac{y_0}{H_1+H_2} - \frac{1}{2}\left(\frac{y_0}{H_1+H_2}\right)^2\right\} \tag{2.35}$$

$$E\left[T^{(a)}\right] = \frac{(H_1+H_2)^2}{3D_2}. \tag{2.36}$$

If we let $D_1 = D_2$ and $k_+ = 0$, then system (b) in Fig. 2.6-(b) becomes the same as system (a) in Fig. 2.6-(a). Hence, for any $y_0 \in [0, H_1 + H_2]$, $E\left[T^{(a)}|y_0, 0\right] = E\left[T^{(b)}|y_0, 0\right]$, which is obvious from Eq. (2.33), (2.34) and (2.35). Therefore, our approach to estimating $E\left[T^{(b)}\right]$ is consistent with the one for $E\left[T^{(a)}\right]$.

Letting $\rho = \frac{H_1}{H_2}$ and $\delta = \frac{D_1}{D_2}$, we can have the ratio of the average life time of the molecule in system (b) to the average life time in system (a) as follows:

$$\frac{E\left[T^{(b)}\right]}{E\left[T^{(a)}\right]} = \frac{2 + 3\rho(\rho+2) + \frac{1}{\delta}(1+K_D)(3\rho^2+2\rho^3)}{2(1+\rho)^3}$$

Since $\rho \ll 1$, $E[T^{(b)}]/E[T^{(a)}]$ is close to one if $(1 + K_D)/\delta$ is small. Therefore, the role of the lower layer in signaling can be important only if it can hold the ligand molecule effectively. If $K_D = 0$ and $\delta < 1$, i.e., there is no membrane protein and $D_1 < D_2$, then

$$\frac{E\left[T^{(b)}\right]}{E\left[T^{(a)}\right]} > \frac{2\rho^3+6\rho^2+6\rho+2}{2(1+\rho)^3} = 1.$$

Similarly, if $\delta = 1$ and $K_D > 0$, we have

$$\frac{E\left[T^{(b)}\right]}{E\left[T^{(a)}\right]} > \frac{2\rho^3+6\rho^2+6\rho+2}{2(1+\rho)^3} = 1.$$

Since the ligand molecule can only bind to the receptor when it is free, the membrane protein ($K_D > 0$) and slow diffusion (when $D_1 < D_2$) holds the ligand molecule from receptors and decreases the diffusion flux of the ligand towards the receptor surface, slowing the association between ligands and receptors. However, as shown in Section 2.3.2, the membrane protein and slow diffusion can increase the concentration of the ligand around the receptor surface. Therefore, if the localized ligand molecule can pass the ligand molecule directly to the receptor, the diffusion flux of the ligand towards the receptor can be increased and the association between the ligand and the receptor can be accelerated. For example, in dorsal-ventral patterning in *Drosophila*, the collagen protein can bind to Sog and to Dpp/Scw, and Sog and Dpp/Scw can bind to each other both in solution and when attached to collagen. If we consider Dpp/Scw as the ligand and Sog as the receptor, the collagen protein localizes Sog and Dpp/Scw around the embryo surface, which can increase the encounter chance of Sog and Dpp/Scw and enhance the formation of Sog/Dpp/Scw complex. Moreover, experiments have shown collagen proteins can enhance the formation of Sog/Dpp/Scw complex [53]. In the following section, we consider the case when the ligand-binding protein can transfer the ligand molecule to receptors directly.

Signaling through partially-absorbing receptors.

In this section, we assume that the membrane protein can pass the ligand molecule directly to the receptor. Moreover, when the ligand molecule is close enough to bind to receptors, we assume that the ligand molecule can bind to a receptor with a finite probability per unit time. As a result, the ligand molecule may diffuse away before it binds to the receptor. We investigate under what conditions the membrane protein can promote signaling. We find that the membrane protein has to pass the ligand molecule to the receptor fast enough, in order for the membrane protein to enhance signaling.

Furthermore, we introduce another kind of species that the membrane protein can pass the ligand molecule to, in order to study the effect of the membrane protein on signal specificity.

Here we consider four systems which have different reactions among ligand molecules, membrane proteins, and receptors. In system (a), we assume that there is no membrane protein and that the ligand molecule binds to the receptor directly. In system (b), we

assume that there are membrane proteins which can pass the ligand molecules to the receptors. In system (b), the ligand molecules can bind to the receptors only through the membrane proteins. In system (c), as in system (b), there are membrane proteins which can pass the ligand molecules to the receptors. In addition, in system (c), the ligand molecule can directly bind to the receptors. In system (d), all settings are the same as those in system (c) except that there is an additional reaction in which the membrane protein can pass the ligand molecule to another signaling pathway. We consider the mean time for the ligand molecule to bind to receptors in these four systems.

Systems (a) and (b) are described in Fig. 2.7-(a) and Fig. 2.7-(b). We denote B as the signaling ligand, BC as the complex of the membrane protein and the ligand, and BR as the ligand-bound receptor. In system (a) of Fig. 2.7, the ligand B can diffuse throughout the domain $[0, L] \times [0, H_1 + H_2]$ with diffusion coefficient D_2 and bind to the receptor on the receptor surface with rate k_a. In the system (b) of Fig. 2.7, we only allow the ligand molecule to bind to the receptors after binding to the membrane proteins in order to find the net effect of binding proteins on signaling. Then, the motion of the ligand in the system (b) is the same as that in Fig. 2.5 except that the ligand molecule cannot bind directly to the receptors and that the complex of the ligand and the membrane protein, BC, can become the ligand-bound receptor, BR, with rate k_b.

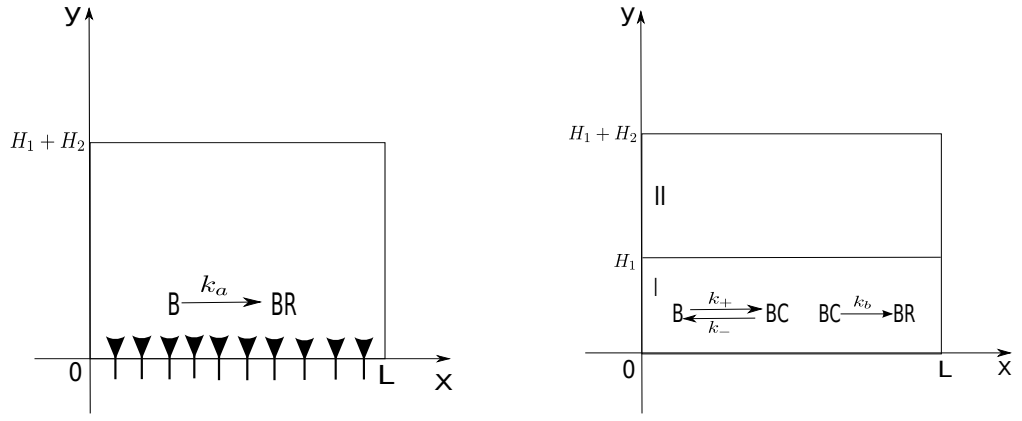

Figure 2.7: Systems with and without localization layers.

We first consider the average time for the ligand molecule to bind to the receptors in system (a). Similarly to Section 2.3.1, we only have to consider the evolution of the

y-coordinate of the molecule position. Define $p^{(a)}(y,t|y_0,0)$ as the probability density function such that $p^{(a)}(y,t|y_0,0)\,dx\,dy$ is the probability that the ligand starting at y_0 at time 0 stays at y at time t. The governing equations are

$$\frac{\partial p^{(a)}(y,t|y_0,0)}{\partial t} = D_2 \Delta p^{(a)}(y,t|y_0,0) \tag{2.37a}$$

$$p^{(a)}(y,t|y_0,0) = \delta(y-y_0), \tag{2.37b}$$

$$D_2 \frac{\partial p^{(a)}(y,t|y_0,0)}{\partial y} = k_a p^{(a)}(y,t|y_0,0), \quad \text{at } y=0, \tag{2.37c}$$

$$\frac{\partial p^{(a)}(y,t|y_0,0)}{\partial y} = 0, \quad \text{at } y = H_1+H_2. \tag{2.37d}$$

Define $T_{br}^{(a)}$ as the random variable of the time when the ligand molecule binds to the receptor in system (a). Then given that the molecule starts at y_0, the conditional expected value of $T_{br}^{(a)}$ can be derived from the following equations:

$$\frac{\partial^2 E\left[T_{br}^{(a)}|y_0,0\right]}{\partial y_0^2} = -\frac{1}{D_2} \tag{2.38a}$$

$$D_2 \frac{\partial E\left[T_{br}^{(a)}|y_0,0\right]}{\partial y_0} = k_a E\left[T_{br}^{(a)}|y_0,0\right], \quad \text{at } y_0 = 0, \tag{2.38b}$$

$$\frac{\partial E\left[T_{br}^{(a)}|y_0,0\right]}{\partial y_0} = 0, \quad \text{at } y_0 = H_1+H_2. \tag{2.38c}$$

Solving (2.38), we obtain

$$E\left[T_{br}^{(a)}|y_0,0\right] = -\frac{1}{2D_2}y_0^2 + \frac{H_1+H_2}{D_2}y_0 + \frac{H_1+H_2}{k_a}.$$

Assuming that y_0 is uniformly distributed in the domain, we have

$$E\left[T_{br}^{(a)}\right] = \frac{(H_1+H_2)^2}{3D_2} + \frac{H_1+H_2}{k_a}. \tag{2.39}$$

We then derive the average time for a ligand molecule to bind to the receptors in system (b). Similar to the systems in Section 2.3.2 and Section 2.3.3, let $[0,L]\times[0,H_1+h]$ be Region I' and $[0,L]\times[H_1-h,H_1+H_2]$ be Region II'. Define $p_{1b}^{(b)}(y,t|y_0,0)$, $p_{1bc}^{(b)}(y,t|y_0,0)$, and $p_{1br}^{(b)}(y,t|y_0,0)$ as the probability density functions such that $p_{1b}^{(b)}(y,t|y_0,0)\,dx\,dy$, $p_{1bc}^{(b)}(y,t|y_0,0)\,dx\,dy$, and $p_{1br}^{(b)}(y,t|y_0,0)\,dx\,dy$ are the probabilities that the ligand starting at y_0 in Region I' as a molecule of species B stays at y at time t as a molecule of

species B, BC or BR without leaving Region I' before time t. For $y_0 \in I'$, the governing equations are

$$\frac{\partial p_{1b}^{(b)}(y,t|y_0,0)}{\partial t} = D_1 \Delta p_{1b}^{(b)}(y,0|y_0,0) - k_+ p_{1b}^{(b)}(y,0|y_0,0) \tag{2.40a}$$

$$+ k_- p_{1bc}^{(b)}(y,0|y_0,0), \tag{2.40b}$$

$$\frac{\partial p_{1bc}^{(b)}(y,t|y_0,0)}{\partial t} = k_+ p_{1b}^{(b)}(y,0|y_0,0) - (k_- + k_b) p_{1bc}^{(b)}(y,0|y_0,0), \tag{2.40c}$$

$$\frac{\partial p_{1br}^{(b)}(y,t|y_0,0)}{\partial t} = k_b p_{1bc}^{(b)}(y,0|y_0,0), \tag{2.40d}$$

$$p_{1b}^{(b)}(y,0|y_0,0) = \delta(y-y_0), \quad p_{1bc}^{(b)}(y,0|y_0,0) = 0, \quad p_{1br}^{(b)}(y,0|y_0,0) = 0, \tag{2.40e}$$

$$\frac{\partial p_{1b}^{(b)}(y,t|y_0,0)}{\partial y} = 0, \quad \text{at } y = 0, \quad p_{1b}^{(b)}(y,t|y_0,0) = 0, \quad \text{at } y = H_1 + h. \tag{2.40f}$$

Assuming the initial position of the molecule is uniformly distributed, we obtain the mean time for the molecule to bind to the receptor in (E4) of Appendix 6.1.5 as shown below:

$$E\left[T_{br}^{(b)}\right] = \frac{H_1 H_2}{D_2 \sum_{i=0}^{\infty} A_i} \left\{ \frac{1}{2k_+ k_b} - \frac{H_1}{H_1 + H_2} \sum_{i=0}^{\infty} \frac{A_i}{(2i\pi + \pi)^2} \right\} + \frac{k_+ + k_- + k_b}{k_+ k_b} + \frac{H_2^3}{3D_2(H_1 + H_2)} \tag{2.41}$$

where $A_i = \frac{1}{k_+ k_b + (\frac{2i\pi+\pi}{2H_1})^2 D_1 (k_- + k_b)}$.

We apply the system (a) and (b) to the biological system of dorsal-ventral patterning in *Drosophila*, in which BMP is the signaling ligand, SBP acts as the membrane protein, and the BMP receptor is the receptor [30, 5]. We compute $E\left[T_{br}^{(a)}\right]$ in Eq. (2.39) and $E\left[T_{br}^{(b)}\right]$ in (2.41) using the parameters given in Table 2.3.

Parameters	D_2	D_1	H_2	H_1	k_a	k_-
Values	73 $\frac{\mu m^2}{sec}$	0.73 $\frac{\mu m^2}{sec}$	0.45 μm	0.05 μm	0.53 $\frac{\mu m}{sec}$	2 $\frac{1}{sec}$

Table 2.3: The parameters for $E(T_{br}^{(a)})$ and $E(T_{br}^{(b)})$ in Fig. 2.7.

In Fig. 2.8, we compare $E\left[T_{br}^{(a)}\right]$ and $E\left[T_{br}^{(b)}\right]$ with different values for k_+ and k_b. Based on whether $E\left[T_{br}^{(a)}\right] > E\left[T_{br}^{(b)}\right]$ or $E\left[T_{br}^{(a)}\right] < E\left[T_{br}^{(b)}\right]$, we determine whether the ligand-binding proteins promote or inhibit signaling. In Fig. 2.8, $E\left[T_{br}^{(b)}\right]$ decreases as k_b and k_+ increase. In Fig. 2.8-(a), where k_b is small, the binding reaction will always inhibit signaling. This is because the membrane protein holds ligand molecules from receptors. Furthermore, in Fig. 2.8-(b), where k_+ is small, the binding reaction will always inhibit signaling. This is because it takes longer for the ligand molecule to bind to membrane proteins than binding to receptors directly. Therefore, when $k_b = 2.7\, sec^{-1}$ in Fig. 2.8-(c), there is a threshold of k_+ for $E\left[T_{br}^{(b)}\right]$ to be less than $E\left[T_{br}^{(a)}\right]$. If k_+ is smaller than this threshold, it takes less time for the ligand to bind to the receptor directly than through binding to membrane proteins and in this case, the ligand-binding protein acts as an inhibitor. If k_+ is bigger than the threshold, i.e., the ligand-binding protein recruits the ligand molecule fast enough, it takes less time for the ligand to bind to the receptor through the membrane protein. In this case, the membrane protein will promote signaling. Similarly, k_b should be larger than the threshold to enhance signaling in Fig. 2.8-(d).

In system (b), the ligand molecule first binds to the membrane protein and then gets transfered to receptors. The association between ligands and receptors involves two steps, as what is assumed in dimensionality reduction. In the system with dimensionality reduction, people assume that the ligand molecule first performs three-dimensional diffusion until it hits the cell surface and then the ligand molecule performs a two-dimensional diffusion to approach receptors on the cell surface. As suggested in [45] and [46], the enhancing effect of dimensionality reduction on signaling is very little when receptors are perfectly absorbing. Our estimation of the expected times in system (a) and (b) can help us understand their conclusion. System (b) can be considered as the system with dimensional reduction, and system (a) can be considered as the three-dimensional direct diffusion to receptors. Letting k_+ go to infinity, Eq. (2.41) gives

$$\lim_{k_+\to\infty} E\left[T_{br}^{(b)}\right] \;=\; \frac{1}{k_b} + \frac{H_2^3}{3D_2(H_1+H_2)}.$$

Then, k_b becomes the effective rate for the ligand molecule to bind to the receptor on the cell membrane. In order that the surface diffusion combined with three-dimensional

diffusion is favorable over the free three-dimensional diffusion to receptors,

$$\lim_{k_+\to\infty} E\left[T_{br}^{(b)}\right] < E\left[T_{br}^{(a)}\right],$$

which leads to the following inequality:

$$\frac{1}{k_b} < \frac{H_1^3}{3D_2(H_1+H_2)} + \frac{H_1H_2}{D_2} + \frac{H_1+H_2}{k_a}. \tag{2.42}$$

Then, as k_a increases to infinity, the region for k_b to satisfy inequality (2.42)) becomes smaller. Therefore, the assumption that the receptors are perfectly absorbing gives a restrict condition for the reduction of dimensionality to enhance signaling.

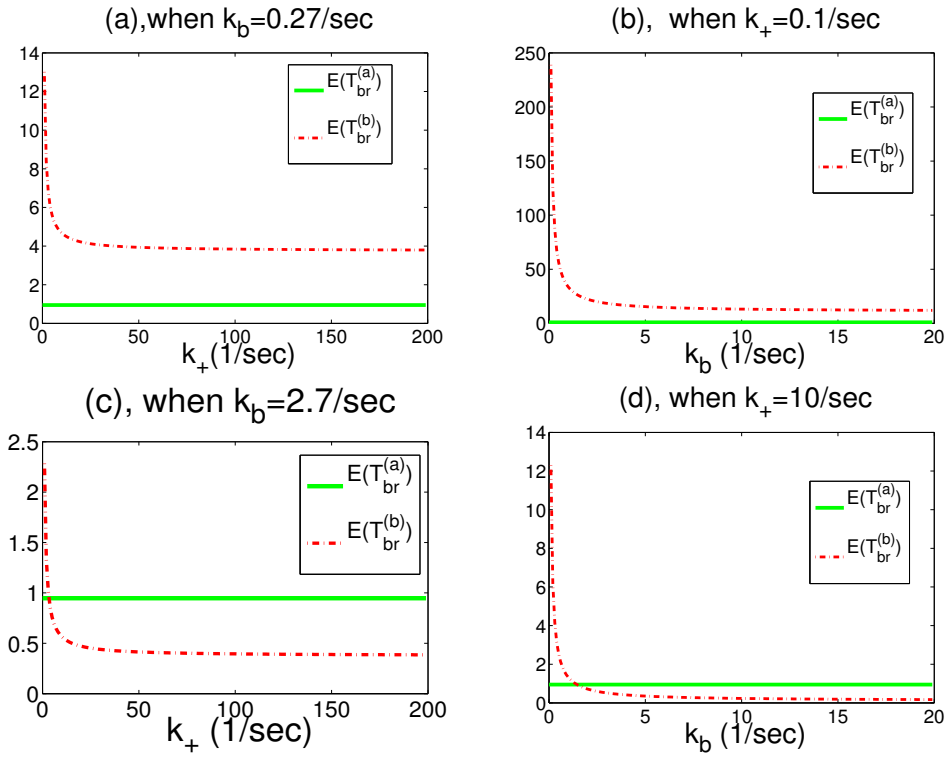

Figure 2.8: The mean time for the ligand to bind to the receptor in system (a) and (b)

Next, we consider system (c) in which we add the direct association between ligands and receptors to system (b) of Fig. 2.7. In the lower layer, the ligand B can bind to the receptor with rate k_{ac}. Define $T_{br}^{(c)}$ as the random variable of the time when the ligand molecule binds to the receptors in system (c). Similarly as in system (b), we assume

that the initial position of the ligand molecule is uniformly distributed in the system and compute the expected value of $T_{br}^{(c)}$ in system (c) as follows:

$$E\left[T_{br}^{(c)}\right] = \frac{H_1 H_2}{D_2 \sum_{i=0}^{\infty} V_i}\left\{\frac{1}{2(k_{ac}k_b + k_{ac}k_- + k_+ k_b)} - \frac{H_1}{H_1+H_2}\sum_{i=0}^{\infty}\frac{4V_i}{(2i\pi+\pi)^2}\right\} + \frac{k_+ + k_b + k_-}{k_{ac}k_b + k_{ac}k_- + k_+k_b} + \frac{H_2^3}{3D_2(H_1+H_2)}, \quad (2.43)$$

where

$$V_i = \frac{1}{k_{ac}k_b + k_{ac}k_- + k_+k_b + \left(\frac{2i\pi+\pi}{2H_1}\right)^2 D_1(k_b+k_-)}$$

.

If there is no binding layer, then system (c) should be the same as system (a). Therefore, letting k_+ go to zero and letting H_1 go to zero in Eq. (2.39) and (2.43), we should have

$$\lim_{H_1\to 0}\lim_{k_+\to 0} E\left[T_{br}^{(c)}\right] = \lim_{H_1\to 0} E\left[T_{br}^{(a)}\right]. \quad (2.44)$$

Using Eq. (2.44), we estimate the reaction rate of the ligand binding to the receptors directly in system (c). Assuming $\lim_{H_1\to 0}\frac{H_1}{D_1} = G \neq 0$,from Eq. (2.44) we get

$$k_a = \frac{k_{ac}H_2}{\frac{H_2}{D_2 G}+1}. \quad (2.45)$$

In the Robin boundary condition of Eq. (2.37) for system (a),

$$D_2\frac{\partial p^{(a)}(y,t|y_0,0)}{\partial y} = k_a p^{(a)}(y,t|y_0,0)$$

at $y = 0$. In Eq. (2.45), k_a is proportional to the reaction rate between the receptor and the ligand molecule, which implies that the faster the receptor surface absorbs the ligand, the sharper the concentration gradient of the ligand in the system. H_1 can be considered as the capture radius of the receptor and D_1 is the diffusion constant of the ligand inside the capture region of receptors. Therefore, Eq. (2.45) shows that the larger the capture radius of the receptor or the more slowly the ligand molecule moves in the capture region, the faster the ligand molecule can be caught by the receptor surface. The dependence of k_a on the slow diffusion near receptors indicates the effect

of localization on the association reaction between receptors and ligands, i.e., the more slowly the ligand molecule diffuses in the capture region, the bigger chance the ligand molecule has to get absorbed before diffusing away. Furthermore, if we consider the reaction between the receptor and the ligand as a bimolecular reaction, Eq. (2.45) also implies that the reaction rate between two molecules is an increasing function of their relative diffusion constant when two molecules are far away from each other, but is a decreasing function of their relative diffusion constant when they are close enough.

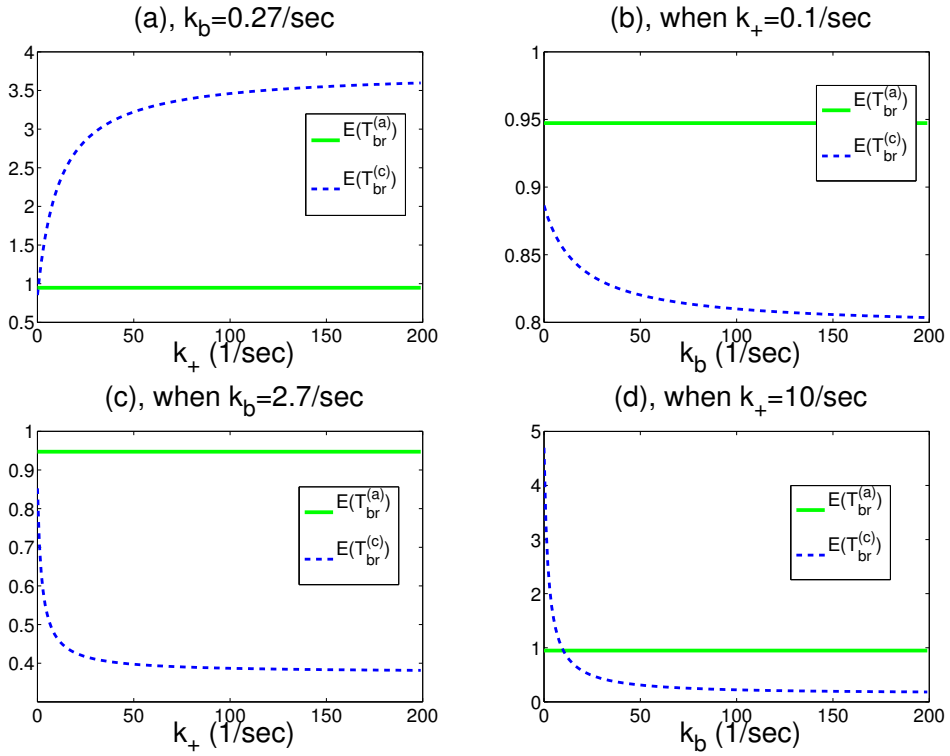

Figure 2.9: The mean time for the ligand to bind to the receptor in system (a) and (c)

Using the parameters given in Table 2.3 in Eq. (2.45) and approximating G by $\frac{H_1}{D_1}$, we get $k_{ac} = 1.28\, sec^{-1}$. Using k_{ac}, we compare the expected time for the ligand molecule to bind to the receptor in system (a) and system (c). As shown in Fig. 2.9-(a), when $k_b = 0.27\, sec^{-1} < k_{ac}$, $E\left[T_{br}^{(c)}\right]$ increases as k_+ increases. When k_b is less than k_{ac}, the binding protein inhibits signaling by holding the ligand molecules from the receptors. Therefore, increasing k_+ promotes competition between the membrane

proteins and the receptors for ligand molecules, where the membrane protein inhibits the association between the ligand and the receptor. However, in Fig. 2.9-(c), when $k_b = 2.7\, sec^{-1} > k_{ac}$, $E\left[T_{br}^{(c)}\right]$ decreases as k_+ increases. If k_b is larger than k_{ac}, it takes less time for the ligand molecule to bind through the membrane protein to the receptors than to bind directly to the receptors by itself. Then, increasing k_+ will enhance the promoting effect of the ligand-binding protein on signaling.

In Fig. 2.9-(b), when $k_+ = 0.1\, sec^{-1} \ll k_{ac}$, it is much easier for the ligand molecule to bind to the receptor than to the ligand-binding protein. Therefore, increasing k_b does not change $E\left[T_{br}^{(c)}\right]$ very much. In Fig. 2.9-(d), when $k_+ = 10\, sec^{-1} > k_{ac}$, there is a threshold of k_b where $E\left[T_{br}^{(a)}\right] = E\left[T_{br}^{(c)}\right]$. In order that the ligand-binding proteins enhance signaling, k_b has to be larger than the threshold.

In conclusion, to enhance signaling, k_b has to be large enough so that the ligand-binding proteins do not sequester the ligands from the receptors. At the same time, k_+ has to be large enough so that the ligand-binding protein can catch the ligand molecules and localize the ligand molecules around the receptors efficiently.

One example of increasing k_+ is the increasing level of SBP in dorsal surface patterning in *Drosophila*, where SBP is produced in proportion to the level of the ligand-bound receptors. Then increasing the concentration of SBP will increase the rate for the membrane protein to catch the ligand molecule. However, SBP can get internalized into the embryo, which remove signaling molecules from the system. As the concentration of SBP increases, the amount of removed signaling molecules increases. As a result, the signal can be inhibited when the level of SBP is high enough.

In addition to SBP, there are other proteins such as scaffold protein that can collect signaling molecules and pass them to different signal pathways. Now, we consider the case the role of membrane proteins in signal specificity. In addition to receptors in the system, we assume that the ligand molecule can be passed by the membrane protein to a molecule of another species to become BD. Once the ligand molecule becomes species BD, it will be removed from the system. Then in system (d), we add the following reaction occurring in the lower layer to system (c):

$$BC \xrightarrow{k_d} BD.$$

Other reactions and diffusions in system (d) are the same as those in system (c). To

estimate the extent to which the membrane protein removes the ligand molecules , we look at the probability that the ligand molecule gets removed before binding to the receptors in system (d). Let p_{BD} as the probability that the ligand molecule gets removed before binding to any receptors. Since the reaction from BC to BD is irreversible, we consider the probability that the ligand molecule becomes a molecule of species BD eventually. Therefore, we estimate p_{BD} at steady state as follows:

$$p_{BD} = \frac{k_+ k_d}{k_{ac}(k_- + k_b + k_d) + k_+(k_b + k_d)}.$$

Obviously, p_{BD} is an increasing function of k_+ and k_d. As the concentration of the membrane protein increases, the fraction of the ligand molecules removed by the membrane proteins increases. Moreover, p_{BD} is a decreasing function of k_b, which is proportional to the concentration of free receptors. Then, as the number of ligand-bound receptors increases, k_b decreases and p_{BD} increases. Therefore, the increase of the membrane protein and the consequent increase of the ligand-bound receptors make more ligand molecules get removed before binding to the receptor.

Chapter 3

Noise propagation in transcription and translation processes

3.1 Introduction

The appropriate regulation of gene expression is essential for cells to proliferate, adapt to environmental conditions, and function within organisms. However, reactions during the process of gene expression often involve small numbers of molecules, leading to large fluctuations [8, 55, 56, 57]. Stochasticity in gene expression has been identified as a major factor underlying the observed phenotypic variability of genetically identical cells [58]. Therefore, understanding how noise propagates in gene expression processes is very important in systems biology.

Stochasticity in gene expression comes from the transcription and translation levels. Transcription happens through three steps: initiation, elongation and termination. During initiation, transcription factors can regulate the recruitment of RNA polymerases (RNAP) to promoters by binding to specific DNA sequences. As a result, the promoter switches between active and inactive states, depending on whether a transcription factor is on or off its functional site of the DNA sequence. After binding to promoters, RNAP opens the double helix and uncovers the template strand for elongation. Elongation

begins with the formation of the transcription elongation complex (TEC) which consists of the RNAP, the DNA and the nascent mRNA. The TEC slides along the DNA sequence and extends the transcript one nucleotide each time until the TEC destabilizes from the DNA sequence. After destabilization, the mRNA is released from the DNA sequence and the transcription process terminates.

Stochasticity in transcription can arise in several steps. For example, the switch of the promoter status is stochastic, due to the small numbers of gene copies and transcription factors. In bacteria, gene copies typically number in one or two, and the number of transcription factors is in tens [59]. Moreover, during elongation, the motion of the TEC can be interrupted by random pauses. In fact, the movement of the TEC along the DNA sequence is a series of bursts of rapid and continuous elongation interrupted by pauses [60]. The lifetime and location of the TEC pauses along the DNA sequence are stochastic and biased by the template sequence [60, 61, 62]. It has been suggested both the switch of the promoter status and TEC pausing can lead to the burst of mRNA production, i.e. the amount of mRNA produced is much larger in some time intervals than the production in other time intervals[63]. How the fluctuations in the promoter status and TEC motions affect the production bursts is very important for understanding stochasticity in gene expression.

Previous studies have been only focused on one of the initiation and elongation steps. Most of the models of the initiation step consist of a telegraph input for the switch of the promoter status and a simple first-order reaction for the production of mRNA[64, 65, 66, 67]. None of them has investigated how the motion of the TEC in the elongation step inherits the stochastic fluctuations from the random switch of the promoter status. For the elongation step, Voliotis et al and Depken et al have focused on the DNA sequence with only one TEC on it and studied the lifetime of the TEC pause [60, 68]. For the DNA sequences with multiple TEC's on them, Voliotis et al and Dobrzynski and Bruggenman have used stochastic simulations to show how the pause leads to the bursts of mRNA production [63, 68]. However, none of them have given any analytical results for the level of mRNA produced in a given time interval.

In this chapter, our objective is to understand how the fluctuations in the promoter status and the TEC motion affect the level of the mRNA produced in a given time interval. To realize our goal, we have studied: 1) the number of mRNAs produced

from the TEC with a random telegraph forming rate and a deterministic motion along a chain in Section 3.2.1; 2) the number of mRNAs produced from the TEC with a Poisson production and random pauses at specific sites of a sequence in Section 3.2.2.

3.2 Reaction chains driven by a random telegraph signal

3.2.1 Noise propagation in linear and deterministic elongation chains

Formulation of the deterministic chain

In this section, we study the statistics of mRNA produced from the TEC with a random production and deterministic downstream steps in a chain as shown in Fig. 3.1. In Fig. 3.1, the TEC arrives at X_1 with rate $S(t)$ and jumps from X_i to X_{i+1} with rate μ until it reaches R.

$$\xrightarrow{S(t)} X_1 \xrightarrow{\mu} X_2 \xrightarrow{\mu} X_3 \cdots X_n \xrightarrow{\mu} R$$

Figure 3.1: The deterministic elongation chain.

A TEC arrives at the 1st site of the DNA sequence and proceeds along the DNA sequence until the terminal site to produce a mRNA. Therefore, we can consider X_i as the TEC at the ith site and R as mRNA. To study a biological system with a large number of identical cells, we let $x_i(t)$ be the concentration of X_i at time t and $r(t)$ be the concentration of the mRNA produced before t. Assuming $x_i(t) = 0$ for all i's and $r(t) = 0$ at time $t = 0$, the kinetics in Fig. 3.1 lead to the following system of stochastic ordinary differential equations:

$$\begin{aligned} \dot{x}(t) &= Ax(t) + S(t)e_1, \\ \dot{r}(t) &= \mu x_n(t), \\ x(0) &= 0, \\ r(0) &= 0, \end{aligned} \tag{3.1}$$

where

$$x(t) = (x_1(t), x_2(t), \cdots, x_n(t))^T,$$

$$A = \begin{pmatrix} -\mu & & & & \\ \mu & -\mu & & & \\ & \mu & -\mu & & \\ & & \ddots & \ddots & \\ & & & \mu & -\mu \end{pmatrix}_{n\times n},$$

and e_k is a n-length vector such that its kth component is 1 and all other components are zero.

During transcription, the recruitment rate of RNAP depends on the promoter status, which switches randomly between the active and inactive states. Therefore, we assume $S(t)$ is a random process switching between s_0 and s_1. In particular, $S(t)$ is a 2-state Markov chain, with exponentially distributed waiting times between jumps. The process $S(t)$ can be characterized by its infinitesimal generator

$$Q = \begin{pmatrix} -\lambda_0 & \lambda_1 \\ \lambda_0 & -\lambda_1 \end{pmatrix}$$

and probability transition matrix

$$P(t) = \frac{1}{\lambda_0+\lambda_1}\begin{pmatrix} \lambda_1+\lambda_0 e^{-(\lambda_0+\lambda_1)t} & \lambda_1-\lambda_1 e^{-(\lambda_0+\lambda_1)t} \\ \lambda_0-\lambda_0 e^{-(\lambda_0+\lambda_1)t} & \lambda_0+\lambda_1 e^{-(\lambda_0+\lambda_1)t} \end{pmatrix},$$

which satisfies the Kolmogorov differential equation $P'(t) = QP(t)$, and the initial condition $P(0) = I$ [65]. Let $p(t) = (p_0(t), p_1(t))^T$ be the probability vector such that the probabilities of $S(t) = s_0$ and $S(t) = s_1$ are $p_0(t)$ and $p_1(t)$ at time t, respectively. Then $p(t) = P(t)p(0)$. If $p(0) = (\frac{\lambda_1}{\lambda_0+\lambda_1}, \frac{\lambda_0}{\lambda_0+\lambda_1})$, then $p(t) = (\frac{\lambda_1}{\lambda_0+\lambda_1}, \frac{\lambda_0}{\lambda_0+\lambda_1})$. For simplicity, we assume $p(0) = (\frac{\lambda_1}{\lambda_0+\lambda_1}, \frac{\lambda_0}{\lambda_0+\lambda_1})$ for the following calculation.[1] Then, we have

$$\begin{aligned} E(S(t)) &= \frac{s_0\lambda_1+s_1\lambda_0}{\lambda_1+\lambda_0}, \\ E(S(t)S(\tau)) &= \left(\frac{s_0\lambda_1+s_1\lambda_0}{\lambda_1+\lambda_0}\right)^2 + \frac{\lambda_0\lambda_1(s_0-s_1)^2 e^{-(\lambda_0+\lambda_1)|t-\tau|}}{(\lambda_1+\lambda_0)^2}. \end{aligned}$$

The first two moments of X_n

From Eq. (3.1), we have

$$x(t) = \int_0^t S(s)e^{A(t-s)}e_1 ds,$$

[1] Please note that our method can be extended to any value of p_0.

which leads to

$$\begin{aligned} x_k(t) &= x(t)\cdot e_k \\ &= \int_0^t e^{-\mu(t-s)}\frac{\mu^{k-1}(t-s)^{k-1}}{(k-1)!}S(s)ds \\ r(t) &= \int_0^t \mu x_n(s)ds. \end{aligned}$$

Therefore,

$$\begin{aligned} E(x_k(t)) &= \int_0^t e^{-\mu(t-s)}\frac{\mu^{k-1}(t-s)^{k-1}}{(k-1)!}E(S(s))ds, \\ &= \frac{s_0\lambda_1+s_1\lambda_0}{(\lambda_1+\lambda_0)\mu}\left(1-e^{-\mu t}\sum_{i=0}^{k-1}\frac{(\mu t)^i}{i!}\right). \\ Var(x_k(t)) &= E(x_k^2(t))-E^2(x_k(t)) \\ &= \frac{2\lambda_0\lambda_1(s_0-s_1)^2}{\mu^2(\lambda_1+\lambda_0)^2} \\ &\quad\times\int_0^{\mu t}\frac{x^{k-1}e^{-\left(1+\frac{\lambda_0+\lambda_1}{\mu}\right)x}}{(k-1)!}\int_0^x\frac{y^{k-1}e^{-\left(1-\frac{\lambda_0+\lambda_1}{\mu}\right)y}}{(k-1)!}dydx. \end{aligned} \tag{3.2}$$

Proposition 1 *Defining* $C_n^k = \begin{pmatrix} n \\ k \end{pmatrix}$, *we have*

1. $\lim_{t\to\infty} E(x_k(t)) = \frac{s_0\lambda_1+s_1\lambda_0}{(\lambda_1+\lambda_0)\mu}$;

2. $\lim_{t\to\infty} Var(x_k(t)) = \frac{\lambda_0\lambda_1(s_1-s_0)^2}{\mu^2(\lambda_0+\lambda_1)^2}\sum_{i=0}^{k-1}\frac{C_{i+k-1}^{k-1}\mu^{k-i}}{2^{i+k-1}(\lambda_0+\lambda_1+\mu)^{k-i}}$ *exponentially;*

3. $$\lim_{k\to\infty}\lim_{t\to\infty} Var(x_k(t)) = 0;$$

4. *if* $\lambda_0+\lambda_1 > \mu$,

$$\frac{\mu^2}{(\lambda_0+\lambda_1)^2-\mu^2}\lim_{t\to\infty} Var(x_k(t)) + \lim_{t\to\infty} Var(x_{k+1}(t))$$

decreases as k *increases;*

5. *if* $\lambda_0 + \lambda_1 < \mu$,

$$\frac{\mu^2}{\mu^2 - (\lambda_0+\lambda_1)^2} \lim_{t\to\infty} Var(x_k(t)) - \lim_{t\to\infty} Var(x_{k+1}(t))$$

decreases as k *increases.*

Proof : The first assertion is easy to see. Here we focus on the remaining assertions. Define

$$V(t) \equiv \int_0^{\mu t} \frac{x^{k-1} e^{-\left(1+\frac{\lambda_0+\lambda_1}{\mu}\right)x}}{(k-1)!} \int_0^x \frac{y^{k-1} e^{-\left(1-\frac{\lambda_0+\lambda_1}{\mu}\right)y}}{(k-1)!} dydx.$$

To show the exponential convergence of $Var(x_k(t))$, it suffices to show that

$$\frac{dV(t)}{dt} \to 0$$

exponentially as $t \to \infty$.

$$\begin{aligned}
\frac{dV(t)}{dt} &= \frac{\mu(\mu t)^{k-1} e^{-(\mu+\lambda_0+\lambda_1)t}}{(k-1)!} \int_0^{\mu t} \frac{y^{k-1} e^{\left(1-\frac{\lambda_0+\lambda_1}{\mu}\right)y}}{(k-1)!} dy \\
&= \frac{\mu(\mu t)^{k-1}}{(k-1)!(\mu-\lambda_0-\lambda_1)^k} \left[e^{-(\mu+\lambda_0+\lambda_1)t} - e^{-2\mu t} \sum_{i=0}^{k-1} \frac{(\mu-\lambda_0-\lambda_1)^i t^i}{i!} \right]
\end{aligned}$$

So $Var(x_k(t))$ converges exponentially. Letting $t \to \infty$ in Eq. (3.2), we have

$$\begin{aligned}
\lim_{t\to\infty} Var(x_k(t)) &= \frac{2\lambda_0\lambda_1(s_0-s_1)^2}{\mu^2(\lambda_1+\lambda_0)^2} \int_0^\infty \frac{x^{k-1} e^{-\left(1+\frac{\lambda_0+\lambda_1}{\mu}\right)x}}{(k-1)!} \int_0^x \frac{y^{k-1} e^{-\left(1-\frac{\lambda_0+\lambda_1}{\mu}\right)y}}{(k-1)!} dydx \\
&= \frac{2\lambda_0\lambda_1(s_0-s_1)^2}{\mu^2(\lambda_1+\lambda_0)^2} \int_0^\infty \frac{y^{k-1} e^{-\left(1-\frac{\lambda_0+\lambda_1}{\mu}\right)y}}{(k-1)!} \int_y^\infty \frac{x^{k-1} e^{-\left(1+\frac{\lambda_0+\lambda_1}{\mu}\right)x}}{(k-1)!} dxdy \\
&= \frac{2\lambda_0\lambda_1(s_0-s_1)^2}{\mu^2(\lambda_1+\lambda_0)^2} \sum_{i=0}^{k-1} \frac{\mu^{k-i}}{i!(\mu+\lambda_0+\lambda_1)^{k-i}} \int_0^\infty \frac{e^{-2y} y^{k+i-1}}{(k-1)!} dy \\
&= \frac{2\lambda_0\lambda_1(s_0-s_1)^2}{\mu^2(\lambda_1+\lambda_0)^2} \sum_{i=0}^{k-1} \frac{\mu^{k-i}(k+i-1)!}{2^{k+i}(\mu+\lambda_0+\lambda_1)^{k-i} i!(k-1)!} \\
&= \frac{\lambda_0\lambda_1(s_1-s_0)^2}{\mu^2(\lambda_0+\lambda_1)^2} \sum_{i=0}^{k-1} \frac{C_{i+k-1}^{k-1} \mu^{k-i}}{2^{i+k-1}(\lambda_0+\lambda_1+\mu)^{k-i}}
\end{aligned}$$

To verify the last three assertions, we define

$$\theta \equiv \frac{\lambda_0+\lambda_1}{\mu}$$

and

$$A_k(\theta) \equiv \frac{1}{2^k(1+\theta)^{k+1}} \sum_{i=0}^{k} \frac{(1+\theta)^i C_{i+k}^k}{2^i}.$$

Then

$$\lim_{t\to\infty} Var(x_{k+1}(t)) = A_k(\theta) \times \frac{\lambda_0\lambda_1(s_0-s_1)^2}{\mu^2(\lambda_1+\lambda_0)^2}.$$

Furthermore, for any θ,

$$\begin{aligned}
A_{k+1}(\theta) &= \frac{1}{2^{k+1}(1+\theta)^{k+2}} \sum_{i=0}^{k+1} \frac{(1+\theta)^i C_{i+k+1}^{k+1}}{2^i} \\
&= \frac{1}{2^{k+1}(1+\theta)^{k+2}} + \frac{1}{2^{k+1}(1+\theta)^{k+2}} \sum_{i=1}^{k+1} \frac{(1+\theta)^i \left(C_{i+k}^{k+1} + C_{i+k}^k\right)}{2^i} \\
&= \frac{1}{2^{k+1}(1+\theta)^{k+2}} \sum_{i=0}^{k} \frac{(1+\theta)^i C_{i+k}^k}{2^i} + \frac{C_{2k+1}^k}{2^{2k+2}(1+\theta)} \\
&\quad + \frac{1}{2^{k+1}(1+\theta)^{k+2}} \sum_{i=1}^{k+1} \frac{(1+\theta)^i C_{i+k}^{k+1}}{2^i} \\
&= A_k(\theta) \times \frac{1}{2(1+\theta)} + \frac{C_{2k+1}^k}{2^{2k+2}(1+\theta)} + \frac{1}{2^{k+1}(1+\theta)^{k+2}} \sum_{i=0}^{k} \frac{(1+\theta)^{i+1} C_{i+k+1}^{k+1}}{2^{i+1}} \\
&= A_k(\theta) \times \frac{1}{2(1+\theta)} + \frac{C_{2k+1}^k}{2^{2k+2}(1+\theta)} + A_{k+1}(\theta) \times \frac{(1+\theta)}{2} - \frac{C_{2k+2}^{k+1}}{2^{2k+3}} \\
&= A_k(\theta) \times \frac{1}{2(1+\theta)} + A_{k+1}(\theta) \times \frac{(1+\theta)}{2} - \frac{C_{2k+1}^k \theta}{2^{2k+2}(1+\theta)},
\end{aligned}$$

where $C_{2k+2}^{k+1} = C_{2k+1}^k + C_{2k+1}^{k+1} = 2C_{2k+1}^k$ is used in the last step. Therefore,

1. if $\theta = 1$,

$$A_k(1) = \frac{C_{2k+1}^k}{2^{2k+1}};$$

2. if $\theta \neq 1$,

$$A_{k+1}(\theta) = A_k(\theta) \times \frac{1}{1-\theta^2} - A_k(1) \times \frac{\theta}{(1-\theta^2)}. \tag{3.3}$$

Then,

$$A_k(1) = \frac{C_{2k+1}^{k+1}}{2^{2k+1}} < \frac{C_{2k+2}^{k+1}}{2^{2k+1}}$$

Stirling's approximation shows that

$$C_{2k+2}^{k+1} \sim \frac{2^{2k+2}}{\sqrt{(k+1)\pi}}$$

as $k \to \infty$. So $A_k(1) \to 0$ as $k \to \infty$. Moreover, it is easy to see that

$$\frac{A_k(1)}{A_{k+1}(1)} = \frac{2(k+2)}{2k+3} > 1.$$

So $A_k(1)$ decreases as k increases.

Since $A_k(\theta)$ is a decreasing function of θ and $A_k(\theta) > 0$, $\lim_{k\to\infty} A_k(1) = 0$ leads to $\lim_{k\to\infty} A_k(\theta) = 0$ for $\theta > 1$. To prove $\lim_{k\to\infty} A_k(\theta) = 0$ for $\theta < 1$, we first assume that when $\theta < 1$ there exists a nonnegative number $\varepsilon(\theta)$ such that $A_k(\theta) > \varepsilon(\theta)$ for all k's. We show the assumption leads to a contradictory. Using Eq. (3.3), we have

$$\begin{aligned}
A_{k+m}(\theta) &= A_{k+m-1}(\theta) \times \frac{1}{1-\theta^2} - A_{k+m-1}(1) \times \frac{\theta}{(1-\theta^2)} \\
&= A_{k+m-2}(\theta) \times \frac{1}{(1-\theta^2)^2} - A_{k+m-2}(1) \times \frac{\theta}{(1-\theta^2)^2} - A_{k+m-1}(1) \times \frac{\theta}{(1-\theta^2)} \\
&\quad \cdots \\
&= A_k(\theta) \times \frac{1}{(1-\theta^2)^m} - \sum_{i=0}^{m-1} A_{k+i}(1) \times \frac{\theta}{(1-\theta^2)^{m-i}} \\
&> \varepsilon(\theta) \times \frac{1}{(1-\theta^2)^m} - \sum_{i=0}^{m-1} A_k(1) \times \frac{\theta}{(1-\theta^2)^{m-i}},
\end{aligned}$$

since $A_k(1)$ decreases as k increases. When k is large enough, Stirling's approximation leads to

$$\begin{aligned}
A_{k+m}(\theta) &> \varepsilon(\theta) \times \frac{1}{(1-\theta^2)^m} - \frac{\theta}{\sqrt{k}} \sum_{i=0}^{m-1} \frac{1}{(1-\theta^2)^{m-i}} \\
&= \varepsilon(\theta) \times \frac{1}{(1-\theta^2)^m} - \frac{1}{\theta(1-\theta^2)^{m-1}\sqrt{k}} + \frac{1}{\theta\sqrt{k}} - \frac{\theta}{\sqrt{k}} \\
&= \frac{1}{(1-\theta^2)^{m-1}} \left(\frac{\varepsilon(\theta)}{1-\theta^2} - \frac{1}{\theta\sqrt{k}} \right) + \frac{1}{\theta\sqrt{k}} - \frac{\theta}{\sqrt{k}}
\end{aligned}$$

k can be chosen large enough so that $\frac{\varepsilon(\theta)}{1-\theta^2} - \frac{1}{\theta\sqrt{k}} > 0$. Then letting $m \to \infty$ leads to $A_{k+m}(\theta) \to \infty$. However, $A_k(\theta) \leqslant 1$. Letting $\theta = 0$ in Eq. (3.3) gives $A_{k+1}(0) = A_k(0)$.

$A_k(0) = A_1(0) = 1$ for all k's. Since $A_k(\theta)$ is a decreasing function of θ, $A_k(\theta) < 1$ for $\theta > 0$. Then the third assertion is proved.

Moreover, if $\theta > 1$, Eq. (3.3) leads to

$$A_k(1) \times \frac{\theta}{(\theta^2 - 1)} = A_{k+1}(\theta) + A_k(\theta) \times \frac{1}{\theta^2 - 1}.$$

Since $A_k(1)$ decreases as k increases, $A_{k+1}(\theta) + A_k(\theta) \times \frac{1}{\theta^2-1}$ decreases as k increases. Therefore, the fourth assertion is verified. Similarly, if $\theta < 1$, the fifth assertion can be proved.

In the above proof, $A_k(0) = 1$ leads to the following equation

$$\sum_{i=0}^{k} \frac{C_{i+k}^{k}}{2^i} = 2^k.$$

Moreover, $\lim_{k\to\infty} \lim_{t\to\infty} Var(x_k(t)) = 0$ indicates that the fluctuations can be ignored when the length of the reaction chain is long enough. This implies that noise may be attenuated along the deterministic chain. Furthermore, when $\lambda_0 + \lambda_1 > \mu$, the fact that increasing k decreases

$$\frac{\mu^2}{(\lambda_0 + \lambda_1)^2 - \mu^2} \lim_{t\to\infty} Var(x_k(t)) + \lim_{t\to\infty} Var(x_{k+1}(t))$$

also implies the attenuation of noise. To understand why the variance approaches zero as $k \to \infty$, we can consider a molecule whose arrival time at X_1 is exponentially distributed with rate s. The molecule jumps from X_i to X_{i+1} at rate μ. Then the time for the molecule to reach X_k increases linearly as k increases. The fluctuations in the arrival time at X_k comes from the fluctuations in the arrival time at X_1. Therefore, the ratio of the fluctuations to the arrival time at X_k decreases as k increases.

The first two moments of R

Using $r(t) = \int_0^t \mu x_n(s)ds$ and following the procedure of calculating $E(x_k(t))$ and $Var(x_k(t))$, we obtain the first two moments of $r(t)$ as follows:

$$E(r(t)) = \frac{s_0\lambda_1 + s_1\lambda_0}{(\lambda_1 + \lambda_0)} \left[t - \frac{n}{\mu} + \frac{e^{-\mu t}}{\mu} \sum_{i=0}^{n-1} \frac{(n-i)(\mu t)^i}{i!} \right]$$

$$
\begin{aligned}
Var(r(t)) &= \frac{\lambda_0\lambda_1(s_0-s_1)^2}{(\lambda_1+\lambda_0)^2}\left\{\frac{2t}{(\lambda_0+\lambda_1)}-\frac{4n}{\mu(\lambda_0+\lambda_1)}-\sum_{i=0}^{n-1}\sum_{j=0}^{n-1}\sum_{b=0}^{j}\frac{C_{i+b}^{i}\mu^{j-b-1}}{2^{i+b}(\mu-\lambda_0-\lambda_1)^{j-b+1}}\right. \\
&+\frac{2}{(\lambda_0+\lambda_1)^2}\left[\frac{\mu^n}{(\mu-\lambda_0-\lambda_1)^n}-\frac{\mu^{2n}}{(\mu-\lambda_0-\lambda_1)^n(\mu+\lambda_0+\lambda_1)^n}-1\right] \\
&+\frac{2e^{-(\lambda_0+\lambda_1)t}}{(\lambda_0+\lambda_1)^2}\left(\frac{\mu}{\mu-\lambda_0-\lambda_1}\right)^n \\
&+\frac{2e^{-\mu t}}{(\lambda_0+\lambda_1)}\sum_{i=0}^{n-1}\frac{(\mu t)^i}{i!}\left[\frac{2(n-i)}{\mu}-\frac{\mu^{(n-i)}}{(\lambda_0+\lambda_1)(\mu-\lambda_0-\lambda_1)^{(n-i)}}+\frac{1}{\lambda_0+\lambda_1}\right] \\
&-\frac{2e^{-(\mu+\lambda_0+\lambda_1)t}\mu^n}{(\lambda_0+\lambda_1)^2(\mu-\lambda_0-\lambda_1)^n}\sum_{i=0}^{n-1}\frac{(\mu t)^i}{i!}\left[1-\frac{\mu^{(n-i)}}{(\mu+\lambda_0+\lambda_1)^{(n-i)}}\right] \\
&\left.+\ e^{-2\mu t}\sum_{i=0}^{n-1}\sum_{j=0}^{n-1}\sum_{b=0}^{j}\sum_{a=0}^{i+b}\frac{C_{i+b}^{i}\mu^{j-b-1}(2\mu t)^a}{2^{b+i}(\mu-\lambda_0-\lambda_1)^{j-b+1}a!}\right\}
\end{aligned}
$$

Letting

$$E_r(t)=\frac{s_0\lambda_1+s_1\lambda_0}{(\lambda_1+\lambda_0)}\left(t-\frac{n}{\mu}\right)$$

and

$$
\begin{aligned}
V_r(t) &= \frac{\lambda_0\lambda_1(s_0-s_1)^2}{(\lambda_1+\lambda_0)^2}\left\{\frac{2t}{(\lambda_0+\lambda_1)}-\frac{4n}{\mu(\lambda_0+\lambda_1)}-\sum_{i=0}^{n-1}\sum_{j=0}^{n-1}\sum_{b=0}^{j}\frac{C_{i+b}^{i}\mu^{j-b-1}}{2^{i+b}(\mu-\lambda_0-\lambda_1)^{j-b+1}}\right. \\
&\left.+\frac{2}{(\lambda_0+\lambda_1)^2}\left(\frac{\mu^n}{(\mu-\lambda_0-\lambda_1)^n}-\frac{\mu^{2n}}{(\mu-\lambda_0-\lambda_1)^n(\mu+\lambda_0+\lambda_1)^n}-1\right)\right\},
\end{aligned}
$$

we have

Proposition 2 *1.* $\lim_{t\to\infty}|E_r(t)-E(r(t))|=0$*;*

2. $\lim_{t\to\infty}|V_r(t)-Var(r(t))|=0$*;*

3. $E_r(t)\neq V_r(t)$ *implies the production of mRNA cannot be a Poisson process.*

3.2.2 Noise propagation in stochastic reaction chains

Formulation of the stochastic reaction chain with TEC pauses

Sequence-specific pausing of TEC is broadly involved in transcription elongation. For example, RNAP pausing in a proximal upstream sequence of the transcription starting

site called the promoter-proximal region has been detected as a general feature of transcription in mammalian cells and numerous cells of other eukaryotes [61, 62]. Moreover, in E. *coli*, A32 and C37 have been identified as the sequence-specific sites for TEC pausing [61]. Once a TEC pauses, the elongation of the incoming upstream TECs will be blocked until the pausing TEC gets reactivated and leaves its current site.

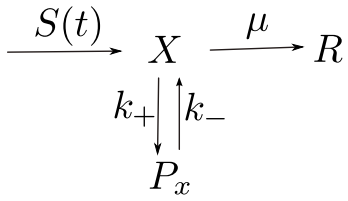

Figure 3.2: The reaction chain with pauses.

In this section, we study how the TEC pause blocks the incoming downstream signal by analyzing the statistics of mRNA produced in a DNA sequence of length 2 as shown in Fig. 3.2. In Fig. 3.2, X represents the TEC formed at site 1 and can pause to become P_x. Moreover, X can jump to site 2 to become a molecule of R. If an upstream TEC arrives at site 1 and site 1 is free, the TEC can occupy site 1 and become X. Otherwise, the TEC will leave. Here we assume that the wating times of the occurrences of all reactions in Fig. 3.2 are exponentially distributed. In particular, the times for a TEC at site 1 to switch between X and P_x are exponentially distributed with rates k_+ and k_-. The time for a TEC of species X to become R is exponentially distributed with rate μ. The upstream TEC arrives at site 1 in a Poisson process with rate $S(t)$. Here we assume $S(t) = s_1$ for any time. Without considering the switch of the promoter site, we focus on the effect of TEC pausing on the production of mRNA here.

Let $(0, i)$ represent the situation when there is no X and i molecules of species R in the system. $(1, i)$ is the situation when there is one molecule of X and i molecules of R in the system. $(1_p, i)$ is the situation when there is one molecule of P and i molecules of R in the system. Then the evolution of the system can be expressed as in Fig. 3.3.

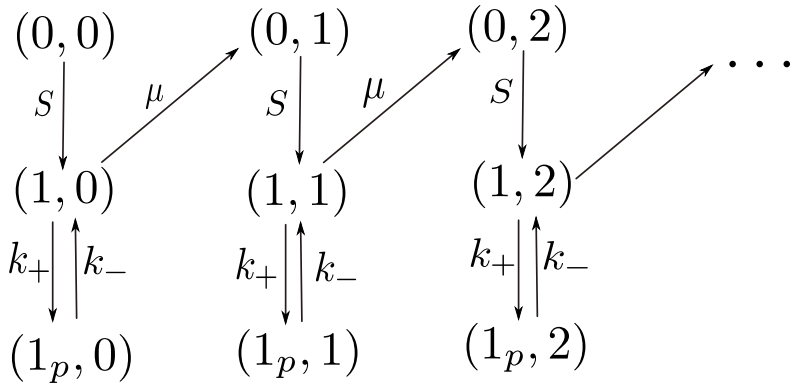

Figure 3.3: The transition of the system status.

The first passage time to produce an mRNA

We first consider the system starting at $(1,0)$. Let $p_{(1,0)}(t)$ and $p_{(1_p,0)}(t)$ be the probability that the system is at $(1,0)$ and $(1_p,0)$ at time t respectively. Then we have the governing equations of $p_{(1,0)}(t)$ and $p_{(1_p,0)}(t)$ as follows:

$$\begin{aligned}
\frac{d}{dt}\begin{pmatrix} p_{(1,0)} \\ p_{(1_p,0)} \end{pmatrix} &= \begin{pmatrix} -(k_+ + \mu) & k_- \\ k_+ & -k_- \end{pmatrix}\begin{pmatrix} p_{(1,0)} \\ p_{(1_p,0)} \end{pmatrix}, \\
\begin{pmatrix} p_{(1,0)} \\ p_{(1_p,0)} \end{pmatrix} &= \begin{pmatrix} 1 \\ 0 \end{pmatrix} \quad \text{at } t = 0.
\end{aligned}$$

By solving the above equations, we obtain

$$p_{(1,0)} + p_{(1_p,0)} = \frac{\sqrt{\Delta} + k_- + k_+ - \mu}{2\sqrt{\Delta}} e^{-\beta_1 t} + \frac{\sqrt{\Delta} - k_- - k_+ + \mu}{2\sqrt{\Delta}} e^{-\beta_2 t},$$

where $\Delta = (k_+ + \mu + k_-)^2 - 4k_-\mu$, $\beta_1 = \frac{(k_- + k_+ + \mu) - \sqrt{\Delta}}{2}$, and $\beta_2 = \frac{(k_- + k_+ + \mu) + \sqrt{\Delta}}{2}$.

Let T_x be the random variable for the waiting time for a transition from X to R. Let $f^{(x)}(t)$ be the probability density function such that the probability of $T_x \in [t, t+dt)$ is $f^{(x)}(t)dt$. Then we have

$$\begin{aligned}
f^{(x)}(t) &= \frac{d[1 - (p_{(1,0)} + p_{(1_p,0)})]}{dt} \\
&= A_1\beta_1 e^{-\beta_1 t} + A_2\beta_2 e^{-\beta_2 t},
\end{aligned}$$

where $A_1 = \frac{1}{2} + \frac{k_- + k_+ - \mu}{2\sqrt{\Delta}}$ and $A_2 = \frac{1}{2} - \frac{k_- + k_+ - \mu}{2\sqrt{\Delta}}$.

Next we consider the system starting at $(0,0)$. Define T_r as the random variable of the time for the system to switch from $(0,0)$ to $(0,1)$. Define $f^{(r)}(t)$ as the probability density function such that the probability of $T_r \in [t, t+dt)$ is $f^{(r)}(t)dt$. Then we have

$$\begin{aligned} f^{(r)}(t) &= \int_0^t s_1 e^{-s_1\tau} f^{(x)}(t-\tau)d\tau, \\ &= \frac{A_1\beta_1 s_1(e^{-\beta_1 t} - e^{-s_1 t})}{s_1 - \beta_1} + \frac{A_2\beta_2 s_1(e^{-\beta_2 t} - e^{-s_1 t})}{s_1 - \beta_2} \qquad (3.4) \\ E(T_r) &= \frac{1}{s_1} + \frac{A_1}{\beta_1} + \frac{A_2}{\beta_2} \\ Var(T_r) &= \frac{1}{s_1^2} + \left(\frac{A_1}{\beta_1} - \frac{A_2}{\beta_2}\right)^2. \end{aligned}$$

The time to produce the nth mNRA

Let $T_{i,r}$ be the random variable of the time for the system to switch from $(0, i-1)$ to $(0,i)$. Then $T_{i,r}$ are independent and have the same distribution as T_r. Therefore, letting $Q(\nu)$ and $Q_n(\nu)$ be the characteristic functions of T_r and $\sum_{i=0}^{n} T_{i,r}$, respectively, we have

$$\begin{aligned} Q(\nu) &= \frac{s_1}{s_1 - i\nu}\left(A_1\frac{\beta_1}{\beta_1 - i\nu} + A_2\frac{\beta_2}{\beta_2 - i\nu}\right) \\ Q_n(\nu) &= Q(\nu)^n \\ &= \sum_{k=0}^{n}\begin{pmatrix} n \\ k \end{pmatrix} A_1^k A_2^{n-k}\left(\frac{s_1}{s_1 - i\nu}\right)^n\left(\frac{\beta_1}{\beta_1 - i\nu}\right)^k\left(\frac{\beta_2}{\beta_2 - i\nu}\right)^{n-k} \end{aligned}$$

Let $f_n(t)$ be the probability density function of $\sum_{i=0}^{n} T_{i,r}$. Noting that the characteristic function of $\frac{s_1 e^{-s_1 t}(s_1 t)^{n-1}}{(n-1)!}$ is $\left(\frac{s_1}{s_1 - i\nu}\right)^n$, we have

$$\begin{aligned} f_n(t) &= \sum_{k=1}^{n-1}\begin{pmatrix} n \\ k \end{pmatrix} A_1^k A_2^{n-k}\left(g_{(n,s_1)} * g_{(k,\beta_1)} * g_{(n-k,\beta_2)}(t)\right), \\ &+ A_1^n g_{(n,s_1)} * g_{(n,\beta_1)}(t) + A_2^n g_{(n,s_1)} * g_{(n,\beta_2)}(t) \end{aligned}$$

where $*$ represents the convolution operator, $g_{(k,\beta)}(t) = \beta e^{-\beta t}\frac{(\beta t)^{k-1}}{(k-1)!}$ is the Gamma distribution for $k \geqslant 1$.

The number of mRNAs produced in $[0, t]$

Let $N(t)$ be the random variable for the number of R molecules produced in $[0, t]$. Using Strong Law for Renewal Sequences in[69], we have

$$\begin{aligned} P(N(t) \geqslant n) &= \int_0^t f_n(\tau) d\tau, \\ \lim_{t\to\infty} \frac{N(t)}{t} &= \frac{1}{E(T_r)}, \quad \text{with probability 1.} \end{aligned}$$

Therefore, the number of mRNA produced in any finite time interval is bounded with probability one. The mean production rate of mRNA defined as the number of mRNA produced in a time interval divided by the length of the time interval is approximately constant when the length of the time interval is large enough.

The bursty production of mRNA

Here we propose a condition to define whether such a biological system as in Fig. 3.2 can generate the bursts of mRNA production. A burst of the production of mRNA occurs when the system begin to generate mRNA molecules at fast rates after a relatively long pause. Therefore, a burst can happen if the time between two successive productions of mRNA is small with a large probability and large with a small probability. Eq. (3.4) shows the production of a single mRNA involves two time scales, so we define the following probabilities:

$$\begin{aligned} P_1 &= P(T_r > \frac{1}{s_1} + \frac{1}{\beta_1}) \\ P_2 &= P(T_r < \frac{1}{s_1} + \frac{1}{\beta_2}) \end{aligned}$$

Then the following condition is defined for the production bursts:

$$\frac{P_1}{P_2} \ll 1.$$

which can be satisfied by the following inequalities

$$\frac{\beta_1}{\beta_2} \ll 1, \quad \frac{\beta_1}{s_1} \ll 1, \quad \frac{A_1}{A_2} \ll 1.$$

$$\frac{\beta_1}{\beta_2} \ll 1 \Leftrightarrow \frac{1 - \frac{\sqrt{\Delta}}{k_+ + k_- + \mu}}{1 + \frac{\sqrt{\Delta}}{k_+ + k_- + \mu}} \ll 1 \Leftrightarrow \frac{4k_-\mu}{(k_+ + k_- + \mu)^2} \ll 1$$

Similarly, $\frac{A_1}{A_2} \ll 1 \Leftrightarrow \frac{4k_+\mu}{(k_-+k_+-\mu)^2} \ll 1$ and $k_- + k_+ < \mu$. Therefore, $k_- \ll \mu$ and $k_+ \ll \mu$. Furthermore,

$$\begin{aligned}
\frac{\beta_1}{s_1} &= \frac{(k_+ + k_- + \mu) - \sqrt{\Delta}}{2s_1} \\
&\approx \frac{(k_+ + k_- + \mu) - (k_+ + k_- + \mu)\left[1 - \frac{4k_-\mu}{(k_+ + k_- + \mu)^2}\right]}{2s_1} \\
&= \frac{2k_-\mu}{s_1(k_+ + k_- + \mu)}.
\end{aligned}$$

Since $k_- \ll \mu$ and $k_+ \ll \mu$, $\frac{\beta_1}{s_1} \ll 1$ leads to $k_- \ll s_1$.

In conclusion, $k_- \ll s_1$, $k_- \ll \mu$ and $k_+ \ll \mu$ can lead to the production bursts of mRNA. $k_+ \ll \mu$ implies that TEC pausing happens rarely at the DNA site. $k_- \ll s_1$ and $k_- \ll \mu$ implies once the TEC pauses, it takes much longer time for the TEC to release than the arrival of new TECs and the jump of the free TEC to the terminal site. As a result, releasing from the pausing status is a limiting step of transcription. Once one TEC pauses, it prevents the incoming upstream TEC's elongating and blocks transcription. After the TEC releases from the pause status, transcription happens at a larger rate than $\frac{1}{\frac{1}{s_1}+\frac{1}{\beta_2}}$ with a large probability P_2 and a burst of mRNA production may occur.

In this chapter, we first examine how the fluctuations from a random switching input propagate along a deterministic first-order reaction chain with the same reaction rate at each step, in order to understand how fluctuations from the initiation step of transcription propagate in elongation. We find that the fluctuations measured by the standard deviation of the number of molecules approach a constant at the steady state exponentially and the fluctuations in each reaction step are bounded by a constant. Therefore, fluctuations from initiation are controlled in elongation. Moreover, if the length of the deterministic chain increases the fluctuations approach zero, which implies that long elongation sequences may be a noise attenuating step in transcription. Then we consider a stochastic elongation chain of length two and TEC can pause at the first step, with the objective to understand the effect of the TEC pausing on mRNA production. Our analysis shows that the mean production rate of mRNA increases linearly with probability one when the length of the observed time interval approaches infinity. Moreover, we find that TEC pausing has to happen rarely and the pausing

time has to be long enough in order for the system to demonstrate bursts of mRNA production.

Chapter 4

Stochastic fluctuations in dorsal surface patterning in *Drosophila*

In this chapter we study how fluctuations propagate at different reaction steps in dorsal surface patterning in *Drosophila*. To realize this goal, we look at the stochastic temporal evolution of the extracellular signal in the slice of the half PV space in Section 4.1. Furthermore, we propose a downstream biological network in nuclei for the feedback loop and examine the propagation of fluctuations in the downstream network in Section 4.2.

During the pattern formation process, a field of cells is exposed to a graded signal and responds in a concentration-dependent manner. For reliable patterning, the cells have to choose a proper response mechanism. Therefore, to characterize fluctuations in patterning, we have to first identify the response and then study how the fluctuations are processed in the response step. During dorsal surface patterning, bound receptors can phosphorylate Mad to pMad, which specifies the amnioserosa at the highest level. Therefore, in Section 4.1, we focus on how the fluctuations in bound receptors in the PV space affect the determination of the amnioserosa boundary. Since the absolute difference of the signal among cells is important to differentiate the cell fates, we first use the standard deviation of the number of Dpp/Scw molecules and bound receptors to compare the signal fluctuations in different locations. Then we define a response mechanism for the determination of the amnioserosa region and study the distribution

of the amnioserosa boundary. To understand noise propagation in the pathway, we compare the fluctuations in Dpp/Scw and bound receptors. However, the number of Dpp/Scw molecules and bound receptors lie in different ranges. Dpp/Scw numbers in ten per nucleus while the bound receptors number in hundreds as shown later. We use the coefficient of variation (CV) that is defined as the standard deviation divided by the mean to scale their fluctuations.

In Section 4.2, we study how reactions and molecular transport of different time scales affect the fluctuations in the production of SBP in the feedback loop. To this end, we consider the amount of SBP in the downstream biological system with different settings. Moreover, to understand the effect of multi-scale reactions on noise propagation, we compare the CV of different species in the downstream network.

As in Section 1.4.4, Dpp/Scw, bound receptors and SBP are denoted as B, BR and C respectively for simplicity.

4.1 Dorsal surface patterning in *Drosophila*

To study fluctuations in the dorsal-surface pattern formation process, we discretize the slice as shown in Fig. 1.8 and use the Gillespie simulation method to simulate the stochastic dynamics of the biochemical system in Fig. 1.5. Using our simulation results, we study the effect of the upstream biological network and the feedback loop on signal fluctuations. Each system in each situation is simulated for 50 times, i.e. , we generate 50 realizations.

4.1.1 The effect of the upstream biological network on signal fluctuations

In this section, we study how the pattern formed in the upstream network affects the fluctuations in the dorsal surface pattern formation process. Before dorsal surface patterning, the PV space is divided into the three sections: the M, the NE and the DR. Dpp, Tld and Tsg are expressed in the DR, while Sog is expressed in the NE. Sog and Tsg can form a heterodimer Sog/Tsg, which has a high affinity for Dpp/Scw (B). The complex formed, Dpp/Scw/Sog/Tsg, can be cleaved by Tld, which releases B. As a result, there exists a flux of Dpp/Scw/Sog/Tsg towards the DM, preventing B from

diffusing far away from the DR. Here we study how the shuttling system constrains the spread of B.

Fig. 4.1 shows the statistics of BR and B in each compartment at 60 minutes. In Fig. 4.1, the yellow bar represents the compartments in the DR, the blue bar represents the compartments in the NE and the red bar represents the compartments in the M. Fig. 4.1-(A) and Fig. 4.1-(B) show the mean number of B and BR molecules in each compartment. The sharp decrease of the BR level occurs around 50, where the amnioserosa boundary lies. However, the sharp decrease of the B level occurs around 30, where the boundary between the DR and the NE lies. Therefore, the density gradient of B inherits the spatial pattern formed in the upstream network.

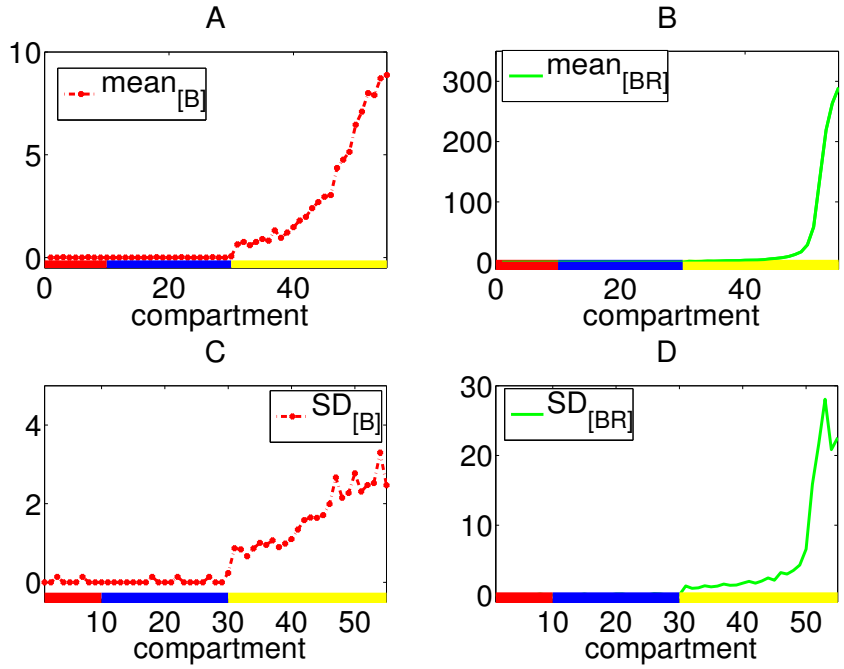

Figure 4.1: The statistics of BR and B in each compartment at 60 minutes.

We use the standard deviation to study the fluctuations in B and BR. Fig. 4.1-(C) and Fig. 4.1-(D) show the standard deviations of the numbers of B and BR molecules in each compartment at 60 minutes, respectively. In compartment 1-30, the small standard deviations of both species indicate that the probability of having B and BR molecules in compartment 1-30 is very small. In the other words, the probability that there are

no B and BR molecules in the NE and M is big. Therefore, the shuttling system plays a very deterministic role in confining signaling molecules in the DR.

Although the standard deviations of B and BR in compartments 31-55 are much larger than those in compartments 1-30, the boundary of the amnioserosa is well defined due to the large difference of the levels of BR between different compartments. The details of fluctuations in compartments 31-55 will be discussed in the following sections.

4.1.2 The effect of the feedback loop on signal fluctuations

In this section, we study the effect of the feedback loop on signal fluctuations. In [5], endocytosis of molecules is treated as degradation, i.e., molecules are removed from the system once they get internalized. As the level of SBP (C) in the feedback loop increases, more B molecules can bind to C and thus get removed from the system. To keep the total level of signaling molecules consistent, the degradation rate of B is decreased when the endocytosis rate is increased in[5]. Here we focus on how the feedback loop and endocytosis interplay to affect signal fluctuations. In particular, we look at the precision of the amnioserosa boundary and the temporal evolution of the noise of B and BR in the compartment near the boundary.

The precision of the boundary location

To simulate the specification of the amnioserosa boundary, we define a threshold concentration of BR. If the concentration of BR is above this, the compartment is defined as type I; otherwise, it is defined as type II. The threshold compartment is defined as the compartment that is of type II and is closest to the DM. We obtain the distribution of the threshold position in the system with/without the feedback loop and with/without endocytosis at 60 minutes.

The simulation results are shown in Fig. 4.2, where ±f (±e) represents the system with/without the feedback loop (endocytosis). Fig. 4.3 shows the mean number of BR molecules in each compartment at 60 minutes. From Fig. 4.2 and 4.3, we reach the following conclusions:

1. With the feedback loop, the amnioserosa contracts. Moreover, in the system with feedback and endocytosis, the threshold position is concentrated in the same one

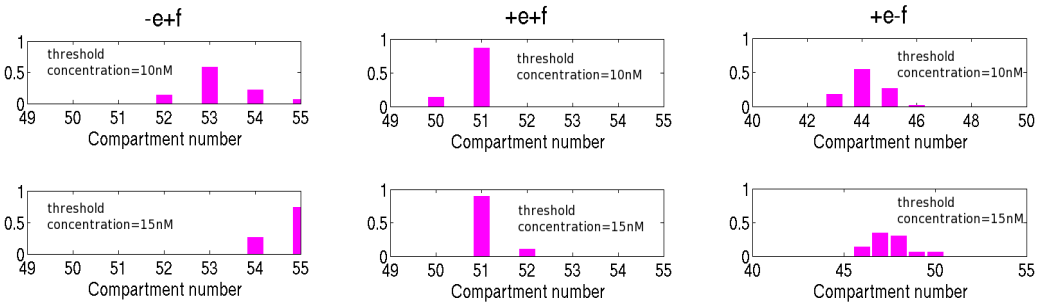

Figure 4.2: The distribution of the threshold positions.

compartment given the two different threshold concentrations. On the contrary, without the feedback loop, the threshold position is more broadly distributed and more sensitive to the threshold concentration. This implies that the feedback loop can help stabilize the aminoserosa boundary. This is because BR in compartments of type I can lead to more C molecules than BR in the compartments of type II. More C molecules in compartments of type I can bind to more B molecules, preventing B from binding to receptors in compartments of type II. As a result, the difference of the numbers of BR molecules between the two types of compartments is amplified by the feedback loop. Then as shown in Fig. 4.3, the gradient of the number of BR molecules is sharper and the boundary is better defined in the system with feedback.

2. Without endocytosis, the threshold moves towards the DM, i.e., the amnioserosa is smaller than the amnioserosa in the system with endocytosis. Moreover, without endocytosis, the threshold position varies more. This can be explained by the temporal evolution of the signal in each compartment. Without endocytosis, we increase the degradation rate of B for the consistency of the signal level as in [5], which decreases the number of B molecules in the early stage of patterning and hence slows the growth of the numbers of BR and C molecules. The smaller number of B molecules in each compartment leads to a narrower signal band around the DM. Furthermore, the difference of the numbers of BR molecules between the two types of compartments is not amplified as much as the difference in the system with endocytosis. So the boundary is less well defined.

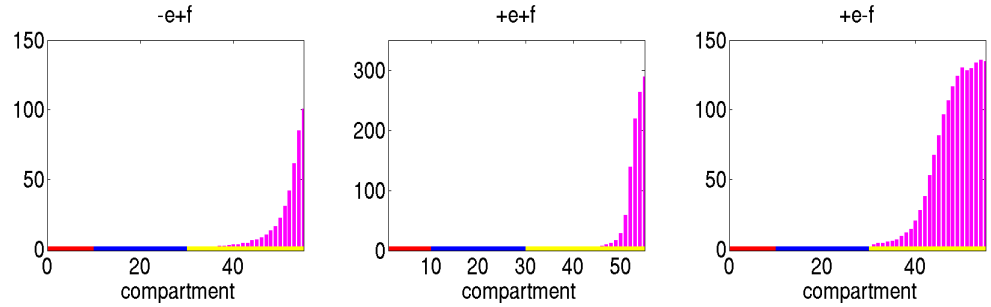

Figure 4.3: The mean number of BR molecules in each compartment at 60 minutes.

The biphasic effect of the feedback loop on noise propagation

In this section, we study the temporal evolution of the signal in the threshold compartments. The threshold compartment is defined as the compartment where the threshold position concentrates. We choose $10nM$ as the threshold concentration. So from Fig. 4.2, the threshold compartment of the system with endocytosis and the feedback loop is compartment 51. The threshold compartment of the system with endocytosis and without the feedback loop is compartment 44. The threshold compartment of the system without endocytosis and with the feedback loop is compartment 53. Fig. 4.4 shows the mean and the CV of the numbers of B and BR molecules in these compartments.

From Fig. 4.4, we can reach the following conclusions:

1. The differences between the mean number of B molecules and the mean number of BR molecules are larger in the systems with the feedback loop than the differences in the system without the feedback loop. This is because C produced in the feedback loop can bind to B and reduce the number of free B molecules.

2. The CV of B is always larger than the CV of BR, which implies the fluctuations are attenuated along the signal pathway. The number of B is around ten per nucleus,and the numbers of receptors and C molecules are over one thousand [5]. The large amount of receptors and C can ensure B molecules are caught effectively, which may attenuate the fluctuations in B.

3. In the systems with the feedback loop, the CV of B first decreases and then increases, while in the system without the feedback loop, the CV of B and the

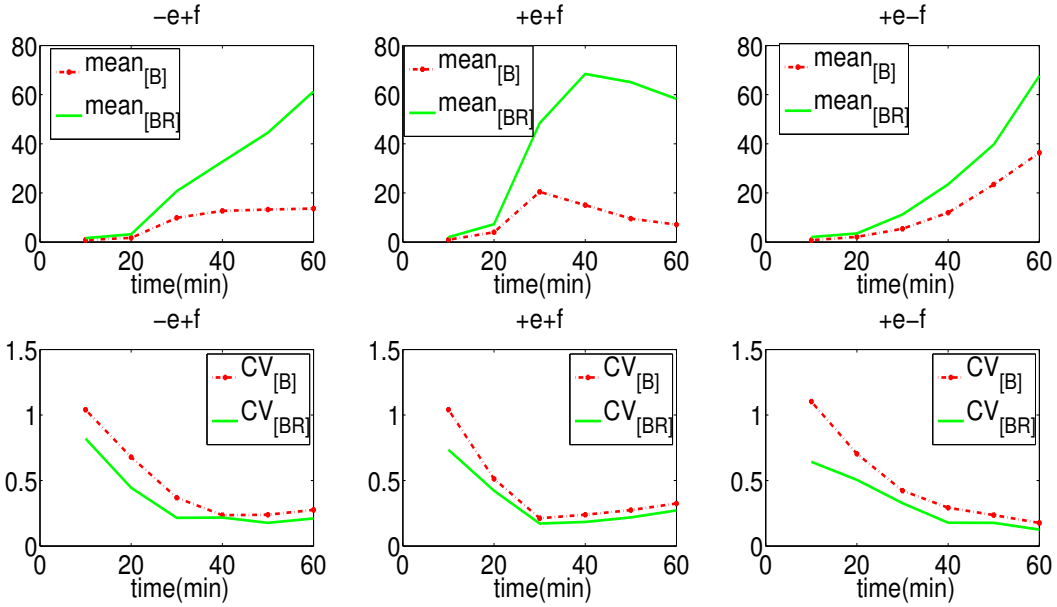

Figure 4.4: The statistics of B and BR in the threshold compartment

CV of BR always decrease. This can be explained by the dual effect of C on signaling. At low levels, C molecules can hold B molecules around receptors and enhance the association between B and receptors, augmenting signaling. However, as the number of C molecules increases, C will compete with receptors for B, which reduces the number of free B molecules and increases the noise. Furthermore, in the system with endocytosis and the feedback loop, C can remove B molecules through endocytosis. As a result, the numbers of B and BR molecules decrease and the fluctuations in them increase.

4.2 The multi-scale downstream biological network in nuclei

In this section, we propose a single cell model to characterize the downstream biological network. By conducting a detailed scale analysis of reaction frequencies and stochastic simulations of the biological system, we aim to understand how reactions of different time scales affect the propagation of fluctuations in the network. Our system is a very

prototypical TGF-β signaling network system, and our conclusions may hold over to other signaling networks. Here we use the same notations as in Section. 4.1, i.e., Dpp/Scw is denoted as B, receptors are denoted as R and SBP is denoted as C. In addition, to differentiate molecules in different locations, we use *p, *c and *n to denote the species in the PV space, the cytoplasm and the nucleus respectively. For example, Bp represents B in the PV space and Bc represents B in the cytoplasm.

4.2.1 Single cell model

Biological network

The single cell model consists of three different domains: the PV space, the cytoplasm, and the nucleus. B diffusion, production and degradation occur all over the PV space. Near the embryo membrane, the reactions are the insertion of R at a constant rate, the secretion of C from cytoplasmic translation, the binding reactions between B, R and C as in [5], endocytosis and exocytosis of R, C, BR, BC and BCR, and the phosphorylation of the cytoplasmic Mad by BR. We use the endocytosis and exocytosis mechanism from [70], in which internalized BR can phosphorylate Mad, and B will disassociate from R and C when BR, BCR and BC get recycled. Moreover, without any quantitative information about intracellular degradation so far, for now we assume the intracellular degradation of BR, BCR, BC, C and R occurs at the same rate as it does in the PV space.

In the cytoplasm, we use the structure of the Smad pathway in humans. Through transgenic experiments, Smad2 in humans is found to function in the same way as Mad in *Drosophila*, and Smad4 works in the same way as Madea [71]. The Smad pathway in humans can be summarized as in Fig. 4.5. In the absence of signaling, the Smad proteins can shuttle between the nucleus and cytoplasm. During signaling, the occupied receptor phosphorylates Smad2, which facilitates the complex formation of Smad2/Smad4 and Smad2/Smad2. Smad2/Smad4 and Smad2/Smad2 can be transported into the nucleus, while Smad2 can only be capable of export in the monomeric form [6, 72]. The unidirectional translocation leads to the accumulation of Smad2/Smad4 and Smad2/Smad2 in the nucleus, where they can bind to DNA, regulate transcription and control feedback reactions. Therefore, the reactions in the cytoplasm are the phosphorylation of Mad,

the association and dissociation reactions between pMad and Madea, the synthesis of C from mRNA translation, the degradation of mRNA, and the intracellular degradation of BR, BCR, BC and C. For simplicity, we denote pMad/Madea as pMMe and pMad/pMad as pMad2. Near the nuclear membrane, the reactions are the nuclear export and import of Mad, pMad, and Madea, the unidirectional import of pMad2 and pMMe, and the nuclear export of mRNA.

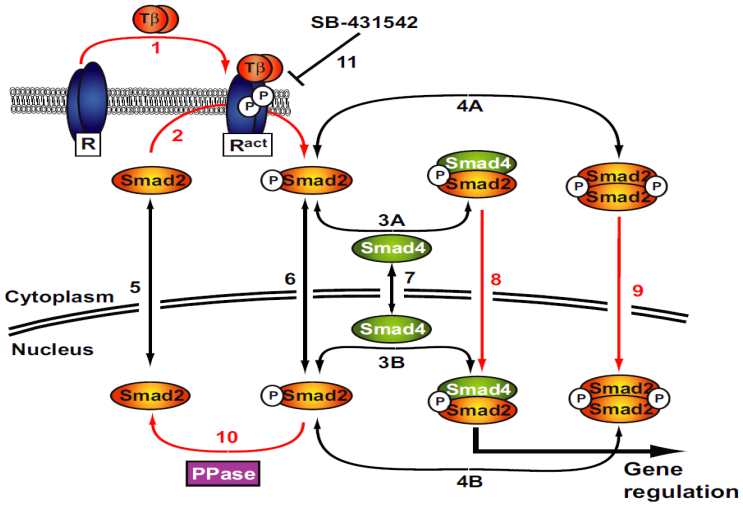

Figure 4.5: The Smad pathway [6].

However, the exact structures of the Smad oligomers have not been fully determined. It has been suggested that the transcription factors should not be Smad2/Smad2 or Smad2/Smad4 but the hetero-trimers consisting of two Smad2's and one Smad4 [73]. Moreover, our estimation in the following section shows the amount of Mad and Madea is much larger than it is necessary for pMad2 and pMMe to activate the downstream gene expressions. Here, we first reduce the amount of Mad and Madea and stick to previous models in [6, 72]; and then we increase the amount of Mad and Madea to the level suggested in [6] and use the trimer as the transcription factor. We compare the temporal evolution of the signal in these two settings.

Then the reactions in the nucleus are the dephosphorylation of pMad, the association and dissociation reactions between pMad and Madea, the binding and unbinding reactions between the transcription factors and the promoter site, and the production

of mRNA. In the nucleus, we assume there exists only one promoter site for the transcription factors to bind to. During transcription, we divide the production of mRNA into two steps: 1) RNAP binds to the DNA sequence to form an elongation complex TEC; 2) TEC proceeds to become mRNA. Depending on the status of the promoter site, the formation rate of TEC switches between the basal rate and the enhanced rate, while TEC always proceeds at the same rate.

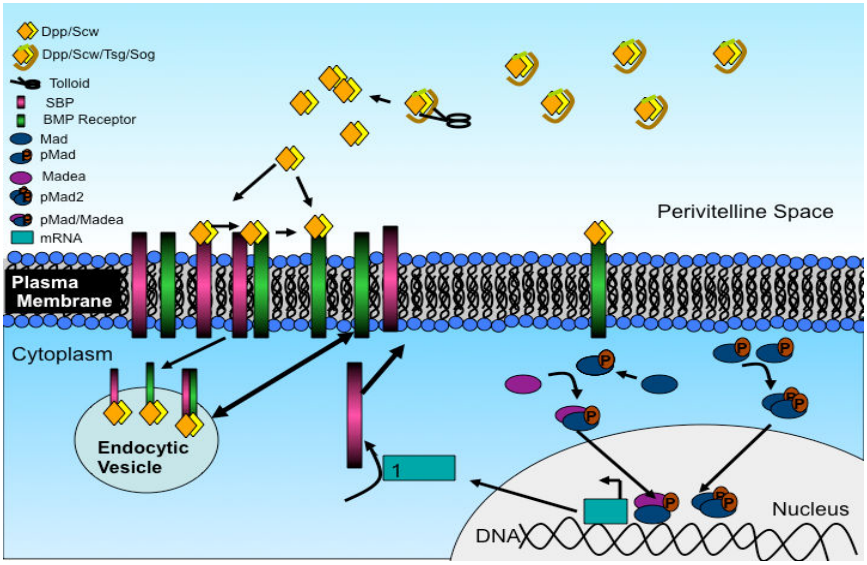

Figure 4.6: The signal transduction pathway in the single cell model.

The model is shown in Fig. 4.6.[1] In addition, we make the following assumptions:

1. Only the species that can be produced undergo degradation. Therefore, B, R, C, BR, BC, BCR and mRNA undergo degradation, and the total amount of Mad and Madea in all forms is constant.

2. Proteins synthesized from mRNA translation can be transported actively and rapidly to their end-destination. So we assume that proteins synthesized from mRNA translation can be transported immediately to the embryo membrane for secretion.

3. All species except DNA and proteins synthesized from mRNA translation diffuse.

[1] This figure is from Christina Brakken-Thal and modified by Likun Zheng.

4. All the species near the embryo membrane, such as R, C, BC and BCR, are treated approximately as being distributed over all the PV space as in [5].

Initially, the concentration of each species is set to zero except the following ones:

1. The concentrations of the receptors in the PV space and the cytoplasm are chosen to be 160 nM and 1600nM respectively, so as to be consistent with the endocytosis and exocytosis rates [5, 70];

2. The concentrations of the cytoplasmic Mad and Madea are one fourth of the concentrations from [6], i.e., the concentrations of the cytoplasmic Mad and Madea are 15.15 nM and 12.7 nM respectively ;

3. The concentrations of the nuclear Mad and Madea are one fourth of the concentrations from [6], i.e., the concentrations of the nuclear Mad and Madea are 7.125 nM and 12.7 nM respectively.

Parameter values

We present the values of all parameters in the attached tables in Appendix 6.2. Parameters are estimated based on experiments and published papers. Here we discuss how we apply known parameters to our system and estimate the parameters that lack references.

Diffusion coefficients: For species that lack published data of diffusion coefficients, we use the following equation from[74] to estimate their diffusion coefficients

$$D = 8.34 * 10^{-8} * \left(\frac{T}{\eta M^{1/3}}\right) \quad cm^2 s^{-1},$$

where T is the temperature, η is the viscosity of the medium and M is the molecular weight. Moreover, for species embedded in the membrane, such as receptors and C, recent studies show their diffusion coefficients are less than $0.02\mu m^2 sec^{-1}$ [75], which is much less than those of the species in fluid. Therefore, for simplicity, we do not consider the diffusion of membrane species here.

Insertion rate of receptors: We assume that the production of receptors in the system is at the steady state and make the insertion rate of receptors the same as their degradation rate in the PV space. The degradation rate of receptors in the PV space is

chosen from [5].

Nucleo-cytoplasmic transport rates of Mad, pMad, pMad2, Madea, pMMe and RNA: The nucleo-cytoplasmic transport rates of Mad, pMad, pMad2, Madea and pMMe are estimated based on the data from [6]. In [6], whole compartment FRAP of nuclear EGFP-Smad2 showed a monophasic and exponentially recovering curve of Smad2 in photo bleached cells. As a result, Shimmer et al concluded that the nuclear transport is governed by mass action kinetics and obtained the transport rates to make their model best fit experiment data. In particular, they treated the nuclear transport as the following first-order reaction:

$$Smadc \underset{k_{out}}{\overset{k_{in}}{\rightleftharpoons}} Smadn,$$

where Smadc and Smadn represent Smad2 in the cytoplasm and nucleus respectively, and k_{out} and k_{in} are the nuclear export and import rate constants. The deterministic governing equation of the temporal evolution of the concentrations of Smadc and Smadn can be expressed by using the mass action rate law. Then k_{out} and k_{in} were estimated so that the solution to the equation can best fit the averaged data from experiments. Similarly, the nuclear import and export rates of other species were obtained in [6].

Without considering diffusion and spatial inhomogeneity, it was assumed that nuclear transport can happen everywhere in [6]. However, we will only allow the nuclear transport to occur near the nuclear membrane, as spatial inhomogeneity may play an important role in signal transduction. During import, molecules bind to cargoes via their nuclear localization signals and then molecular cargoes bind to cognate soluble transport factors that facilitate the passage of the resulting transport factor-cargo complexes through the nuclear pore complexes [76]. Assuming molecules can be localized around the nuclear membrane once they reach there, we divide the import process into two steps: 1) in the first step, the molecule diffuses freely to the nuclear membrane and gets localized; and 2) in the second step, the molecule near the nuclear membrane undergoes a first-order reaction to become a nuclear molecule. To obtain the first-order reaction rate, we solve the following equation

$$\frac{1}{k_{in}} = E(T) + \frac{1}{k'_{in}},$$

where k_{in} is the import rate from [6], k'_{in} is the first-order transport rate across the nuclear membrane, and $E(T)$ is the expected time for a molecule to reach the nuclear

membrane given its initial position is uniformly distributed in the cytoplasm. Similarly, we obtain the other nucleo-cytoplasmic transport rates.

mRNA transport from the transcription site to the nuclear pore complexes is characterized as nucleoplasmic diffusion with diffusion coefficient ranging over $0.005-0.03\mu m^2 s^{-1}$ [77, 78]. The time for a mRNA molecule to travel throughout a nucleus of radius $5-8\mu m$ is $20-30$ min [77]. However, the export of a mRNA molecule proceeds rapidly (about 0.5 s) once the mRNA molecule is attached to the nuclear envelope [77]. Therefore, we let mRNA get exported immediately once mRNA reaches the nuclear membrane by nucleoplasmic diffusion.

The rate of pMad2 and pMMe binding to the promoter site on DNA: We use $1\times10^9 M^{-1}sec^{-1}$ and $1.11\times10^{-3}sec^{-1}$ from [79] as references for the on and off rates of pMad2 and pMMe binding to the promoter site. In [79], experiments were carried out under the pseudo-first-order condition, in which the free DNA concentration remains constant. The number of DNA-target-bound proteins was counted over time and was fitted by a monoexponential equation.

In our system, we assume there is only one promoter site for pMad2 and pMMe. Since the binding reactions between the promoter site and transcription factors are much faster than diffusion-limited associations, we increase the size of the promoter site to account for the fast association reaction. In particular, we discretize the nucleus into identical compartments of dimension $3\mu m\times3\mu m\times3\mu m$ and put the promoter site in the central compartment. The transcription factor in the central compartment can bind to the site at rate $1\times10^9 M^{-1}s^{-1}$.

Basal and enhanced transcription rates: As far as we know, there is no quantitative information about transcription and translation steps in the feedback loop. We use the known quantitative information of other species to estimate the transcription rates. In bacteria and mammalian cells, the basal transcription rate ranges over $0.01-0.05sec^{-1}$ and the transcription rate can be increased by 8-30 times by transcription factors binding to promoter sites [80, 81, 82]. Therefore, in our system, we choose the basal transcription rate as $0.03\,sec^{-1}$ and the enhanced transcription rate as $0.3\,sec^{-1}$.

System dimensions: The average nucleus diameters during nuclear cycles 10-14 are 10 μm, 10.5 μm, 9.2 μm, 8.2 μm, and 6.5 μm [32]. For simplicity, we approximate the

nucleus as a cuboid of dimension $9\mu m \times 4\mu m \times 9\mu m$. The cytoplasmic space is approximated as a cuboid of dimension $9\mu m \times 0.5\mu m \times 9\mu m$ between the embryo membrane and the nuclear cuboid, and the PV space is approximated as a cuboid of dimension $9\mu m \times 0.5\mu m \times 9\mu m$ above the embryo membrane. The system is shown in Fig. 4.7, which consists of three cuboids: the PV cuboid, the cytoplasmic cuboid, and the nuclear cuboid. Here the x-axis is along the D-V axis. The PV cuboid is built based on [5]. We discuss our settings of the cytoplasmic cuboid and the nuclear cuboid as below.

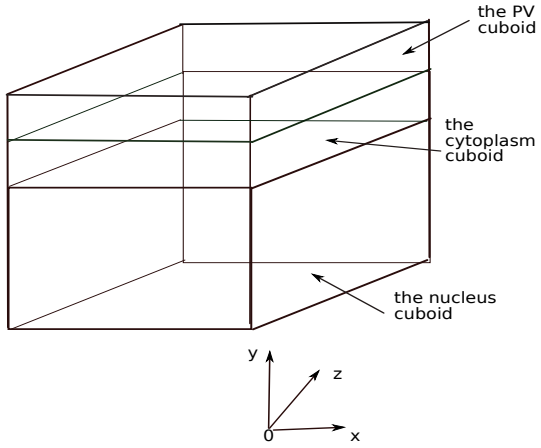

Figure 4.7: The cuboid approximation of the single cell system.

The volume of the cytoplasmic cuboid is smaller than the volume of the cytoplasmic space and the amount of cytoplasmic Mad and Madea may be underestimated. However, our analysis in Section 4.2.2 shows that phosphorylation occurs so slowly that only a small amount of Mad can get phosphorylated. Therefore, underestimating the amount of Mad has little effect on downstream signaling. Underestimating the volume of the cytoplasmic space also changes the time for molecules to reach the nuclear membrane $E(T)$. However, our analysis of nuclear import in Section 4.2.2 indicates that $E(T) \sim 4\,sec$ and $\frac{1}{k_{in}} \sim 300\,sec$. So the transport across the nuclear membrane is the limiting step of nuclear import. Therefore, the effect of $E(t)$ on nuclear import is small.

The volume of the nuclear cuboid is the same as the volume of the nucleus in the 14th cycle. Therefore, the amount of signaling molecules is well approximated. In addition, similar to nuclear import, the limiting step of the export of pMad, Mad and Madea is the transport across the nuclear membrane. Therefore, the effect of the dimension of

the nuclear cuboid on the nuclear export of pMad, Mad and Madea is small.

Next, we discuss the effect of the nuclear cuboid on mRNA export. Since nucleoplasmic diffusion of mRNA is very slow and the nuclear envelope can export mRNA once mRNA gets attached to it, the limiting step of mRNA export is nucleoplasmic diffusion. As a result, the dimension of the nuclear cuboid, where mRNA can get exported, and where mRNA is located after export is important for mRNA export. In our system, we let the nuclear membrane at $y = 0$ and $y = 4\,\mu m$ export mRNA immediately once mRNA reaches there and the remaining part of the nuclear membrane is reflective. As a result, the expected time for mRNA to get exported is $\frac{2}{D_{mRNA}}$, where D_{mRNA} is the diffusion coefficient of mRNA. If mRNA is produced at the center of a sphere of diameter $6.5\,\mu m$ and can get absorbed once it hits the surface of the sphere, then the mean time for mRNA to get absorbed is $\frac{1.98}{D_{mRNA}}$. Therefore, the mean export time of mRNA is well approximated.

After export, the location of mRNA is determined based on Fig. 4.8, which is a cross section of the cytoplasm. In Fig. 4.8, the rectangle representing the cytoplasmic space contains a circle representing the nucleus in its center. Here the cytoplasmic space is approximated as a cube of dimension $9\mu m \times 9\mu m \times 9\mu m$ and the nucleus is approximated as a sphere with its diameter equal to $6.5\mu m$. If we divide the cytoplasmic space into 3 identical compartments as in Fig. 4.8, then the length of the side of each compartment along the x-axis is $3\,\mu m$. Given a mRNA molecule starting at the center of the nucleus, the probability for it to locate in the middle compartment above the dashed line after export is $\frac{\theta}{2\pi}$, where θ is the angle corresponding to a cord of length $3\,\mu m$ in a circle of diameter $6.5\,\mu m$. The probability to locate in any one of the other two compartments above the dashed line after export is $\frac{1}{4} - \frac{\theta}{4\pi}$. If the mRNA molecule locates below the dashed line after nuclear export, it takes at least $\frac{3^2}{0.03*3} = 100\,sec$ for it to reach the embryo membrane, which is much larger than the mean life time of mRNA ($10\,sec$) in our system. Therefore, we assume that mRNA locating below the dashed line always stays below the dashed line. Moreover, we assume that proteins synthesized below the dashed line can be transported with equal probability to each compartment above the dashed line. Therefore, the fraction of mRNA to produce proteins in the middle compartment is $\frac{\theta}{2\pi} + \frac{1}{6}$. The fraction of mRNA in any one of the other two compartments is $\frac{5}{12} - \frac{\theta}{4\pi}$. Therefore, after export, we locate a mRNA

molecule in the middle compartment with probability $\frac{\theta}{2\pi} + \frac{1}{6}$. The probability to locate it in any one of the other two compartments is $\frac{5}{12} - \frac{\theta}{4\pi}$. If we divide the cytoplasmic space into any number of identical compartments, the determination of the location of mRNA follows the similar way. Moreover, after export, the mRNA molecule is put close to the embryo membrane. Since we assume synthesized proteins from translation are transported immediately to the embryo membrane for secretion, the y-coordinate of the position of the mRNA molecule will not affect signaling.

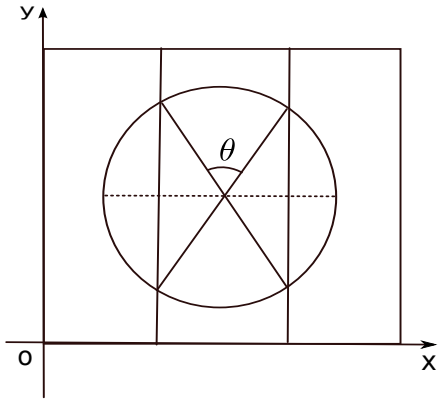

Figure 4.8: The cross section of an embryo in the cytoplasm.

4.2.2 Time scales of reactions

In this section, we compare the time scales of different reaction steps to understand the temporal scale of the signal evolution. We first estimate the maximal numbers of molecules of different species based on literature and then use them to estimate reaction frequencies. We find that the major rate limiting steps are the phosphorylation of Mad and the nucleo-cytoplasmic transport of mRNA.

We estimate the maximal number of molecules of each species in its respective cuboid. For example, the PV cuboid is of dimension $9\mu m \times 0.5\mu m \times 9\mu m$, and the concentration of free BMP is in the range of 0-5nM [5]. So the maximal number of B molecules in the PV cuboid is

$$5nM \times 6.02 \times 10^{23} \frac{molecules}{mol} \times 9\mu m \times 9\mu m \times 0.5\mu m = 122 \tag{4.1}$$

For simplicity of modeling it is assumed receptors are distributed in the whole PV cuboid

as in [5]. Therefore, the maximal number of receptors in the PV cuboid is

$$160nM \times 6.02 \times 10^{23} \frac{molecules}{mol} \times 9\mu m \times 9\mu m \times 0.5\mu m = 3900, \tag{4.2}$$

where the concentration of receptors $160nM$ is taken from [5]. Similarly, the maximal numbers of molecules of other species can be estimated. Table. 4.1 shows the maximal number of molecules of species in different cuboids. The total amount of receptors and C molecules is much larger than the amount of B. So that C and receptors can catch B molecules effectively and attenuate the fluctuations in B.

Variable	Space	Concentration	Number of Molecules	Reference
B	PV	$5nM$	122	[5]
R	PV	$160nM$	3900	[5]
C	PV	$340nM$	8400	[5]
Mad	Cytoplasm	$60.6nM$	1477	[6]
$Madea$	Cytoplasm	$50.8nM$	1238	[6]
Mad	Nucleus	$28.5nM$	5559	[6]
$Madea$	Nucleus	$50.8nM$	9908	[6]

Table 4.1: Maximum estimated numbers of molecules

To estimate reactions frequencies, we calculate the maximal propensity function of each reaction, which gives the largest probability of the occurrence of the reaction during unit time. In particular, we calculate the propensity function by Eq. (4.3)

$$X_1 \times X_2 \times rate \times V \times 6.02 \times 10^{23}, \tag{4.3}$$

where X_1 and X_2 are the concentrations of the reactant species in a bimolecular reaction ($X_2 = 1$ for a unimolecular reaction), $rate$ is the reaction rate constant, and V is the volume of the respective cuboid. X_1 and X_2 are chosen as the maximal concentrations of the reactant species in the cuboid. Table 4.2 summaries the propensity functions of the reactions. There is a two orders of magnitude difference between the slowest and fastest reactions in the PV space. Forming active signaling complexes by B binding to R is very slow, but the formation of active signaling complexes through binding to C is very likely, leading to almost all active signaling complexes forming through C. In the intracellular space, the major rate limiting step appears to be the phosphorylation of Mad to pMad.

Reaction	Species 1	Species 2	Rate	Propensity
$B + C \rightarrow BC$	B ($5nM$)	C ($200nM$)	$1\frac{1}{nM*min}$	$405\frac{1}{sec}$
$BC \rightarrow B + C$	BC ($30nM$)		$2\frac{1}{min}$	$241\frac{1}{sec}$
$BC + R \rightarrow BCR$	BC ($30nM$)	R ($160nM$)	$0.5\frac{1}{nM*min}$	$975\frac{1}{sec}$
$BCR \rightarrow BC + R$	BCR ($80nM$)		$10\frac{1}{min}$	$332\frac{1}{sec}$
$BR + C \rightarrow BCR$	BR ($30nM$)	C ($200nM$)	$1.3 * 10^{-1}\frac{1}{nM*min}$	$317\frac{1}{sec}$
$BCR \rightarrow BR + C$	BCR ($80nM$)		$10\frac{1}{min}$	$332\frac{1}{sec}$
$B + R \rightarrow BR$	B ($5nM$)	R ($160nM$)	$2.4 * 10^{-2}\frac{1}{nM*min}$	$8\frac{1}{sec}$
$BR \rightarrow B + R$	BR ($30nM$)		$4\frac{1}{min}$	$490\frac{1}{sec}$
$BR + Mad \rightarrow pMad$	BR ($30nM$)	Mad ($60.6nM$)	$2.4 * 10^{-2}\frac{1}{nM*min}$	$17\frac{1}{sec}$
$2 * pMad \rightarrow pMad2$	$pMad$ ($60.6nM$)	$pMad$ ($60.6nM$)	$1.1 * 10^{-1}\frac{1}{nM*min}$	$164\frac{1}{sec}$
$pMad + Me \rightarrow pMMe$	$pMad$ ($60.6nM$)	Me ($50.8nM$)	$1.1 * 10^{-1}\frac{1}{nM*min}$	$137\frac{1}{sec}$
$pMad2 \rightarrow 2pMad$	$pMad2$ ($30.3nM$)		$1\frac{1}{min}$	$12\frac{1}{sec}$
$pMMe \rightarrow pMad + Me$	$pMMe$ ($50.8nM$)		$1\frac{1}{min}$	$20\frac{1}{s}$
$pMad \rightarrow Mad$	$pMad$ ($28.5nM$)		$3.96 * 10^{-1}\frac{1}{min}$	$37\frac{1}{sec}$

Table 4.2: Propensity functions for reactions.

The maximal propensity function for the nucleo-cytoplasmic transport is calculated by Eq. (4.4)

$$X_1 \times rate \times V \times 6.02 \times 10^{23} \tag{4.4}$$

where X_1 is the maximal concentration of the respective species, *rate* is the transport rate constant from [6], and V is the volume of the cuboid where the transport starts. In [6], all species are assumed to be evenly distributed in the system. Therefore, we can use the total number of molecules in the cuboid in Eq. (4.4). Table 4.3 summarizes the propensity functions for transport across the nuclear membrane, where *c and *n present species in the cytoplasmic and nuclear cuboids. The transport rate is several orders of magnitude smaller than the maximal rate of reactions between pMad and Madea, but is in the same order as the phosphorylation rate. Due to the slow phosphorylation step, the number of pMad increases slowly and hence all the cytoplasmic reactions may happen slowly. As a result,large fluctuations may arise in the cytoplasm.

Species	Concentration	Rate	Propensity Function
Madc	$60.6nM$	$5.16 * 10^{-3} \frac{1}{sec}$	$7.6 \frac{1}{sec}$
Madn	$28.5nM$	$0.29 \frac{1}{sec}$	$3627 \frac{1}{sec}$
pMadc	$60.6nM$	$5.16 * 10^{-3} \frac{1}{sec}$	$7.6 \frac{1}{sec}$
pMadn	$28.5nM$	$0.29 \frac{1}{sec}$	$3627 \frac{1}{sec}$
pMad2c	$30.3nM$	$0.0294 \frac{1}{sec}$	$22 \frac{1}{sec}$
pMMec	$60.6nM$	$0.0294 \frac{1}{sec}$	$44 \frac{1}{sec}$
Medeac	$50.8nM$	$0.00516 \frac{1}{sec}$	$6.4 \frac{1}{sec}$
Medeac	$50.8nM$	$0.00305 \frac{1}{sec}$	$68 \frac{1}{sec}$

Table 4.3: Propensity functions for transport across the nuclear membrane

We estimate the time scale for a molecule to diffuse throughout the cuboid where it lies. In particular, the time scale is estimated by Eq (4.5)

$$\frac{L^2}{D} \tag{4.5}$$

where D is the diffusion coefficient, and L is the maximum length of the cuboid. Table 4.4 summarizes the time scales for molecules of different species to diffuse throughout

the respective cuboid. The diffusion of mRNA is several orders of magnitude slower than all other diffusion processes. Therefore, the transport of mRNA can also be a limiting step of the signal evolution.

Species	Diffusion Constant	L^2/D
B	$7.3 * 10 \frac{\mu m^2}{sec}$	$1.1 sec$
$Madc$	$1.6 * 10 \frac{\mu m^2}{sec}$	$5.06 sec$
$pMadc$	$1.6 * 10 \frac{\mu m^2}{sec}$	$5.06 sec$
$pMad2c$	$1.3 * 10 \frac{\mu m^2}{sec}$	$6.23 sec$
$Medeac$	$1.4 * 10 \frac{\mu m^2}{sec}$	$5.79 sec$
$pMMec$	$1.2 * 10 \frac{\mu m^2}{sec}$	$6.75 sec$
$mRNAc$	$3.0 * 10^2 \frac{\mu m^2}{sec}$	$2700 sec$
$Madn$	$1.6 * 10 \frac{\mu m^2}{sec}$	$5.06 sec$
$pMadn$	$1.6 * 10 \frac{\mu m^2}{sec}$	$5.06 sec$
$pMad2n$	$1.3 * 10 \frac{\mu m^2}{sec}$	$6.23 sec$
$Medean$	$1.4 * 10 \frac{\mu m^2}{sec}$	$4.57 sec$
$pMMec$	$1.2 * 10 \frac{\mu m^2}{sec}$	$5.33 sec$
$mRNAn$	$3.0 * 10^{-2} \frac{\mu m^2}{sec}$	$2130 sec$

Table 4.4: The time scales of diffusion

Therefore, the downstream network is a multi-scale network, which allows us to reduce the system for stochastic simulations. Since the diffusion time of Mad and Madea is much less than the time of phosphorylation and nuclear transport , we can assume that Mad and Madea are always well mixed in the nucleus and cytoplasm. By making this assumption, we can reduce the simulation time by half to one third. Moreover, the phosphorylation of Mad is much slower than other reactions, which implies a small number of pMad molecules and large fluctuations in the cytoplasm. Furthermore, the nucleo-cytoplasmic transport of mRNA is much slower than other reactions and diffusion processes, which may play an important role in the propagation of fluctuations.

4.2.3 Stochastic Simulation

In this section, we use the Gillespie simulation method to understand how reactions of different time scales affect the propagation of fluctuations in the single cell system with different settings. 50 realizations are generated for each case.

Simulation settings

To apply the Gillespie simulation method, we discretize the three cuboids into compartments and assume each compartment is well mixed. In particular, we divide the PV cuboid into $Px \times Py \times Pz$ identical compartments. Px, Py and Pz are the number of discretizations along the x-axis, the y-axis and the z-axis, respectively. The cytoplasmic cuboid is discretized into $Cx \times Cy \times Cz$ identical compartments. Cx, Cy and Cz are the number of discretizations along the x-axis, the y-axis and the z-axis, respectively. The nuclear cuboid is divided into $Nx \times Ny \times Nz$ identical compartments. Nx, Ny and Nz are the number of discretizations along the x-axis, the y-axis and the z-axis, respectively. Letting $Px = Cx = Nx = Pz = Cz = Nz$, each compartment in each layer is of dimension $\frac{9}{Nx}\mu m \times l_y^* \times \frac{9}{Nx}$, where l_y^* is the length of the side along y-axis. Here we choose $Cx = 3$, $Py = Cy = 1$ and $Ny = 3$. So the compartments in the PV, cytoplasmic and nuclear cuboids are of dimension $3\mu m \times 0.5\mu m \times 3\mu m$, $3\mu m \times 0.5\mu m \times 3\mu m$ and $3\mu m \times 1.3\mu m \times 3\mu m$ respectively.

Since we are only interested in patterning in the D-V axis, we assume that the system is uniform in the z-direction. We focus on a slice of the single cell in the $x - y$ plane. Fig. 4.9 shows the discretization of the system and the slice of the single cell we study.

In order to study fluctuations caused by a small number of signaling molecules, we assume B is only produced in one compartment in the PV cuboid at rate $1nM/min$ and the boundaries of the PV cuboid are reflective.

The temporal evolution of the system

Using the parameters from tables in Appendix 6.2, we simulate the biochemical system presented in Section 4.2.1. The mean number of molecules of each species in each compartment is given in Fig. 4.10. Ctotal equals the total number of molecules of

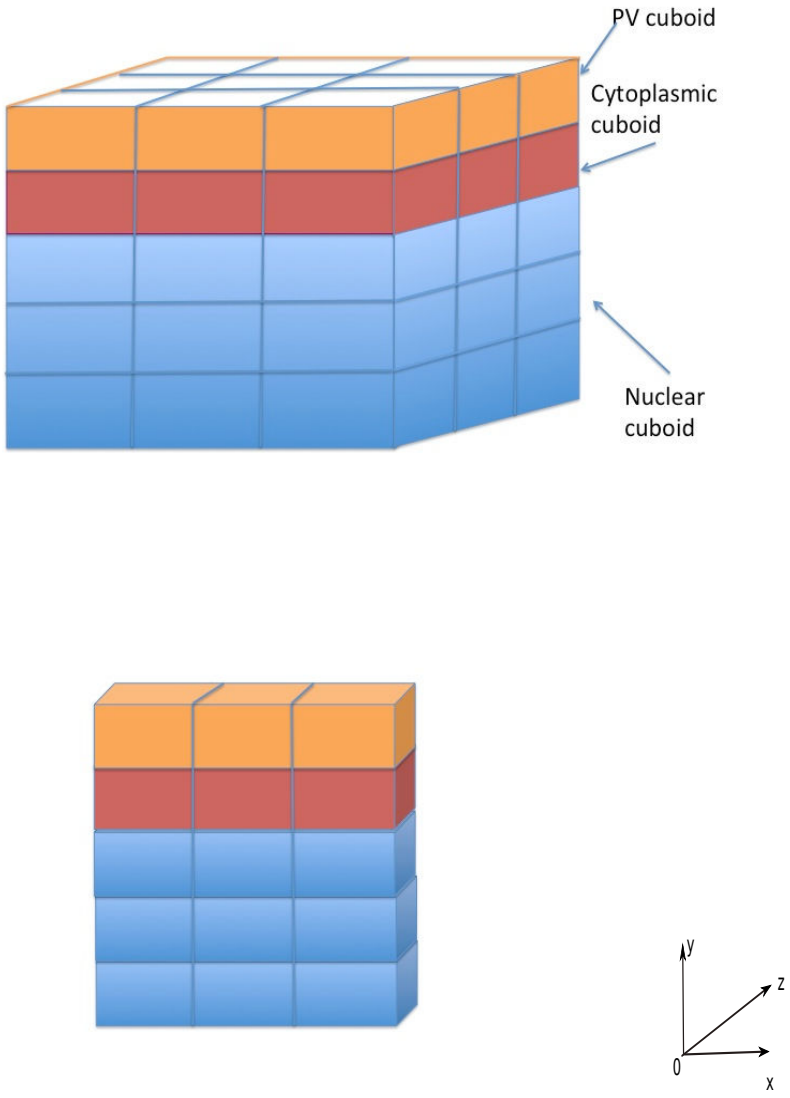

Figure 4.9: The discretization of the single cell system.

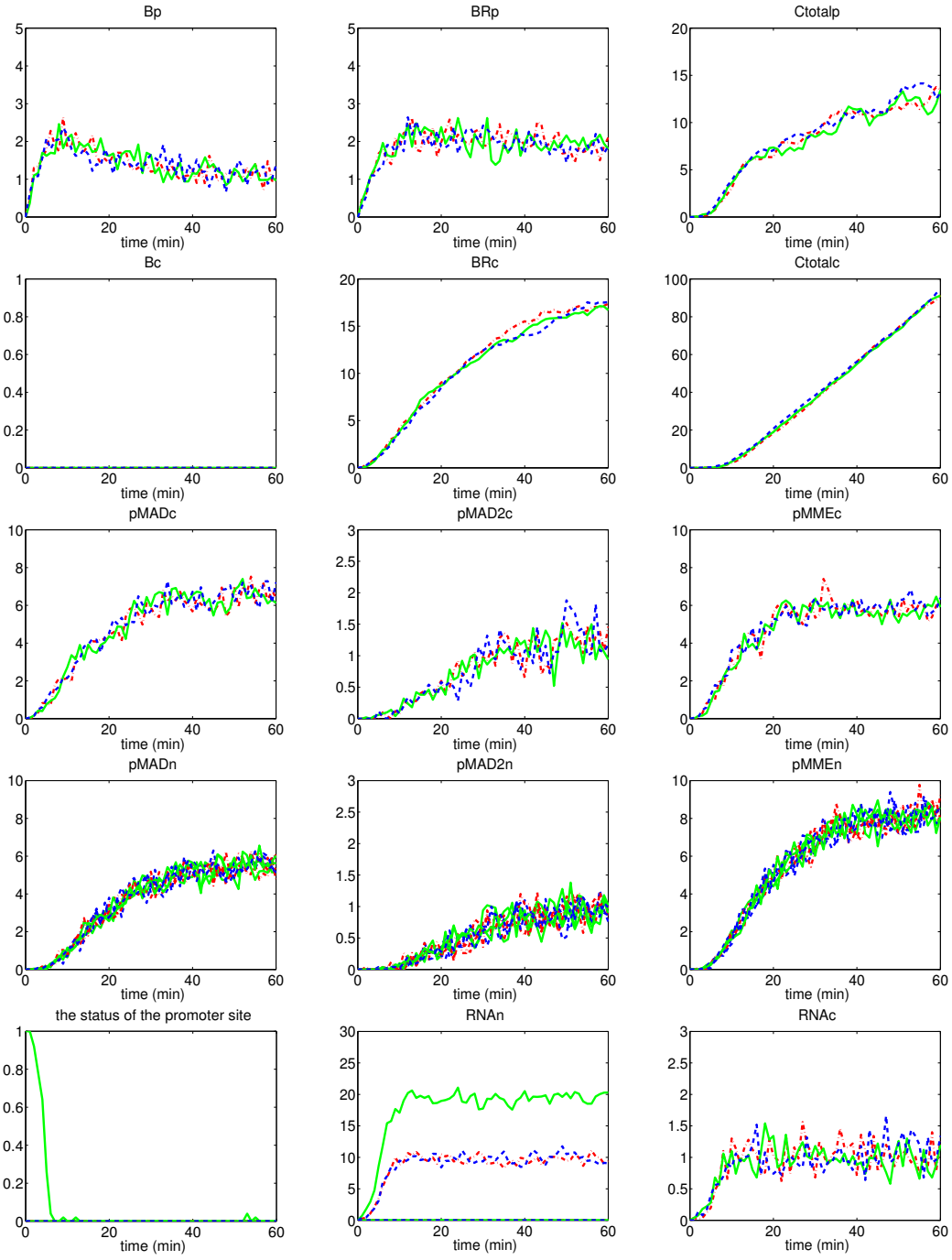

Figure 4.10: The temporal evolution of the single cell system.

BC, BCR and C. The status of the promoter site presents whether the promoter site is free or occupied. If it is one, the site is free; and if it is zero, the site is occupied. So averaging the status of the promoter site over all the realizations gives the probability that the promoter site is free. From Fig. 4.10, we can reach the following conclusions:

1. The signal level in the single cell system is consistent with the signal level in the half PV space in Section 4.1. In particular, the levels of B, BR and Ctotal are consistent with results in Section 4.1 and [5]. For example, the mean number of BR molecules is 2 in a PV compartment and 18 in a cytoplasmic compartment. So the total average number of BR molecules that can phosphorylate Mad in a cytoplasmic compartment is 20, which is equivalent to a density of $7.5nM$. In Section 4.1, the concentration threshold of BR for the amnioserosa boundary is around 10nM. Therefore, our single cell can be considered as a cell around the amnioserosa boundary. Similarly, Ctotal and B can be found to be consistent with previous results.

2. In spite of the local production of B and transport of molecules across membranes, all species except mRNA are well mixed in each cuboid. This can be explained by comparing two time scales: 1) B diffusion is much faster than the downstream reactions and 2) except mRNA, transport of other species across the nuclear membrane is much slower than diffusion. Therefore, we focus on one compartment in each cuboid in the following discussion. In particular, in the PV and cytoplasmic cuboids, we focus on the middle compartments. In the nuclear cuboid, we focus on the Central compartment, where the promoter site is located.

3. From 5 minutes on, the promoter site stays occupied and rarely becomes free anymore. This can be explained by comparing the propensity functions of the binding and unbinding reactions between transcription factors and the promoter site. The binding rate (k_{on}) is $60nM/min$ and the unbinding rate (k_{off}) is $0.067/min$. Therefore, once there is one transcription factor in the Central compartment, the propensity function of the binding reaction is 25. If the promoter site is occupied, the propensity function of the unbinding reaction is 0.067. So once the promoter site is occupied, it can be occupied most of time.

4. The mean number of B molecules in PV compartments first increases but decreases later. As more C molecules are produced, more B molecules will bind to C and endocytosis of BC decreases the amount of B. Since internalized B cannot get recycled, C can inhibit signaling at its high level. In addition, since internalized B cannot signal and cannot get recycled, we do not consider B in the cytoplasm. So the mean number of Bp is zero in all cytoplasmic compartments.

Signal sensitivity to transcription parameters

Since the propensity function of the binding reaction between transcription factors and the promoter site is much larger than that of the unbinding reaction, the promoter site will stay occupied once it is occupied. Here we study how the signal evolves if we increase the unbinding rate. Fig. 4.11 shows the temporal evolution of the status of the promoter site, the mean number of RNAn and the mean number of Ctotalp in the systems with different unbinding rates. As the unbinding rate increases, the times for the promoter site and RNAn to approach their quasi steady states increase. The increase of Ctotalp becomes slower, too. However, as k_{off} increases from $0.067min^{-1}$ to $6.7min^{-1}$, the change of the temporal evolution of the signal is much smaller than the change caused by increasing k_{off} from $6.7min^{-1}$ to $67min^{-1}$. This implies that the unbinding rate has to be increased enough to cause change in the downstream gene expression. To understand this, recall that the propensity function of the promoter site being occupied is 25 once there is a transcription factor in the central compartment. So the mean fraction of the occupancy status of the promoter site is larger than $\frac{25}{25+k_{off}}$. The transcription rate is increased by 10 times when the promoter site is occupied by transcription factors, so the mean transcription rate is at least

$$k_{bt}\frac{k_{off}+10*25}{k_{off}+25},$$

where k_{bt} is the basal transcription rate. As a result, k_{off} has to be increased substantially to cause reduction in $\frac{k_{off}+10*25}{k_{off}+25}$. Therefore, the system is robust to the change of unbinding rates. To study the fluctuations in the promoter site and the downstream gene expressions, we choose $6.7min^{-1}$ as the unbinding rates in the following sections.

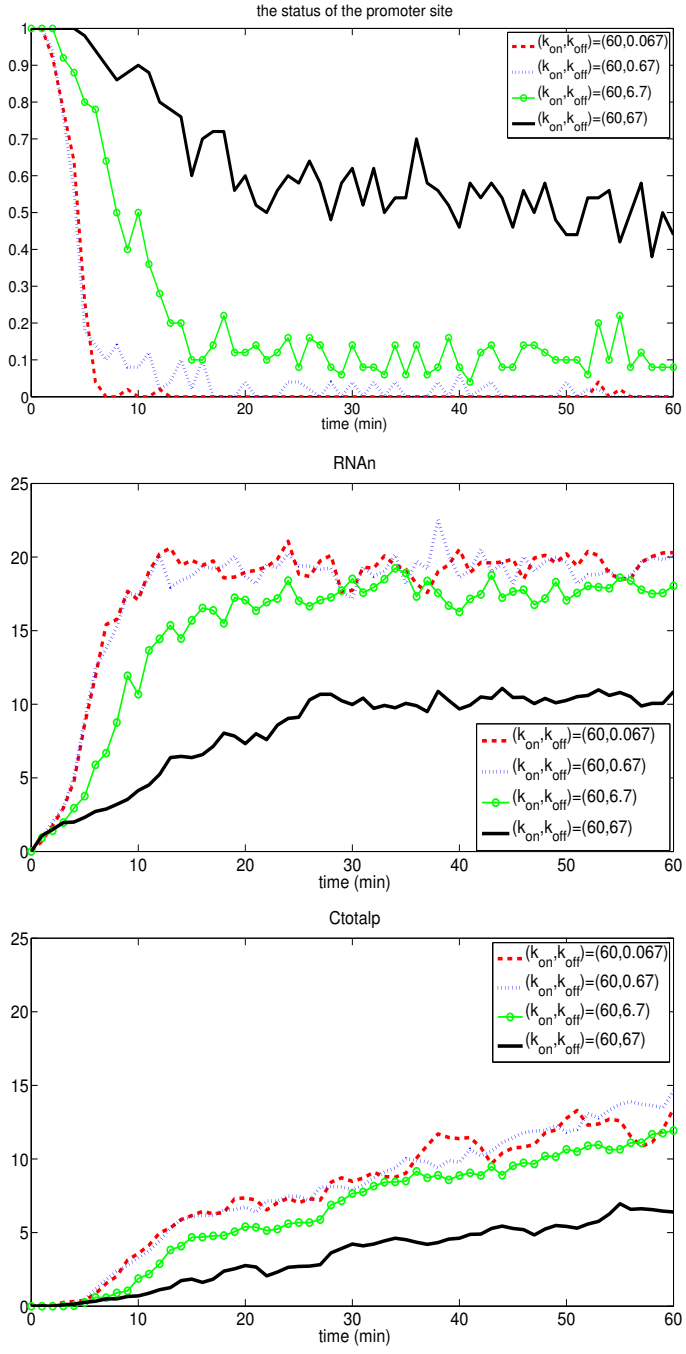

Figure 4.11: The signal sensitivity to transcription unbinding rates.

Noise propagation

Here we study how noise propagates along the signal transduction pathway by considering the CV of the number of molecules in one compartment. Fig. 4.14 shows different functions of the CV, depending whether the CV is around one or zero. The CV's of the numbers of molecules of Bp, BRp, BRc, pMadc, pMadn,P2c and P2n are represented by the exponential function of them. P2c (P2n) is the total number of molecules of pMad2 and pMMe in one cytoplasmic (nuclear) compartment. The CV's of the numbers of molecules of Ctotalp, RNAc, RNAn, and the promoter site (Site) are represented by the logarithm function of them. Fig. 4.14 shows the noise of BRc is smaller than that of BRp, which may be explained by the accumulation of BR in the cytoplasm by endocytosis. However, the noise of pMad is much larger than that of BRc, which can be caused by the slow phosphorylation step. In the nuclear compartment, the the noise of RNAn is much smaller than that of the promoter site, which can be explained by fast transcription. The noise of RNAc is larger than that of RNAn, due to the slow export of RNAn. The noise of Ctotalp is much smaller than that in RNAc, which may be explained by fast synthesis of C from cytoplasmic translation and rapid transport to the embryo membrane. In conclusion, the fast synthesis of C, cytoplasmic accumulation of BR by endocytosis and fast transcription may reduce noise while the slow phosphorylation of Mad and nuclear export of mRNA increase noise. However, the difference between the noises of pMadc, P2c, pMadn and P2n cannot be seen. Therefore, the effect of the nuclear accumulation of pMad, pMad2 and pMMe on the propagation of noise is little.

The hetero-trimers

It has been suggested that the transcription factor should be the hetero-trimer (pMad2/Madea) consisting of 2 pMad's and one Madea [73]. To test this hypothesis, we add the following reactions in the cytoplasm and nucleus:

$$pMad + pMMe \underset{k_{-8}}{\overset{k_8}{\rightleftharpoons}} pMad2/Madea \underset{k_{-8}}{\overset{k_8}{\rightleftharpoons}} pMad2 + Madea.$$

Moreover, pMad2/Madea can only be transported from the cytoplasm to the nucleus as pMad2 and pMMe. pMad2/Madea acts as the transcription factor that can enhance transcription, while pMad2 and pMMe are not transcription factors. Due to the

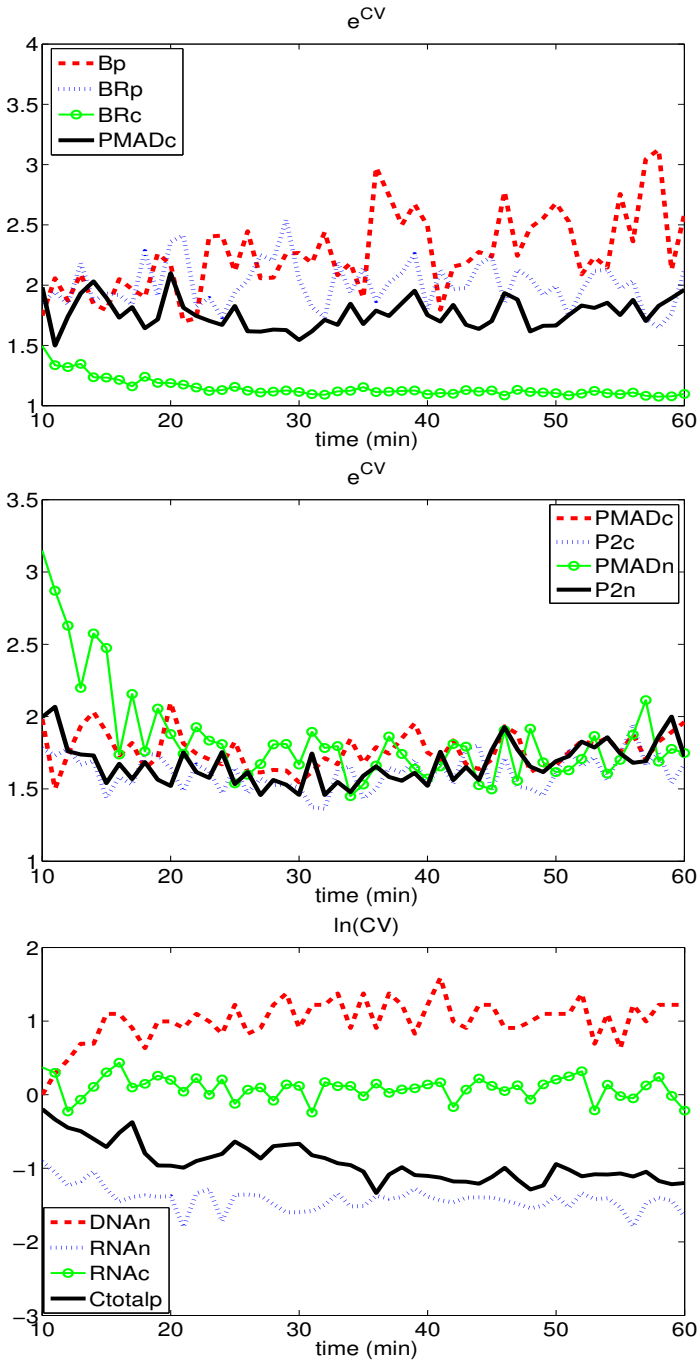

Figure 4.12: Noise propagation in the system with $(k_{on}, k_{off}) = (60, 6.7)$.

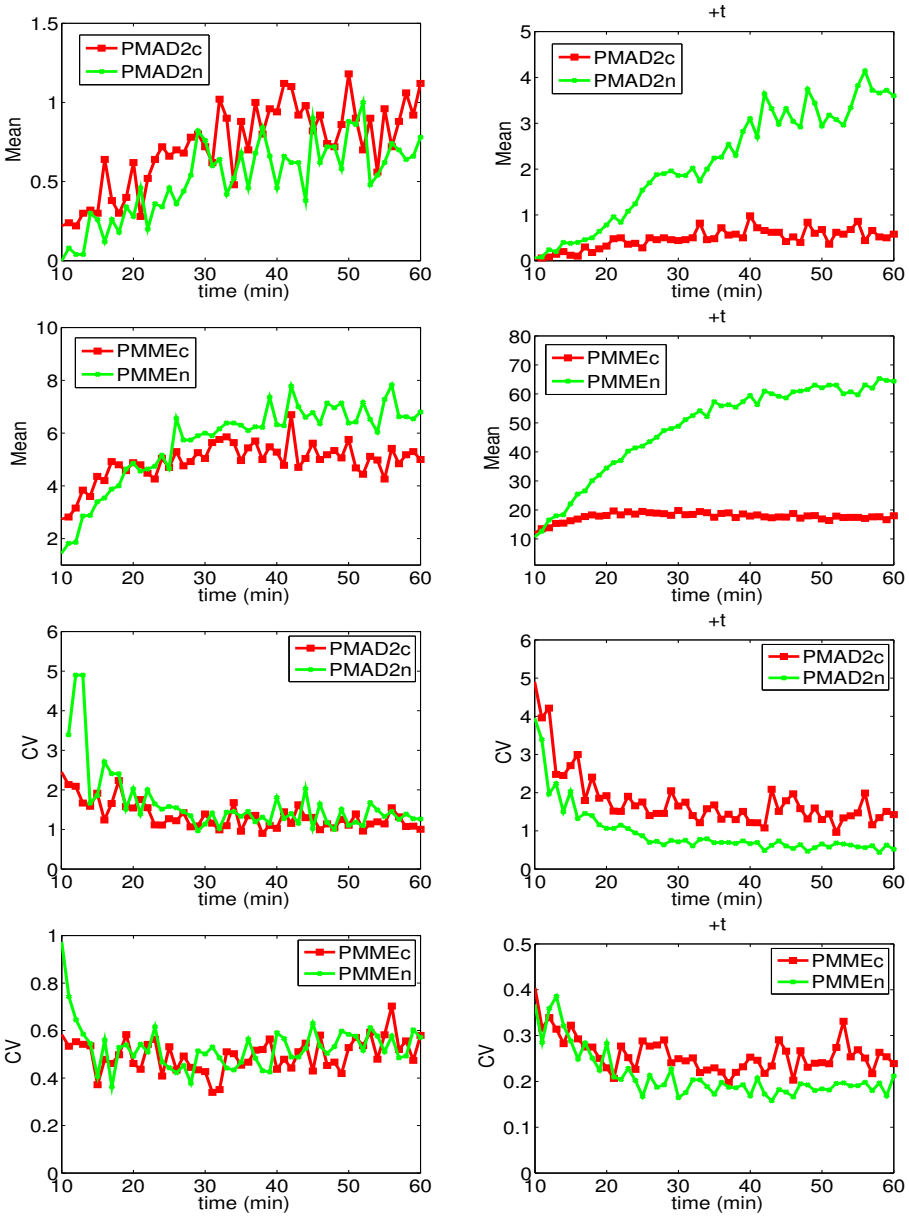

Figure 4.13: The trimer pMad2/Madea can amplify the nuclear accumulation.

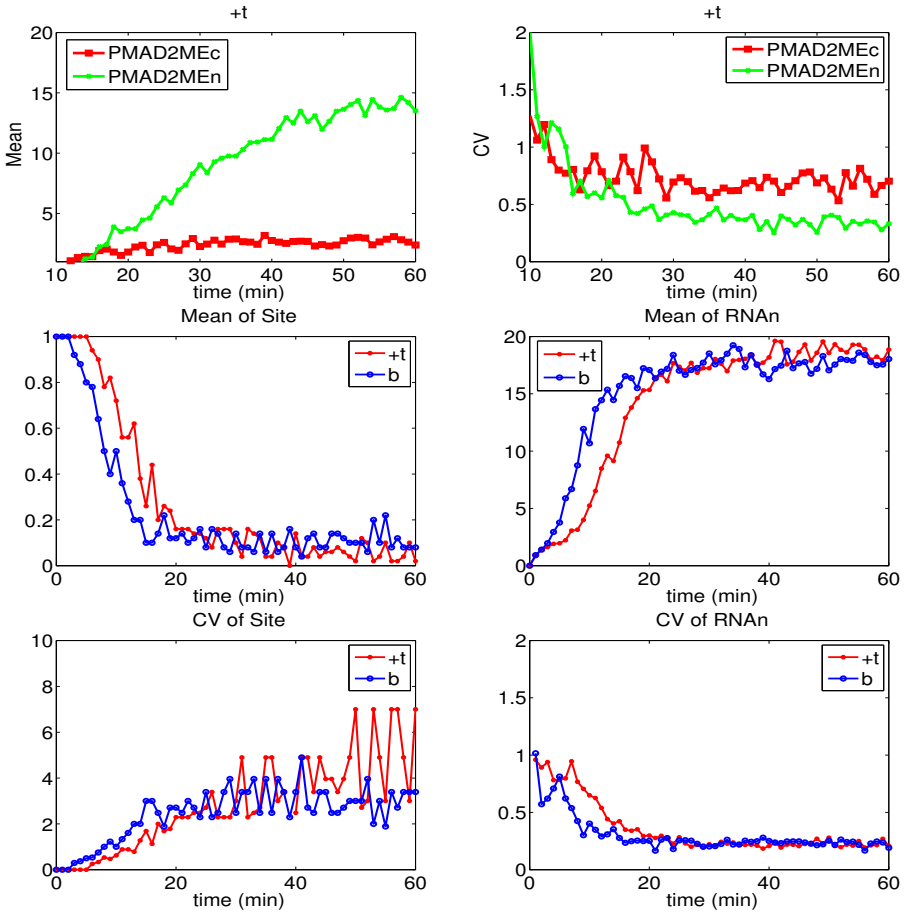

Figure 4.14: The response of the downstream signal to the formation of trimers.

slow phosphorylation of Mad, the formation of pMad2/Madea is much lower than that of pMad2 and pMMe. Therefore, for the consistency of the signal level, we increase the initial concentrations of Mad and Madea by four times. We simulate the system with pMad2/Madea and compare it with the basal system in Section4.2.3. As the system in Section 4.2.3, molecules of species except RNAn are well-mixed in each cuboid. Therefore, we focus on the middle cytoplasmic compartment and the central nuclear compartment. We compare the mean and CV of the numbers of pMad2 and pMMe molecules in the two systems. The comparison results are shown in Fig. 4.13. In Fig. 4.13, figures with the title $+t$ show the results of the system with pMad2/Madea as transcription factors, and the remaining ones show the results from the system in Section 4.2.3. Fig. 4.13 shows the CV's of the nuclear pMad2 and pMMe are less than those of the cytoplasmic pMad2 and pMMe in the system with the trimer formation, which can not be observed in the system in Section 4.2.3. It may be because that the unidirectional transport of pMAd2/Madea can enhance the nuclear accumulation enough to attenuate the fluctuations in the nucleus, which can be seen from the mean numbers of pMad2 and pMMe molecules in Fig. 4.13.

Fig. 4.14 shows how the downstream signal responds to the change of the transcription factor. In Fig. 4.14, PMAD2MEc and PMAD2MEn represent pMad2/Madea in the cytoplasm and the nucleus respectively. The system labeled with $+t$ is the system with the formation of the trimer and the system labeled with b is the system in Section 4.2.3. Fig. 4.14 shows the nuclear accumulation of pMad2/Madea leads to the reduction of the fluctuations of pMad2/Madea in the nucleus. However, due to the slow phosphorylation of Mad, the trimers pMad2/Madea are formed at a much lower rate than pMad2 and pMMe. As a result, the promoter site and RNAn approach their quasi-steady state more slowly.

Chapter 5

Conclusion and Future Work

Biochemical systems are stochastic due to random motion and collision of signaling molecules, and environmental fluctuations. Stochasticity is identified as the major reason for the phenotypic difference among genetically identical cells. However, the development of organisms is highly reproducible. How the biological system filters noise is the major topic we study in this thesis.

First, we have studied the effect of the localization of signaling molecules on the signal transduction pathway, in the deterministic and stochastic views. Using sensitivity analysis of the deterministic models, we have found slow diffusion and the fast degradation of the ligand near the receptor surface can interact with each other to sharpen the gradient of the signal and accelerate the relaxation of the biochemical system to the steady state. By analyzing the stochastic motion of a ligand molecule in a system with locally distributed receptors and membrane proteins, we have estimated the extent of localization in terms of diffusion coefficients and binding reaction rates. Our results also demonstrate that although the membrane protein can concentrate the ligand molecule around receptors, it has to pass the localized ligand molecule to receptors fast enough, in order to enhance signaling. Otherwise, the localization will inhibit signaling. The effect of localization on signal specificity has also been discussed. So far, we have assumed that the receptors and the membrane proteins are in excess, which leads to first-order reaction-diffusion systems. In the future, we plan to consider the change in the levels of free receptors and membrane proteins.

Ligand molecules bind to receptors to initiate downstream networks that may lead

to gene expression. Therefore, we study how the noise from the initiation step of transcription evolves along the elongation step and affects the production of mRNA. Our analysis shows that if the transcription complex forms at a random telegraph rate and the complex proceeds deterministically along the DNA sequence, the noise can approach zero as the length of the DNA sequence is long enough. During elongation, the complex pausing at the DNA sequence is commonly observed in transcription. We consider a system in which the complex arrives at the promoter site in a Poisson process and can pause at specific sites of the DNA sequence. We show that the transcription pause has to happen rarely and lasts long enough to lead to the bursts of mRNA production. In the future, we will study how the randomly switching of the status of the promoter site and the complex pausing interplay with each other to affect the production of mRNA.

During the process of determining the amnioserosa boundary in *Drosophila*, receptors bound by Dpp/Scw initiate the downstream network, which leads to the expression of an auxiliary membrane protein SBP (C). C can localize Dpp/Scw around receptors and affect signaling as a coreceptor, thereby forming a feedback loop. The feedback loop has been demonstrated by deterministic models in [5]. Here we use stochastic simulations to show how the feedback loop can help the system specify the amnioserosa boundary among a field of cells. Moreover, we propose a detailed single cell model for the downstream network. Our estimation of the time scales of reactions identifies the phosphorylation of Mad and nuclear export of mRNA are the two limiting steps in signal transduction. Our stochastic simulations imply that fluctuations are amplified at these steps. Moreover, we consider the system with the heterotrimer pMad2/Madea as the transcription factor and compare it with the system with the dimers as the transcription factor. The formation of the trimer can enhance the nuclear accumulation of pMad2 and pMMe, and reduce the fluctuations in the nucleus. However, due to the slow phosphorylation of Mad, the formation of the trimer is slow and the temporal evolution of the signal is slower than the system with the dimer as transcription factors. In the future, we will implement the single cell system in the whole pattern formation process, to understand how reactions of different time scales affect the communication between cells. However, the computation time can become a problem. Since the single cell system is a multi-scale reaction network, we may be able to simplify the system in an appropriate way to reduce the simulation time.

References

[1] D. StJohnston and W. Churchill. The beginning of the end. *EMBO JOURNAL*, 20(22):6169–6179, 2001.

[2] A. Stathopoulos and M. Levine. Dorsal gradient networks in the Drosophila embryo. *Developmental Biology*, 246(1):57–67, 2002.

[3] A. Eldar, R. Dorfman, D. Weiss, H. Ashe, BZ Shilo, and N. Barkai. Robustness of the BMP morphogen gradient in Drosophila embryonic patterning. *Nature*, 419(6904):304–8, 2002.

[4] R.P. Zinzen, J. Cande, M. Ronshaugen, D. Papatsenko, and M. Levine. Evolution of the ventral midline in insect embryos. *Developmental Cell*, 11(6):895–902, 2006.

[5] D.M. Umulis, M. Serpe, M.B. OConnor, and H.G. Othmer. Robust, bistable patterning of the dorsal surface of the Drosophila embryo. *Proceedings of the National Academy of Sciences*, 103(31):11613, 2006.

[6] B. Schmierer, A.L. Tournier, P.A. Bates, and C.S. Hill. Mathematical modeling identifies Smad nucleocytoplasmic shuttling as a dynamic signal-interpreting system. *Proceedings of the National Academy of Sciences*, 105(18):6608, 2008.

[7] B. Fett, J. Bruck, and M.D. Riedel. Synthesizing stochasticity in biochemical systems. In *Proceedings of the 44th annual conference on Design automation*, pages 640–645. ACM Press New York, NY, USA, 2007.

[8] M. Kaern, T.C. Elston, W.J. Blake, J.J. Collins, et al. Stochasticity in gene expression: from theories to phenotypes. *Nat Rev Genet*, 6(6):451–464, 2005.

[9] J. Hasty, F. Isaacs, M. Dolnik, D. McMillen, and JJ Collins. Designer gene networks: towards fundamental cellular control. *Chaos: An Interdisciplinary Journal of Nonlinear Science*, 11:207, 2001.

[10] R. Erban, J. Chapman, and P. Maini. A practical guide to stochastic simulations of reaction-diffusion processes. *Lecture Notes*, 2007.

[11] J. Crank. *The mathematics of diffusion*. Oxford University Press, 1983.

[12] http://science.jrank.org/pages/1397/Chemoreception.html.

[13] NG van Kampen. Stochastic Processes in Physics and Chemistry. *Amsterdam, New York*, 1992.

[14] CW Gardiner. Handbook of stochastic methods(for physics, chemistry and the natural sciences). 2009.

[15] D.T. Gillespie. The multivariate Langevin and Fokker–Planck equations. *American Journal of Physics*, 64:1246, 1996.

[16] D.T. Gillespie. The chemical Langevin equation. *The Journal of Chemical Physics*, 113:297, 2000.

[17] T.G. Kurtz. The relationship between stochastic and deterministic models for chemical reactions. *The Journal of Chemical Physics*, 57:2976, 2003.

[18] DT Gillespie. A general method for numerically simulating the stochastic time evolution of coupled chemical reactions (1976). *J. Comp. Phys*, 22:403–434.

[19] C. Gadgil, C.H. Lee, and H.G. Othmer. A stochastic analysis of first-order reaction networks. *Bulletin of Mathematical Biology*, 67(5):901–946, 2005.

[20] D.T. Gillespie et al. Exact stochastic simulation of coupled chemical reactions. *The Journal of Physical Chemistry*, 81(25):2340–2361, 1977.

[21] S.A. Isaacson and C.S. Peskin. Incorporating diffusion in complex geometries into stochastic chemical kinetics simulations. *SIAM JOURNAL ON SCIENTIFIC COMPUTING*, 28(1):47, 2006.

[22] S.A. Isaacson. The reaction-diffusion master equation as an asymptotic approximation of diffusion to a small target. *SIAM Journal on Applied Mathematics*, 70(1):77–111, 2009.

[23] H-W. Kang, L.Zheng, and H.G. Othmer. A new method for choosing the computational cell in stochastic reaction-diffusion systems. *Submitted*.

[24] L.A. Goentoro, G.T. Reeves, C.P. Kowal, L. Martinelli, T. Schüpbach, and S.Y. Shvartsman. Quantifying the Gurken morphogen gradient in Drosophila oogenesis. *Developmental Cell*, 11(2):263–272, 2006.

[25] V. Morel and F. Schweisguth. Repression by Suppressor of Hairless and activation by Notch are required to define a single row of single-minded expressing cells in the Drosophila embryo. *Genes & Development*, 14(3):377–388, 2000.

[26] http://www.bio.uu.nl/ cpio/handouts/DrosophilaHandout.pdf.

[27] MP Belvin, Y. Jin, and KV Anderson. Cactus protein degradation mediates Drosophila dorsal-ventral signaling. *Genes & Development*, 9(7):783–793, 1995.

[28] http://www.sdbonline.org/fly/torstoll/cactus1.htm.

[29] N. Kirov, S. Childs, M. O'Connor, and C. Rushlow. The Drosophila dorsal morphogen represses the tolloid gene by interacting with a silencer element. *Molecular and Cellular Biology*, 14(1):713–722, 1994.

[30] Y.C. Wang and E.L. Ferguson. Spatial bistability of Dpp–receptor interactions during Drosophila dorsal–ventral patterning. *Nature*, 434(7030):229–234, 2005.

[31] S.D. Podos and E.L. Ferguson. Morphogen gradients: new insights from DPP. *Trends in Genetics*, 15(10):396–402, 1999.

[32] T. Gregor, E.F. Wieschaus, A.P. McGregor, W. Bialek, and D.W. Tank. Stability and nuclear dynamics of the bicoid morphogen gradient. *Cell*, 130(1):141–152, 2007.

[33] P. Joly, B.H. Jennings, and S.N. Jayasinghe. Development and fertility studies on post-bio-electrosprayed Drosophila melanogaster embryos. *Biomicrofluidics*, 3:44107, 2009.

[34] R.R. Dubreuil, P. Wang, S. Dahl, J. Lee, and L.S.B. Goldstein. Drosophila β Spectrin functions independently of α Spectrin to polarize the Na, K ATPase in epithelial Cells. *Journal of Cell Biology*, 149(3):647–656, 2000.

[35] R.G. Thorne, A. Lakkaraju, E. Rodriguez-Boulan, and C. Nicholson. In vivo diffusion of lactoferrin in brain extracellular space is regulated by interactions with heparan sulfate. *Proceedings of the National Academy of Sciences*, 105(24):8416, 2008.

[36] D. Umulis, M.B. O'Connor, and S.S. Blair. The extracellular regulation of bone morphogenetic protein signaling. *Development*, 136(22):3715, 2009.

[37] A. Levchenko, J. Bruck, and P.W. Sternberg. Scaffold proteins may biphasically affect the levels of mitogen-activated protein kinase signaling and reduce its threshold properties. *Proceedings of the National Academy of Sciences of the United States of America*, 97(11):5818, 2000.

[38] M. González-Gaitán. Signal dispersal and transduction through the endocytic pathway. *Nature Reviews Molecular Cell Biology*, 4(3):213–224, 2003.

[39] M.J. Marinissen and J.S. Gutkind. Scaffold proteins dictate Rho GTPase-signaling specificity. *Trends in biochemical sciences*, 30(8):423–426, 2005.

[40] V. Greco, M. Hannus, and S. Eaton. Argosomes:: a potential vehicle for the spread of morphogens through epithelia. *Cell*, 106(5):633–645, 2001.

[41] E.S. Seto, H.J. Bellen, and T.E. Lloyd. When cell biology meets development: endocytic regulation of signaling pathways. *Genes & development*, 16(11):1314, 2002.

[42] T. Bollenbach, K. Kruse, P. Pantazis, M. González-Gaitán, and F. Jülicher. Morphogen transport in epithelia. *Physical Review E*, 75(1):011901, 2007.

[43] G. Adam and M. Delbrück. Reduction of dimensionality in biological diffusion processes. *Structural chemistry and molecular biology*, pages 198–215, 1968.

[44] J.A. Papin, T. Hunter, B.O. Palsson, and S. Subramaniam. Reconstruction of cellular signalling networks and analysis of their properties. *Nature Reviews Molecular Cell Biology*, 6(2):99–111, 2005.

[45] H.C. Berg and E.M. Purcell. Physics of chemoreception. *Biophysical journal*, 20(2):193–219, 1977.

[46] FW Wiegel and C. DeLisi. Evaluation of reaction rate enhancement by reduction in dimensionality. *American Journal of Physiology- Regulatory, Integrative and Comparative Physiology*, 243(5):R475, 1982.

[47] O.G. Berg, R.B. Winter, and P.H. Von Hippel. Diffusion-driven mechanisms of protein translocation on nucleic acids. 1. Models and theory. *Biochemistry*, 20(24):6929–6948, 1981.

[48] M. Coppey, O. Bénichou, R. Voituriez, and M. Moreau. Kinetics of target site localization of a protein on DNA: a stochastic approach. *Biophysical journal*, 87(3):1640–1649, 2004.

[49] B.N. Kholodenko, J.B. Hoek, and H.V. Westerhoff. Why cytoplasmic signalling proteins should be recruited to cell membranes. *Trends in Cell Biology*, 10(5):173–178, 2000.

[50] C. Wofsy and B. Goldstein. Effective rate models for receptors distributed in a layer above a surface: application to cells and Biacore. *Biophysical journal*, 82(4):1743–1755, 2002.

[51] D.M. Umulis. Analysis of dynamic morphogen scale invariance. *Journal of the Royal Society Interface*, 6(41):1179, 2009.

[52] D. Umulis, M.B. O'Connor, and H.G. Othmer. Robustness of embryonic spatial patterning in Drosophila melanogaster. *Current topics in developmental biology*, 81:65–111, 2008.

[53] X. Wang, R.E. Harris, L.J. Bayston, and H.L. Ashe. Type IV collagens regulate BMP signalling in Drosophila. *Nature*, 455(7209):72–77, 2008.

[54] JH Fessler and LI Fessler. Drosophila extracellular matrix. *Annual review of cell biology*, 5(1):309–339, 1989.

[55] V. Shahrezaei and P.S. Swain. The stochastic nature of biochemical networks. *Current opinion in biotechnology*, 19(4):369–374, 2008.

[56] A. Raj and A. van Oudenaarden. Nature, nurture, or chance: stochastic gene expression and its consequences. *Cell*, 135(2):216–226, 2008.

[57] A. Eldar and M.B. Elowitz. Functional roles for noise in genetic circuits. *Nature*, 467(7312):167–173, 2010.

[58] V. Elgart, T. Jia, A.T. Fenley, and R. Kulkarni. Connecting protein and mrna burst distributions for stochastic models of gene expression. *Physical Biology*, 8:046001, 2011.

[59] P. Swain. Modelling stochastic gene expression. *Notes*.

[60] M. Depken, E.A. Galburt, and S.W. Grill. The origin of short transcriptional pauses. *Biophysical journal*, 96(6):2189–2193, 2009.

[61] M.L. Kireeva and M. Kashlev. Mechanism of sequence-specific pausing of bacterial rna polymerase. *Proceedings of the National Academy of Sciences*, 106(22):8900, 2009.

[62] P.B. Rahl, C.Y. Lin, A.C. Seila, R.A. Flynn, S. McCuine, C.B. Burge, P.A. Sharp, and R.A. Young. C-myc regulates transcriptional pause release. *Cell*, 141(3):432–445, 2010.

[63] M. Dobrzyński and F.J. Bruggeman. Elongation dynamics shape bursty transcription and translation. *Proceedings of the National Academy of Sciences*, 106(8):2583, 2009.

[64] V. Shahrezaei and P.S. Swain. Analytical distributions for stochastic gene expression. *Proceedings of the National Academy of Sciences*, 105(45):17256, 2008.

[65] M.W. Smiley and S.R. Proulx. Gene expression dynamics in randomly varying environments. *Journal of mathematical biology*, 61(2):231–251, 2010.

[66] T. Jia and R.V. Kulkarni. Post-transcriptional regulation of noise in protein distributions during gene expression. *Physical review letters*, 105(1):18101, 2010.

[67] A. Raj, C.S. Peskin, D. Tranchina, D.Y. Vargas, and S. Tyagi. Stochastic mrna synthesis in mammalian cells. *PLoS biology*, 4(10):e309, 2006.

[68] M. Voliotis, N. Cohen, C. Molina-París, and T.B. Liverpool. Fluctuations, pauses, and backtracking in dna transcription. *Biophysical journal*, 94(2):334–348, 2008.

[69] B. Fristedt and L.F. Gray. *A modern approach to probability theory*. Birkhauser, 1997.

[70] J.M.G. Vilar, R. Jansen, and C. Sander. Signal processing in the tgf-β superfamily ligand-receptor network. *PLoS Computational Biology*, 2(1):e3, 2006.

[71] Peter ten Dijke and Carl-Henrik Heldin. Smad signal transduction: Smads in proliferation, differentiation and disease. *Proteins and Cell Regulation*, 5, 2006.

[72] B. Schmierer and C.S. Hill. Kinetic analysis of smad nucleocytoplasmic shuttling reveals a mechanism for transforming growth factor β-dependent nuclear accumulation of smads. *Molecular and cellular biology*, 25(22):9845, 2005.

[73] B.Y. Qin, B.M. Chacko, S.S. Lam, M.P. de Caestecker, J.J. Correia, and K. Lin. Structural basis of smad1 activation by receptor kinase phosphorylation. *Molecular cell*, 8(6):1303–1312, 2001.

[74] ME Young, PA Carroad, and RL Bell. Estimation of diffusion coefficients of proteins. *Biotechnology and Bioengineering*, 22(5):947–955, 1980.

[75] B. Marom, E. Heining, P. Knaus, and Y.I. Henis. Formation of stable homomeric and transient heteromeric bmp receptor complexes regulates smad signaling. *Journal of Biological Chemistry*, 2011.

[76] A. Zilman, S. Di Talia, B.T. Chait, M.P. Rout, M.O. Magnasco, et al. Efficiency, selectivity, and robustness of nucleocytoplasmic transport. *PLoS Comput Biol*, 3(7):e125, 2007.

[77] A. Mor, S. Suliman, R. Ben-Yishay, S. Yunger, Y. Brody, and Y. Shav-Tal. Dynamics of single mrnp nucleocytoplasmic transport and export through the nuclear pore in living cells. *Nature cell biology*, 12(6):543–552, 2010.

[78] D.Y. Vargas, A. Raj, S.A.E. Marras, F.R. Kramer, and S. Tyagi. Mechanism of mrna transport in the nucleus. *Proceedings of the National Academy of Sciences of the United States of America*, 102(47):17008, 2005.

[79] E.A. Nalefski, E. Nebelitsky, J.A. Lloyd, and S.R. Gullans. Single-molecule detection of transcription factor binding to dna in real time: specificity, equilibrium, and kinetic parameters. *Biochemistry*, 45(46):13794–13806, 2006.

[80] A.M. Kierzek, L. Zhou, and B.L. Wanner. Stochastic kinetic model of two component system signalling reveals all-or-none, graded and mixed mode stochastic switching responses. *Mol. BioSyst.*, 6(3):531–542, 2009.

[81] A. Tiwari, G. Balázsi, M.L. Gennaro, and O.A. Igoshin. The interplay of multiple feedback loops with post-translational kinetics results in bistability of mycobacterial stress response. *Physical Biology*, 7:036005, 2010.

[82] D.M. Suter, N. Molina, D. Gatfield, K. Schneider, U. Schibler, and F. Naef. Mammalian genes are transcribed with widely different bursting kinetics. *Science*, 332(6028):472, 2011.

[83] S. Thomsen, S. Anders, S.C. Janga, W. Huber, and C.R. Alonso. Genome-wide analysis of mrna decay patterns during early drosophila development. *Genome biology*, 11(9):R93, 2010.

Chapter 6

Appendices

6.1 Ligand signaling in a complex medium

6.1.1 The smallest pole (in magnitude) for $\mathcal{L}[u](\bar{y}, s)$

When $\theta = 1$, $\mathcal{L}[u](\bar{y}, s)$ has an essential singularity and the smallest pole (in magnitude) can not be used to estimate the relaxation time of u to the steady state. Therefore, we assume $\theta \neq 1$. Here we find the smallest pole (in magnitude) for $\theta > 1$ and the result can be extended to the case when $\theta < 1$. For $\theta > 1$, there exists a nonzero real pole of Eq. (2.11) in $(-1, -\frac{1}{\theta})$. For any real $s \in [(-1, -\frac{1}{\theta})]$, Eq. (2.12) becomes:

$$\begin{aligned} &\Gamma\sqrt{\delta}\sqrt{s+1}\cos\left(\alpha\sqrt{-(s+\frac{1}{\theta})}\right)\sinh\left(\beta\sqrt{s+1}\right) \\ &-\sqrt{-\delta(s+\frac{1}{\theta})}\sin\left(\alpha\sqrt{-(s+\frac{1}{\theta})}\right)\cosh\left(\beta\sqrt{s+1}\right) = 0. \end{aligned} \tag{A1}$$

When $s = -1$, the left-side term in Eq. (A1) is less than zero. On the other hand, when $s = -\theta$, the left-side term in Eq. (A1) is greater than zero. Therefore, at least one real zero of Eq. (A1) exists in $(-1, -\frac{1}{\theta})$. Let s_{re} be a real zero of Eq. (A1) in $(-1, -\frac{1}{\theta})$.

Let $x + yi$ be the smallest pole of Eq. (2.11) in magnitude. Then, $|x + yi| \leqslant 1$, $|x| < 1$ and $|y| < 1$. Now, we will show that $|y| \ll 1$. For simple notation, we set

$$(a + bi)^2 \equiv (x + 1) + yi, \tag{A2}$$

$$(m + ni)^2 \equiv (x + \frac{1}{\theta}) + yi. \tag{A3}$$

Therefore, $|a|^2+|b|^2=\sqrt{(|x|+1)^2+|y|^2}<\sqrt{5}$ and $|m|^2+|n|^2<\sqrt{(|x|+1)^2+|y|^2}<\sqrt{5}$. Moreover, $a+bi$ and $m+ni$ satisfy the following:

$$\begin{aligned}&\Gamma\sqrt{\delta}(a+bi)\cosh\{\alpha(m+ni)\}\sinh\{\beta(a+bi)\}\\&+(m+ni)\sinh\{\alpha(m+ni)\}\cosh\{\beta(a+bi)\}=0.\end{aligned}\tag{A4}$$

Multiplying the complex conjugate of the second term in Eq. (A4) to both sides of Eq. (A4), we get

$$\begin{aligned}&\Im[(a+bi)\cosh\{\alpha(m+ni)\}\sinh\{\beta(a+bi)\}\\&\times(m-ni)\sinh\{\alpha(m-ni)\}\cosh\{\beta(a-bi)\}]=0,\end{aligned}$$

where $\Im$ is the ideal part of a complex number. For simple notation, we set

$$\bar{m}=\alpha m,\quad \bar{n}=\alpha n,\quad \bar{a}=\beta a,\quad \bar{b}=\beta b.$$

Then Eq. (A5) gives

$$\begin{aligned}&\{\bar{m}\sinh(2\bar{m})-\bar{n}\sin(2\bar{n})\}\left\{\bar{b}\sinh(2\bar{a})+\bar{a}\sin(2\bar{b})\right\}\\&=\{\bar{n}\sinh(2\bar{m})+\bar{m}\sin(2\bar{n})\}\left\{\bar{a}\sinh(2\bar{a})-\bar{b}\sin(2\bar{b})\right\}.\end{aligned}\tag{A5}$$

Moreover, $|\bar{m}|=|\alpha||m|<5^{\frac{1}{4}}|\alpha|\ll 1$. Similarly, $|\bar{n}|\ll 1$, $|\bar{a}|\ll 1$ and $|\bar{b}|\ll 1$. Using Taylor expansion in Eq. (A5), we have

$$\begin{aligned}&\left\{\bar{m}\left(2\bar{m}+O\left(\bar{m}^3\right)\right)-\bar{n}\left(2\bar{n}+O\left(\bar{n}^3\right)\right)\right\}\left\{\bar{b}\left(2\bar{a}+O\left(\bar{a}^3\right)\right)+\bar{a}\left(2\bar{b}+O\left(\bar{b}^3\right)\right)\right\}\\&=\left\{\bar{n}\left(2\bar{m}+O\left(\bar{m}^3\right)\right)+\bar{m}\left(2\bar{n}+O\left(\bar{n}^3\right)\right)\right\}\left\{\bar{a}\left(2\bar{a}+O\left(\bar{a}^3\right)\right)-\bar{b}\left(2\bar{b}+O\left(\bar{b}^3\right)\right)\right\}.\end{aligned}$$

Therefore,

$$\left\{m^2-n^2+O\left(\alpha^2\right)\right\}\left\{2ab+O\left(\beta^2\right)\right\}=\left\{2mn+O\left(\alpha^2\right)\right\}\left\{a^2-b^2+O\left(\beta^2\right)\right\}.\tag{A6}$$

Since $a^2-b^2=x+1$, $m^2-n^2=x+\theta$, and $2ab=2mn=y$ from Eq. (A2) and (A3), Eq. (A6) becomes

$$\left\{x+\frac{1}{\theta}+O(\alpha^2)\right\}\left\{y+O(\beta^2)\right\}\;=\;\left\{y+O(\alpha^2)\right\}\left\{x+1+O(\beta^2)\right\}.\tag{A7}$$

Simplifying Eq. (A7) for α^2 and β^2 gives

$$y\;\approx\;O\left(\alpha^2\right)(x+1-y)+O\left(\beta^2\right)(y-x-\frac{1}{\theta})+O\left(\alpha^2\beta^2\right).$$

Since $|x| < 1$ and $|y| < 1$, using $\alpha \ll 1$ and $\beta \ll 1$, we get $y \ll 1$.

We find the smallest pole of Eq. (2.11) below. Plugging $x + yi$ in Eq. (2.12), we have

$$\begin{aligned}
&\Gamma\sqrt{\delta}\sqrt{x+1+yi}\cosh\left\{\alpha\sqrt{x+\frac{1}{\theta}+yi}\right\}\sinh\left\{\beta\sqrt{x+1+yi}\right\} \\
&+\sqrt{x+\frac{1}{\theta}+yi}\sinh\left\{\alpha\sqrt{x+\frac{1}{\theta}+yi}\right\}\cosh\left\{\beta\sqrt{x+1+yi}\right\} \\
&= 0. \qquad \text{(A8)}
\end{aligned}$$

Therefore, the left hand side of Eq. (A8) only depends on $x+1+yi$ and $x+\frac{1}{\theta}+yi$. Due to $y \ll 1$, we can consider $x+1$ and $x+\frac{1}{\theta}$ to find the smallest nonzero pole in magnitude, i.e., we can estimate the smallest nonzero real pole, $s_{\min}$, of Eq. (2.11) in magnitude. Letting $y = 0$ in Eq. (A8), for any $x > -\frac{1}{\theta}$, the left hand side of Eq. (A8) is always positive. So $s_{\min} < -\frac{1}{\theta}$ and $s_{\min}$ obeys the following equation

$$\Gamma\sqrt{\delta}\sqrt{s+1}\tanh\left(\beta\sqrt{s+1}\right)+\sqrt{-\delta(s+\frac{1}{\theta})}\tan\left(\alpha\sqrt{-(s+\frac{1}{\theta})}\right) \;=\; 0. \qquad \text{(A9)}$$

Since there exist at least one real pole of Eq. (2.11) in $[-1, -\frac{1}{\theta}]$, we have $|s_{\min}| < 1$. Due to $\alpha \ll 1$ and $\beta \ll 1$, we have $\alpha\sqrt{-(s_{min}+\frac{1}{\theta})} \ll 1$ and $\beta\sqrt{s_{\min}+1} \ll 1$. So Taylor expansion of Eq. (A9) gives

$$\begin{aligned}
&\Gamma\sqrt{\delta}\sqrt{s+1}\left\{\beta\sqrt{s+1}-\frac{\left(\beta\sqrt{s+1}\right)^3}{3}\right\} \\
+\quad &\sqrt{-(s+\theta)}\left\{\alpha\sqrt{-(s+\frac{1}{\theta})}-\frac{\left(\alpha\sqrt{-(s+\frac{1}{\theta})}\right)^3}{3}\right\}\approx 0
\end{aligned}$$

which is a quadratic equation for s_{min}. Solving Eq. (A10) for s, we get

$$s \;\approx\; \frac{-2\left(\frac{1}{\theta}\alpha^3+\Gamma\beta^3\sqrt{\delta}\right)+3\left(\alpha+\Gamma\beta\sqrt{\delta}\right)\pm\sqrt{\triangle}}{2(\alpha^3+\Gamma\beta^3\sqrt{\delta})} \qquad \text{(A10)}$$

where

$$\triangle \;=\; 9(\alpha+\Gamma\beta\sqrt{\delta})^2+4\alpha\beta\Gamma\sqrt{\delta}\left\{3(\alpha^2-\beta^2)(1-\frac{1}{\theta})-\alpha^2\beta^2(1-\frac{1}{\theta})^2\right\}.$$

Using $\alpha \ll 1$ and $\beta \ll 1$ and $\sqrt{1+z} \approx 1 + \frac{z}{2}$ for $|z| \ll 1$, we approximate $\sqrt{\triangle}$ as follows:

$$\sqrt{\triangle} \approx 3\left(\alpha + \Gamma\beta\sqrt{\delta}\right)\left[1 + \frac{4\alpha\beta\Gamma\sqrt{\delta}(1-\frac{1}{\theta})\left\{3(\alpha^2-\beta^2) - \alpha^2\beta^2(1-\frac{1}{\theta})\right\}}{18\left(\alpha + \Gamma\beta\sqrt{\delta}\right)^2}\right].$$

Since $|s_{\min}| < 1$, we get

$$s \approx \frac{-2\left(\frac{1}{\theta}\alpha^3 + \Gamma\beta^3\sqrt{\delta}\right) + 3\left(\alpha + \Gamma\beta\sqrt{\delta}\right) - \sqrt{\triangle}}{2(\alpha^3 + \Gamma\beta^3\sqrt{\delta})} \tag{A11}$$

Using $\alpha = \sqrt{\frac{\delta(1-\epsilon)^2}{\Lambda}}$, $\beta = \sqrt{\frac{\epsilon^2}{\Lambda}}$, and $\frac{\beta}{\alpha} = \frac{\rho}{\sqrt{\delta}}$ where $\rho = \frac{\epsilon}{1-\epsilon}$, we rewrite Eq. (A11) as

$$s_{\min} \approx -1 + \frac{1-\frac{1}{\theta}}{1+\Gamma\rho} + \frac{\Gamma\rho^3(1-\frac{1}{\theta})^2}{3\Lambda(1+\rho)^2(1+\frac{\Gamma\rho^3}{\sqrt{\delta}})(1+\Gamma\rho)}.$$

6.1.2 The solution to the immobilization equations

The system governed by Eq. (2.18) can be rewritten in the following vector form

$$\begin{pmatrix} p_{1b} \\ p_{1bc} \end{pmatrix}_t = \begin{pmatrix} D_1\Delta & \\ & 0 \end{pmatrix}\begin{pmatrix} p_{1b} \\ p_{1bc} \end{pmatrix} + \begin{pmatrix} -k_+ & k_- \\ k_+ & -k_- \end{pmatrix}\begin{pmatrix} p_{1b} \\ p_{1bc} \end{pmatrix}. \tag{B1}$$

subject to the following initial and boundary conditions:

$$\begin{aligned} p_{1b}(y,0|y_0,0) &= \delta(y-y_0), \\ p_{1bc}(y,0|y_0,0) &= 0, \\ \frac{\partial p_{1b}}{\partial y}(y,t|y_0,0) &= 0, \quad \text{at } y = 0, \\ p_{1b}(y,t|y_0,0) &= 0, \quad \text{at } y = H_1. \end{aligned}$$

Let $D = \begin{pmatrix} D_1 & \\ & 0 \end{pmatrix}$ and $K = \begin{pmatrix} -k_+ & k_- \\ k_+ & -k_- \end{pmatrix}$. Then the solution to Eq. (B1) has the form $\begin{pmatrix} p_{1b} \\ p_{1bc} \end{pmatrix} = \sum_{n=0}^{\infty} e^{\lambda_n t}\Psi_n(y)$, where $\Psi_n(y)$ is the eigenfunction and λ_n is the eigenvalue. Therefore, $\Psi_n(y)$ is the solution to

$$D\Delta\Psi_n + (K - \lambda_n I)\Psi_n = 0, \qquad \frac{\partial \Psi_n}{\partial y}|_{y=0} = 0, \qquad \Psi_n|_{y=H_1} = 0.$$

Then it is easy to check that $\Psi_n = \begin{pmatrix} \nu_{1n} \\ \nu_{2n} \end{pmatrix} \psi_n$, where ψ_n is a solution to the following scalar eigenvalue problem

$$\Delta\psi_n + \omega_n^2 \psi_n = 0 \quad \text{for } y \in [0, H_1], \qquad \frac{\partial \psi_n}{\partial y}|_{y=0} = 0, \qquad \psi_n(y, t|y_0, 0)|_{y=H_1} = 0. \quad \text{(B2)}$$

Moreover, $\nu_n = \begin{pmatrix} \nu_{1n} \\ \nu_{2n} \end{pmatrix}$ satisfies the algebraic eigenvalue problem

$$(K - \omega_n^2 D - \lambda_n I)\nu_n = 0, \quad \text{(B3)}$$

where I is the 2×2 identity matrix.

From Eq. (B2), we obtain $\omega_n = \frac{(2n+1)\pi}{2H_1}$ and $\psi_n = \cos\frac{(2n+1)\pi y}{2H_1}$. From Eq. (B3)), we have $\det(K - \omega_n^2 - \lambda_n I) = 0$ and obtain

$$\lambda_{n\pm} = \frac{-(k_+ + k_- + \omega_n^2 D_1) \pm \upsilon_n}{2}$$

, where

$$\upsilon_n = \sqrt{(k_+ + k_- + \omega_n^2 D_1)^2 - 4k_-\omega_n^2 D_1}$$

. Define $\nu_{n\pm}$ such that $\begin{pmatrix} p_{1b} \\ p_{1bc} \end{pmatrix} = \sum_{n=0}^{\infty} e^{\lambda_{n+}t}\psi_n\nu_{n+} + e^{\lambda_{n-}t}\psi_n\nu_{n-}$. Then we have $(K - \omega_n^2 D - \lambda_{n+}I)\nu_{n+} = 0$ and $(K - \omega_n^2 D - \lambda_{n-}I)\nu_{n-} = 0$. Using the initial condition of $\begin{pmatrix} p_{1b} \\ p_{1bc} \end{pmatrix}$, we obtain

$$\begin{aligned}
\nu_{n+} &= \frac{1}{H_1\upsilon_n}\cos\frac{(2n+1)\pi y_0}{2H_1}\begin{pmatrix} k_- - k_+ - \omega_n^2 D_1 + \upsilon_n \\ \\ 2k_+ \end{pmatrix} \\
\nu_{n-} &= \frac{1}{H_1\upsilon_n}\cos\frac{(2n+1)\pi y_0}{2H_1}\begin{pmatrix} k_+ - k_- + \omega_n^2 D_1 + \upsilon_n \\ \\ -2k_+ \end{pmatrix}.
\end{aligned}$$

Following the above procedure, we solve Eq. (2.21) and get p_2 as follows:

$$p_2(y,t|y_0,0) = \sum_{n=0}^{\infty} \frac{2}{H_2} e^{-\left(\frac{2n\pi+\pi}{2H_2}\right)^2 D_2 t} \sin\frac{(2n+1)\pi(y_0-H_1)}{2H_2} \sin\frac{(2n+1)\pi(y-H_1)}{2H_2}.$$

6.1.3 The probability density function of the molecule at the steady state

The Laplace transform of Eq. (2.28) with respect to t gives

$$\begin{aligned} & \mathcal{L}[G_{1B}](s,y|y_0) \\ = \; & \mathcal{L}[p_{1B}](s,y|y_0) + \mathcal{L}[G_{1B}](s,y|H_1-h) \\ \times \; & \{s\mathcal{L}[S_1](s|y_0,0) - S_1(0|y_0,0)\}\{s\mathcal{L}[S_2](s|H_1+h,0) - S_2(0|H_1+h,0)\}, \end{aligned} \quad \text{(C1)}$$

where $\mathcal{L}[f](s)$ represents the Laplace transform of $f(t)$. Based on the definition of $S_1(t|y_0,0)$ and $S_2(t|H_1+h,0)$, we have $S_1(0|y_0,0)=1$ and $S_2(0|H_1+h,0)=1$.

Letting $y_0 = H_1 - h$ in Eq. (C1), we obtain

$$\begin{aligned} & \mathcal{L}[G_{1B}](s,y|H_1-h) \\ = \; & \frac{\mathcal{L}[p_{1B}](s,y|H_1-h)}{s\mathcal{L}[S_1](s|H_1-h) + s\mathcal{L}[S_2](s|H_1+h) - s^2\mathcal{L}[S_1](s|H_1-h)\mathcal{L}[S_2](s|H_1+h)} \end{aligned}$$

Therefore, for any $y_0 \in [0, H_1+h]$, we have

$$\begin{aligned} & \mathcal{L}[G_{1B}](s,y|y_0) \\ = \; & \mathcal{L}[p_{1B}](s,y|y_0) + \frac{\mathcal{L}[p_{1B}](s,y|H_1-h)\{s\mathcal{L}[S_1](s|y_0)-1\}\{s\mathcal{L}[S_2](s|H_1+h)-1\}}{1-\{s\mathcal{L}[S_1](s|H_1-h)-1\}\{s\mathcal{L}[S_2](s|H_1+h)-1\}}. \end{aligned} \quad \text{(C2)}$$

Then we get

$$\begin{aligned} \lim_{t\to\infty} G_{1B}(y,t|y_0) &= \lim_{s\to 0} s\mathcal{L}[G_{1B}](s,y|y_0) \\ &= \frac{\mathcal{L}[p_{1B}](0,y|H_1-h)}{\mathcal{L}[S_1](0|H_1-h) + \mathcal{L}[S_2](0|H_1+h)}. \end{aligned} \quad \text{(C3)}$$

By computing Laplace transforms of Eq. (C3), we get

$$\lim_{t\to\infty} G_{1B}(y,t|y_0)$$

$$= \frac{\sum_{n=0}^{\infty} \frac{(H_1+h)}{D_1(2n\pi+\pi)^2} \cos\frac{(2n\pi+\pi)(H_1-h)}{2(H_1+h)} \cos\frac{(2n\pi+\pi)y}{2(H_1+h)}}{\sum_{n=0}^{\infty} \frac{2(-1)^n(H_1+h)^2(k_++k_-)}{D_1k_-(2n\pi+\pi)^3} \cos\frac{(2n\pi+\pi)(H_1-h)}{2(H_1+h)} + \sum_{n=0}^{\infty} \frac{2(H_2+h)^2}{D_2(2n\pi+\pi)^3} \sin\frac{h(2n\pi+\pi)}{H_2+h}}.$$

Using the similar approach of deriving $\lim_{t\to\infty} G_{1B}(y,t|y_0)$, we get

$$\lim_{t\to\infty} G_1(y,t|y_0) \tag{C4}$$

$$= \frac{\sum_{n=0}^{\infty} \frac{(H_1+h)(k_++k_-)}{k_-D_1(2n\pi+\pi)^2} \cos\frac{(2n\pi+\pi)(H_1-h)}{2(H_1+h)} \cos\frac{(2n\pi+\pi)y}{2(H_1+h)}}{\sum_{n=0}^{\infty} \frac{2(-1)^n(H_1+h)^2(k_++k_-)}{D_1k_-(2n\pi+\pi)^3} \cos\frac{(2n\pi+\pi)(H_1-h)}{2(H_1+h)} + \sum_{n=0}^{\infty} \frac{2(H_2+h)^2}{D_2(2n\pi+\pi)^3} \sin\frac{h(2n\pi+\pi)}{H_2+h}}$$

$$= (1+K_D) \lim_{t\to\infty} G_{1B}(y,t|y_0)$$

and

$$\lim_{t\to\infty} G_2(y,t|y_0) \tag{C5}$$

$$= \frac{\sum_{n=0}^{\infty} \frac{(H_2+h)}{D_2(2n\pi+\pi)^2} \sin\frac{h(2n\pi+\pi)}{H_2+h} \sin\frac{(2n\pi+\pi)(y-H_1+h)}{2(H_2+h)}}{\sum_{n=0}^{\infty} \frac{2(-1)^n(H_1+h)^2(k_++k_-)}{D_1k_-(2n\pi+\pi)^3} \cos\frac{(2n\pi+\pi)(H_1-h)}{2(H_1+h)} + \sum_{n=0}^{\infty} \frac{2(H_2+h)^2}{D_2(2n\pi+\pi)^3} \sin\frac{h(2n\pi+\pi)}{H_2+h}}.$$

Letting h go to zero in Eq. (C4), we get [1]

$$\lim_{h\to 0}\lim_{t\to\infty} G_{1B}(y,t|y_0) = \frac{\frac{1}{D_1}\sum_{n=0}^{\infty} \frac{(-1)^n \cos\frac{(2n\pi+\pi)y}{2H_1}}{(2n\pi+\pi)}}{\frac{H_1(1+K_D)}{4D_1} + \frac{H_2}{4D_2}}.$$

To calculate $\sum_{n=0}^{\infty} \frac{(-1)^n \cos\frac{(2n\pi+\pi)y}{2H_1}}{(2j\pi+\pi)}$, we consider a function $f(x)$ such that for any integer k,

$$f(x) = \begin{cases} 1, & \text{if } x \in (4k-1, 4k+1), \\ -1, & \text{if } x \in (4k+1, 4k+3), \\ 0, & \text{if } x = 4k-1, 4k+1 \text{ or } x = 4k+3. \end{cases}$$

[1] Here, we use $\sum_{n=0}^{\infty} \frac{1}{(2n+1)^2} = \frac{\pi^2}{8}$.

The Fourier expansion of $f(x)$ is as follows:

$$f(x) = 4\sum_{n=0}^{\infty} \frac{(-1)^n}{(2n\pi+\pi)} \cos\frac{(2n\pi+\pi)x}{2}.$$

Therefore for $y \in (0, H_1)$, we have

$$\sum_{n=0}^{\infty} \frac{(-1)^n}{(2n\pi+\pi)} \cos\frac{(2n\pi+\pi)y}{2H_1} = \frac{1}{4}.$$

So

$$\lim_{h\to 0}\lim_{t\to\infty} G_{1B}(y,t|y_0) = \frac{\frac{1}{D_1}}{\frac{H_1(1+K_D)}{D_1}+\frac{H_2}{D_2}}.$$

Similarly, letting h goes to zero in Eq. (C4) and (C5), we get

$$\lim_{h\to 0}\lim_{t\to\infty} G_1(y,t|y_0) = \frac{\frac{(1+K_D)}{D_1}}{\frac{H_1(1+K_D)}{D_1}+\frac{H_2}{D_2}},$$

$$\lim_{h\to 0}\lim_{t\to\infty} G_2(y,t|y_0) = \frac{\frac{1}{D_2}}{\frac{H_1(1+K_D)}{D_1}+\frac{H_2}{D_2}}.$$

6.1.4 The probability of escaping a perfectly absorbing surface

Define $P_{a,c}(b)$ as the probability that the molecule starts at $y = b$ hits $y = a$ before hitting $y = c$. To connect Region I' and II', we consider the probability $P_{H_1+h,0}(y_0)$ that the molecule starting at $y = y_0$ in Region I' reaches $y = H_1 + h$ before getting absorbed at $y = 0$. We consider the steady-state probability density function of a molecule in a one-dimensional system with absorbers at $y = 0$ and $y = H_1 + h$. Since the system (b) in Section 2.3.3 is uniform in x-direction, we only need to consider the one-dimensional system here. Then $P_{H_1+h,0}(y_0)$ is the ratio of the outward flux at $y = y_0$ to the total flux at $y = y_0$. Define $C(y|y_0)$ as the steady-state probability density function such that $C(y|y_0)\,dy$ gives the probability of the ligand molecule starting at y_0 to stay at $[y, y + dy)$ in the steady-state. The governing equation is given as

$$\begin{aligned} D_1\frac{d^2C(y|y_0)}{dy^2} &= -\delta(y-y_0) \\ C(0|y_0) &= 0 \end{aligned} \qquad \text{(D1)}$$

$$C(H_1+h|y_0) \;=\; 0.$$

By using Fourier transform, we solver the above equation and get

$$C(y|y_0) \;=\; \begin{cases} C_0\left(\frac{-y_0}{D_1(H_1+h)}+\frac{1}{D_1}\right)y, & \text{if } y \leqslant y_0, \\ C_0\left(\frac{-y_0 y}{D_1(H_1+h)}+\frac{y_0}{D_1}\right), & \text{if } y \geqslant y_0, \end{cases}$$

where C_0 is a constant.

Then we get

$$\begin{aligned} P_{H_1+h,0}(y_0) &= \frac{\lim\limits_{y\to y_0^+} -D_1\frac{dC(y|y_0)}{dy}}{\lim\limits_{y\to y_0^+} -D_1\frac{dC(y|y_0)}{dy}+\lim\limits_{y\to y_0^-} D_1\frac{dC(y|y_0)}{dy}} \\ &= \frac{y_0}{H_1+h}. \end{aligned}$$

To test $P_{H_1+h,0}(y_0)$, we assume that $H_1=(2^N-1)h$, where N is an integer.

$$P_{H_1+h,0}(H_1-h) \;=\; 1-P_{0,H_1+h}(H_1-h). \tag{D2}$$

Since the molecule starting at $y=H_1-h$ should pass $y=H_1-3h$ to reach $y=0$, we rewrite the right-side term in Eq. (D2) as

$$Eq.(\text{D2}) \;=\; 1-P_{H_1-3h,H_1+h}(H_1-h)P_{0,H_1+h}(H_1-3h). \tag{D3}$$

Since $y=H_1-3h$ and $y=H_1+h$ are symmetric with respect to $y=H_1-h$, we get

$$P_{H_1-3h,H_1+h}(H_1-h)=\frac{1}{2}. \tag{D4}$$

Using Eq. (D4), we rewrite Eq. (D3) as

$$Eq.(\text{D3}) \;=\; 1-\frac{1}{2}P_{0,H_1+h}(H_1-3h). \tag{D5}$$

Repeating the procedure in Eq. (D2)-(D5), we compute $P_{H_1+h,0}(H_1-h)$ as

$$P_{H_1+h,0}(H_1-h) \;=\; 1-\left(\frac{1}{2}\right)^{N-1}P_{0,H_1+h}(H_1-(2^N-1)h). \tag{D6}$$

Since $H_1=(2^N-1)h$, we get

$$\begin{aligned} P_{H_1+h,0}(H_1-h) &= 1-\left(\frac{1}{2}\right)^{N-1} \\ &= \frac{H_1-h}{H_1+h}. \end{aligned}$$

6.1.5 The mean time for the ligand molecule to bind to receptors.

Following the procedure in Section 6.1.2, we solve Eq. (2.40) and obtain

$$
\begin{aligned}
&p_{1b}^{(b)}(x,y,t|x_0,y_0,0)\\
&=\sum_{i,j=0}^{\infty}\eta_{ij}e^{-\left(\frac{k_++k_-+k_b-C_{ij}}{2}\right)t}\left[\cosh(\omega_{ij}t)+\frac{-k_++k_-+k_b+C_{ij}}{2\omega_{ij}}\sinh(\omega_{ij}t)\right]\\
&\times\cos\frac{i\pi x}{L}\cos\frac{(2j+1)\pi y}{2(H_1+h)},
\end{aligned}
\tag{E1a}
$$

$$
\begin{aligned}
&p_{1bc}^{(b)}(x,y,t|x_0,y_0,0)\\
&=k_+\sum_{i,j=0}^{\infty}\frac{\eta_{ij}}{\omega_{ij}}e^{-\left(\frac{k_++k_-+k_b-C_{ij}}{2}\right)t}\sinh(\omega_{ij}t)\cos\frac{i\pi x}{L}\cos\frac{(2j+1)\pi y}{2(H_1+h)}
\end{aligned}
\tag{E1b}
$$

$$
\begin{aligned}
&p_{1br}^{(b)}(x,y,t|x_0,y_0,0)\\
&=k_+k_b\sum_{i,j=0}^{\infty}\frac{\eta_{ij}}{\omega_{ij}}\cos\frac{i\pi x}{L}\cos\frac{(2j+1)\pi y}{2(H_1+h)}\\
&\left[e^{-\left(\frac{-k_++k_-+k_b-C_{ij}}{2}\right)t}\left\{\frac{e^{\omega_{ij}t}}{k_+-(k_-+k_b)+C_{ij}+2\omega_{ij}}\right.\right.\\
&\left.\left.-\frac{e^{-\omega_{ij}t}}{k_+-(k_-+k_b)+C_{ij}-2\omega_{ij}}\right\}+\frac{\omega_{ij}}{k_+k_b-C_{ij}(k_-+k_b)}\right],
\end{aligned}
\tag{E1c}
$$

where $C_{ij}=-\left[\left(\frac{i\pi}{L}\right)^2+\left(\frac{(2j+1)\pi}{2(H_1+h)}\right)^2\right]D_1$, $\omega_{ij}^2=\left(\frac{-k_++k_-+k_b+C_{ij}}{2}\right)^2+k_-k_+$, and

$$
\eta_{ij}=\begin{cases}\frac{4}{L(H_1+h)}\cos\frac{i\pi x_0}{L}\cos\frac{(2j+1)\pi y_0}{2(H_1+h)}, & \text{if } i\neq 0\\ \frac{2}{L(H_1+h)}\cos\frac{(2i+1)\pi y_0}{2(H_1+h)}, & \text{if } i=0.\end{cases}
$$

Let $P_{1b}^{(b)}(t,x_0,y_0)$, $P_{1bc}^{(b)}(t,x_0,y_0)$ and $P_{1br}^{(b)}(t,x_0,y_0)$ be the probabilities that the molecule starting from (x_0,y_0) at time 0 lies in Region I' at time t as a molecule of species B, BC and BR respectively, without leaving I' before time t. Using Eq. (E1), we get

$$
\begin{aligned}
&P_{1b}^{(b)}(t,x_0,y_0)\\
=\;&\int_0^L\int_0^{H_1+h}p_{1b}^{(b)}(x,y,t|x_0,y_0,0)\,dy\,dx\\
=\;&\sum_{j=0}^{\infty}\frac{(-1)^j\eta_{0j}L(H_1+h)}{2\omega_{ij}(2j+1)\pi}\left[(-k_++k_-+k_b+C_{ij}+2\omega_{ij})e^{\left(\frac{-k_+-k_--k_b+C_{ij}+2\omega_{ij}}{2}\right)t}\right.
\end{aligned}
$$

$$-(-k_+ + k_- + k_b + C_{ij} - 2\omega_{ij})e^{\left(\frac{-k_- - k_b - k_+ + C_{ij} - 2\omega_{ij}}{2}\right)t}\Bigg]$$

$$\begin{aligned}
& P_{1bc}^{(b)}(t, x_0, y_0) \\
= & \int_0^L \int_0^{H_1+h} p_{1bc}^{(b)}(x, y, t|x_0, y_0, 0)\, dy\, dx \\
= & k_+ \sum_{j=0}^{\infty} \frac{(-1)^j \eta_{0j} L(H_1 + h)}{\omega_{0j}(2j+1)\pi} \left[e^{\left(\frac{-k_+ - k_- - k_b + C_{0j} + 2\omega_{0j}}{2}\right)t} - e^{\left(\frac{k_+ - k_- - k_b + C_{0j} - 2\omega_{0j}}{2}\right)t} \right] \\
& P_{1br}^{(b)}(t, x_0, y_0) \\
= & \int_0^L \int_0^{H_1+h} p_{1br}^{(b)}(x, y, t|x_0, y_0, 0)\, dy\, dx \\
= & k_+ k_b \sum_{j=0}^{\infty} \frac{2(-1)^j \eta_{0j} L(H_1 + h)}{\omega_{0j}(2j+1)\pi} \left[\frac{e^{\left(\frac{k_+ - k_- - k_b + C_{0j} + 2\omega_{0j}}{2}\right)t}}{k_+ - k_- - k_b + C_{0j} + 2\omega_{0j}} \right. \\
& \left. - \frac{e^{\left(\frac{k_+ - k_- - k_b + C_{0j} + 2\omega_{0j}}{2}\right)t}}{k_+ - k_- - k_b + C_{0j} - 2\omega_{0j}} + \frac{\omega_{0j}}{k_+ k_b - C_{0j}(k_- + k_b)} \right],
\end{aligned}$$

Let $TR_{1h}^{(b)}$ be the random variable of the time when the molecule leaves Region I' for the first time or the molecule becomes of species BR before leaving Region I'. Let $T_{1h}^{(b)}$ be the time when the molecule leaves Region I' for the first time. Then we have

$$\begin{aligned}
P\left(T_{1h}^{(b)} < t|x_0, y_0\right) &= 1 - \left(P_{1b}^{(b)}(t, x_0, y_0) + P_{1bc}^{(b)}(t, x_0, y_0) + P_{1br}^{(b)}(t, x_0, y_0)\right) \\
P\left(TR_{1h}^{(b)} < t|x_0, y_0\right) &= 1 - \left(P_{1b}^{(b)}(t, x_0, y_0) + P_{1bc}^{(b)}(t, x_0, y_0)\right)
\end{aligned}$$

Let $T_h^{(b)}$ be the time when the molecule becomes of species BR. Then

$$E\left[T_h^{(b)}|x_0, y_0\right] \tag{E2}$$

$$\begin{aligned}
= & E\left[TR_{1h}^{(b)}|y_0\right] \\
& + \int_0^{\infty} \left\{E\left[T_{2h}^{(b)}|H_1 + h\right] + E\left[T_h^{(b)}|H_1 - h\right]\right\} \frac{dP\left(T_{1h}^{(b)} < t|y_0\right)}{dt}\, dt
\end{aligned} \tag{E3}$$

where $T_{2h}^{(b)}$ is the random variable for the time when the molecule starting in Region II' leaves Region II' for the first time and $\frac{dP\left(T_{1h}^{(b)} < t|y_0\right)}{dt}dt$ is the probability that the molecule leaves Region I' during time interval $[t, t + dt)$. Letting $y_0 = H_1 - h$, we have

$$E\left[T_h^{(b)}|H_1 - h\right]$$

$$
\begin{aligned}
&= E\left[TR_{1h}^{(b)}|H_1-h\right] + \int_0^\infty \left\{E\left[T_{2h}^{(b)}|H_1+h\right] + E\left[T_h^{(b)}|H_1-h\right]\right\} \frac{dP\left(T_{1h}^{(b)} < t|y_0\right)}{dt}\, dt \\
&= \int_0^\infty \left\{P_{1b}^{(b)}(t, H_1-h) + P_{1bc}^{(b)}(t, H_1-h)\right\} dt \\
&\quad + \left\{E\left[T_{2h}^{(b)}|H_1+h\right] + E\left[T_h^{(b)}|H_1-h\right]\right\} \int_0^\infty \frac{dP\left(T_1^{(b)} < t|H_1-h\right)}{dt}\, dt \\
&= \int_0^\infty \left\{P_{1b}^{(b)}(t, H_1-h) + P_{1bc}^{(b)}(t, H_1-h)\right\} dt \\
&\quad + \left\{E\left[T_{2h}^{(b)}|H_1+h\right] + E\left[T_h^{(b)}|H_1-h\right]\right\} \lim_{t\to\infty}\left(1 - P_{1br}^{(b)}(t, H_1-h)\right)
\end{aligned}
$$

Therefore,

$$
\begin{aligned}
& E\left[T_h^{(b)}|H_1-h\right] \\
&= \frac{E\left[T_{2h}^{(b)}|H_1+h\right] \lim_{t\to\infty}\left(1-P_{1br}^{(b)}(t,H_1-h)\right) + \int_0^\infty \left\{P_{1b}^{(b)}(t,H_1-h)+P_{1bc}^{(b)}(t,H_1-h)\right\} dt}{\lim_{t\to\infty} P_{1br}^{(b)}(t,H_1-h)}.
\end{aligned}
$$

If (x_0, y_0) is in Region II', we have

$$
\begin{aligned}
\frac{\partial p_2^{(b)}(x,y,t|x_0,y_0,0)}{\partial t} &= D_2 \Delta p_2^{(b)}(x,y,t|x_0,y_0,0) \\
p_2^{(b)}(x,y,0|x_0,y_0,0) &= \delta(x-x_0)\delta(y-y_0), \\
\frac{\partial p_2^{(b)}(x,y,t|x_0,y_0,0)}{\partial x} &= 0, \quad \text{at } x=0 \text{ and } x=L, \\
p_2^{(b)}(x,y,t|x_0,y_0,0) &= 0, \quad \text{at } y = H_1-h, \\
\frac{\partial p_2^{(b)}(x,y,t|x_0,y_0,0)}{\partial y} &= 0, \quad \text{at } y = H_1+H_2.
\end{aligned}
$$

Similar to Section 2.3.1, we can get

$$
E\left[T_{2h}^{(b)}|y_0\right] = \sum_{i=0}^{\infty} \frac{16(H_2+h)^2 \sin\frac{(2i+1)\pi(y_0-(H_1-h))}{2(H_2+h)}}{D_2(2i\pi+\pi)^3}.
$$

Then the average time for the molecule starting at $y = H_1 - h$ is

$$
E\left[T_h^{(b)}|H_1-h\right]
$$

$$= \frac{\sum_{i=0}^{\infty} \frac{16(H_2+h)^2 \sin\frac{(2i+1)\pi h}{H_2+h}}{D_2(2i\pi+\pi)^3} \left(1 - k_+k_b \sum_{j=0}^{\infty} X_j\right) + (k_+ + k_- + k_b) \sum_{i=0}^{\infty} X_i}{k_+k_b \sum_{i=0}^{\infty} X_i},$$

where $X_i = \frac{4(-1)^i \cos\frac{(2i+1)\pi(H_1-h)}{2(H_1+h)}}{(2j+1)\pi(k_+k_b - C_{0i}(k_- + k_b))}$.

If $y_0 < H_1$, we can substitute $E\left[T_h^{(b)}|H_1 - h\right]$ into Eq. (E3) and get $E\left[T_h^{(b)}|y_0\right]$. If $y_0 > H_1$, we have

$$E\left[T_{br}^{(b)}|y_0\right] = E\left[T_{2h}^{(b)}|y_0\right] + E\left[T_{br}^{(b)}|H_1 - h\right]$$

If the initial position of the molecule is uniformly distributed in the whole domain, we have the average time for the molecule to become of species BR as follows:

$$\begin{aligned} E\left[T_{br}^{(b)}\right] &= \lim_{h\to 0} \int_0^{H_1+H_2} \frac{E\left[T_h^{(b)}|y_0\right]}{H_1+H_2}\, dy_0 \\ &= \frac{H_1H_2}{D_2 \sum_{i=0}^{\infty} A_i} \left\{ \frac{1}{2k_+k_b} - \frac{H_1}{H_1+H_2} \sum_{i=0}^{\infty} \frac{A_i}{(2i\pi+\pi)^2} \right\} \\ &\quad + \frac{k_+ + k_- + k_b}{k_+k_b} + \frac{32H_2^3}{D_2(H_1+H_2)} \sum_{i=0}^{\infty} \frac{1}{(2i\pi+\pi)^4}, \end{aligned} \tag{E4}$$

where $A_i = \frac{1}{k_+k_b + \left(\frac{2i\pi+\pi}{2H_1}\right)^2 D_1(k_- + k_b)}$.

6.2 Stochastic fluctuations in dorsal surface patterning in *Drosophila*

Parameter	Description	Value	Reference
	Diffusion	**Diffusion Coefficients**	
D_B	B in the PV space	$7.3 * 10\frac{\mu m^2}{sec}$	[5]
D_{Mad}	Mad in the cytoplasm and in the nucleus	$1.6 * 10\frac{\mu m^2}{sec}$	estimated

D_{pMad}	pMad in the cytoplasm and in the nucleus	$1.6 * 10 \frac{\mu m^2}{sec}$	estimated
D_{mRNA}	mRNA in the cytoplasm and in the nucleus	$3 * 10^{-2} \frac{\mu m^2}{sec}$	[77, 78]
D_{pMad2}	pMad2 in the cytoplasm and in the nucleus	$1.3 * 10 \frac{\mu m^2}{sec}$	estimated
D_{Me}	Madea in the cytoplasm and in the nucleus	$1.4 * 10 \frac{\mu m^2}{sec}$	estimated
D_{pMMe}	D pMad/Madea in the cytoplasm and in the nucleus	$1.2 * 10 \frac{\mu m^2}{sec}$	estimated
$D_{pMad2ME}$	pMad2/Madea in the cytoplasm and in the nucleus	$1.05 * 10 \frac{\mu m^2}{sec}$	estimated
	Production / Degradation		
k_{sb}	$\varnothing \rightarrow B$ in the PV space	$1 \frac{nM}{min}$	estimated
k_{db}	$B \rightarrow \varnothing$ in the PV space	$3.3 * 10^{-2} \frac{1}{min}$	[5]
k_{sr}	$\varnothing \rightarrow R$ in the PV space	$5 * 10^{-4} \frac{nM}{min}$	estimated
k_{dr}	$R \rightarrow \varnothing$ in the PV space and cytoplasm	$5 * 10^{-4} \frac{1}{min}$	[5]
k_{dc}	$C \rightarrow \varnothing$ in the PV space and cytoplasm	$1.67 * 10^{-4} \frac{1}{min}$	[5]
k_{dbr}	$BR \rightarrow \varnothing$ in the PV space and cytoplasm	$1.67 * 10^{-4} \frac{1}{min}$	[5]
k_{dbc}	$BC \rightarrow \varnothing$ in the PV space and cytoplasm	$1.67 * 10^{-4} \frac{1}{min}$	[5]
k_{dbcr}	$BCR \rightarrow \varnothing$ in the PV space and cytoplasm	$1.67 * 10^{-4} \frac{1}{min}$	[5]
k_{dmrna}	$mRNA \rightarrow \varnothing$ in the cytoplasm	$6.6 \frac{1}{min}$	[83]
k_{sc}	$mRNA \rightarrow C_{cyto} + mRNA$	$1 \frac{1}{min}$	estimated

	in the cytoplasm		
k_{dmrnan}	$mRNA \rightarrow \varnothing$	0	estimated
k_{bt}	$DNA \rightarrow TEC + DNA$ Basal transcription rate	$2\frac{1}{min}$	[81]
k_{et}	$DNA \rightarrow TEC + DNA$ Transcription enhanced by transcription factors binding	$20\frac{1}{min}$	[81]
	Receptor Interactions		
k_4	$B + C \rightarrow BC$	$1\frac{1}{nM*min}$	[5]
k_{-4}	$BC \rightarrow B + C$	$2\frac{1}{min}$	[5]
k_5	$B + R \rightarrow BR$	$2.4 * 10^{-2}\frac{1}{nM*min}$	[5]
k_{-5}	$BR \rightarrow B + R$	$4\frac{1}{min}$	[5]
k_6	$BC + R \rightarrow BCR$	$0.5\frac{1}{nM*min}$	[5]
k_{-6}	$BCR \rightarrow BC + R$	$10\frac{1}{min}$	[5]
k_7	$BR + C \rightarrow BCR$	$1.3 * 10^{-1}\frac{1}{nM*min}$	[5]
k_{-7}	$BCR \rightarrow BR + C$	$10\frac{1}{min}$	[5]
	Cytoplasmic Interactions		
k_{Mad}	$BR + Mad \rightarrow pMad + BR$	$2.4 * 10^{-2}\frac{1}{nM*min}$	[6]
k_8	$2pMad \rightarrow pMad2$ $pMad + Me \rightarrow pMMe$	$1.1 * 10^{-1}\frac{1}{nM*min}$	[6]
k_{-8}	$pMad2 \rightarrow 2pMad$ $pMMe \rightarrow pMad + Me$	$1\frac{1}{min}$	[6]
	Nuclear Interactions		
k_{-pMadn}	$pMad \rightarrow Mad$	$3.96 * 10^{-1}\frac{1}{min}$	[6]
k_8	$2pMad \rightarrow pMad2$ $pMadn + Me \rightarrow pMMe$	$1.1 * 10^{-1}\frac{1}{nM*min}$	[6]
k_{-8}	$pMad2 \rightarrow 2pMad$ $pMMe \rightarrow pMad + Me$	$1\frac{1}{min}$	[6]
k_{on}	$pMad2 + DNA \rightarrow pMad2DNA$ $pMMe + DNA \rightarrow pMMeDNA$	$60\frac{1}{nM*min}$	[79]
k_{off}	$pMad2DNA \rightarrow pMad2n + DNA$	$6.7 * 10^{-2}\frac{1}{min}$	[79]

	$pMMeDNA \rightarrow pMMe + DNA$		
$k_{rnaprod}$	$TEC \rightarrow mRNA$	$6.7 * 10^{-2} \frac{1}{min}$	estimated
	Movement Across Membrane		
k_{endo}	Endocytosis rate of BR, BCR, C and BC	$3.33 * 10^{-1} \frac{1}{min}$	[70]
k_{ex}	Exocytosis rate of BR, BCR, C and BC	$3.33 * 10^{-2} \frac{1}{min}$	[**?**]
k_{min}	Nuclear import rate of Mad,pMad and Madea	$1.56 * 10^{-1} \frac{1}{min}$	[6]
k_{in}	Nuclear import rate of pMad2 and pMME	$9 * 10^{-1} \frac{1}{min}$	[6]
k_{out}	Nuclear outport rate of Mad and pMad	$3.36 * 10^{-1} \frac{1}{min}$	[6]
k_{mout}	Nuclear import rate of Madea	$1.56 * 10^{-1} \frac{1}{min}$	[6]
k_{sec}	$C_{cyto} \rightarrow C$ Secretion rate of C	$1 \frac{1}{min}$	estimated